

**Excited States and Electron Transfer in Solution:
Models Based on Density Functional Theory**

by

Timothy Daniel Kowalczyk

B.S., University of Southern California (2007)

Submitted to the Department of Chemistry
in partial fulfillment of the requirements for the degree of

Doctor of Philosophy

at the

MASSACHUSETTS INSTITUTE OF TECHNOLOGY

June 2012

© Massachusetts Institute of Technology 2012. All rights reserved.

Author
Department of Chemistry
May 14, 2012

Certified by.....
Troy Van Voorhis
Associate Professor
Thesis Supervisor

Accepted by.....
Robert W. Field
Chairman, Department Committee on Graduate Theses

This doctoral thesis has been examined by a Committee of the
Department of Chemistry as follows:

Professor Jianshu Cao
Chairman, Thesis Committee
Professor of Chemistry

Professor Troy Van Voorhis
Thesis Supervisor
Associate Professor of Chemistry

Professor Keith A. Nelson
Member, Thesis Committee
Professor of Chemistry

Excited States and Electron Transfer in Solution: Models Based on Density Functional Theory

by

Timothy Daniel Kowalczyk

Submitted to the Department of Chemistry
on May 14, 2012, in partial fulfillment of the
requirements for the degree of
Doctor of Philosophy

Abstract

Our understanding of organic materials for solar energy conversion stands to benefit greatly from accurate, computationally tractable electronic structure methods for excited states. Here we apply two approaches based on density functional theory (DFT) to predict excitation energies and electron transfer parameters in organic chromophores and semiconductors in solution. First, we apply constrained DFT to characterize charge recombination in a photoexcited donor-acceptor dyad and to understand the photophysical behavior of a fluorescent sensor for aqueous zinc. Second, we discover that the delta-self-consistent-field (Δ SCF) approach to excited states in DFT offers accuracy comparable to that of the better-established but more indirect linear-response time-dependent DFT approach, and we offer some justification for the similarity. Finally, we investigate a spin-restricted analog of Δ SCF known as restricted open-shell Kohn-Sham (ROKS) theory. We resolve a known ambiguity in the formal solution of the ROKS equations for the singlet excited state by presenting a self-consistent implementation of ROKS with respect to the mixing angle between the two open shells. The excited state methods developed and applied in this work contribute to the expanding toolkit of electronic structure theory for challenging problems in the characterization and design of organic materials.

Thesis Supervisor: Troy Van Voorhis
Title: Associate Professor

Acknowledgments

First I thank my advisor, Troy Van Voorhis, on both professional and personal levels for the support and guidance that set the foundation for this work. Troy has helped me take full advantage of my strengths while giving me the time and resources to work on my weaknesses. He has also gone out of his way to accommodate my peculiar travel schedule, which has made a world of difference over the past several years.

I thank my thesis committee chair, Jianshu Cao, and committee member Keith Nelson for their input and advice on my work. Together with Bob Field and Mounqi Bawendi, they also helped shape my overwhelmingly positive experiences as a teaching assistant. I also thank my undergraduate research mentors, T. Daniel Crawford and Anna Krylov, for giving me the opportunity and the experience to hit the ground running.

Bob Silbey: I will never forget your special talent of asking a question, at the end of an otherwise impenetrable seminar, that suddenly made the whole audience understand the main point of the talk. Nor your riveting stories about quantum physicists from another era. Thank you for all you've done for us. We all miss you.

Thanks to my wonderful colleagues who, at one time or another, shared that space we all love to hate, The Zoo. In particular, I thank Ben Kaduk for technical assistance with the cluster and with Q-Chem; Lee-Ping Wang for insightful discussions about chemistry, energy, and navigating the academic world; Shane Yost for talking through some of my crazier ideas with me; Seth Difley for thought-provoking commentary; Oleg Vydrov for lunches and healthy doses of skepticism; and Jiahao Chen, for being a second mentor to me these past few years. Chiao-Lun Cheng, Jeremy Evans, Xiaogeng Song, Steve Presse, Qin Wu, Jianlan Wu, Eric Zimanyi, Xin Chen, Young Shen, Sina Yeganeh, Laken Top, Eric Hontz, Tamar Mentzel, Jeremy Moix, Liam Cleary, Bas Vlaming, Hang Chen, Mike Mavros, Helen Xie, Matt Welborn, Tom Avila, Chern Chuang, Javier Cerrillo Moreno and Takashi Tsuchimochi: it's been great working alongside you. Thanks also to Li Miao and Peter Giunta for their hard work keeping us stocked, fed, and reimbursed; and to Susan Brighton and Melinda Cerny in the

Chemistry Education office, who made the department feel like home.

I am grateful for the support of friends and colleagues beyond the Zoo who have brought balance to my time at MIT. I thank Andy Smith and Danny Liu for late-night conversations at 12 Michael Way; Jonathan Linkus for dragging me out to Harvard for coffee, dinner and architecture appreciation; fellow ChemREFS for their efforts to support their comrades through the various challenges of graduate school; and fellow organizers of the Boston-area theory seminars for helping create a broader sense of community. It has been an honor to collaborate with Stephen Lippard and his metalloneurochemistry subgroup, especially Bryan Wong and Daniella Buccella; I thank them for the opportunity.

A significant portion of the work presented in this thesis — including several key “aha!” moments — transpired under the roof of the Vagelos Laboratories at the University of Pennsylvania. I thank Patrick Walsh for entertaining my use of his group’s desk space and bandwidth. My sporadic time in Philadelphia was graced by friendships both within and beyond the confines of the Penn chemistry department. I’m especially grateful to Chris MacDermaid and Ariane Perez-Gavilan for having opened up their homes and their hearts (and more than a few good meals) to Genette and me through all of the ups and downs of graduate school.

I thank my grandmothers, Doris H. Smith and Blanche Kowalczyk, for supporting me in spite of my resistance to getting a haircut.

Most of all, I am so grateful for the love and support of the four people whose contributions behind the scenes are too many to report here: my mother Ginny, my father Dan, my brother Jeff, and my best friend (and wife) Genette. You are the implicit co-authors of all my work. Naturally, this thesis is dedicated to you.

Contents

1	Introduction	17
1.1	Marcus theory of electron transfer	19
1.2	Computational models for excited states and ET in solution	22
1.2.1	Density functional methods for the chromophore	23
1.2.2	Classical models for the solvent	27
1.3	Structure of this thesis	30
1.4	Acknowledgment	32
2	Simulation of Solution Phase Electron Transfer in a Compact Donor-Acceptor Dyad	33
2.1	Introduction	33
2.2	Model system: the FAAQ dyad	36
2.3	Computational model for electron transfer	38
2.4	Computational Details	39
2.5	Results	41
2.5.1	Construction of free energy profiles	41
2.5.2	Characterization of the electronic coupling	46
2.6	Discussion	48
2.6.1	Role of solute flexibility in ET kinetics	48
2.6.2	Reaction coordinate based on a simplified electrostatic model	51
2.7	Conclusion	52
2.8	Acknowledgment	55
2.A	Appendix: Parameterization of the quartic free energy model	55

2.B	Appendix: Electrostatic energy gap models	57
2.C	Appendix: Force field parameters for polarizable DMSO	59
3	Fluorescence quenching by photoinduced electron transfer in a luminescent Zn²⁺ sensor	61
3.1	Introduction	61
3.2	The Zn ²⁺ chemosensor ZP1	64
3.3	Computational Details	66
3.4	Results and Discussion	67
3.4.1	TDDFT with a conventional hybrid functional	67
3.4.2	TDDFT with long-range corrected functionals	71
3.4.3	CT excited states via CDFE	74
3.5	Conclusion	77
4	Assessment of ΔSCF density functional theory for electronic excitations in organic dyes	79
4.1	Introduction	79
4.2	Test Set	81
4.3	Computational Methods	85
4.4	Results	85
4.5	Discussion and Analysis	89
4.5.1	Linear response TDDFT	89
4.5.2	Δ SCF densities	91
4.5.3	Δ SCF energy expressions	92
4.6	Conclusion	95
4.7	Acknowledgment	96
5	Self-consistent implementation of restricted open-shell Kohn-Sham methods for excited states	97
5.1	Introduction	97
5.2	Theory	100

5.2.1	The influence of orbital mixing between open shells	103
5.2.2	Variational treatment of open-shell mixing	104
5.3	Computational details	106
5.4	Results and Discussion	107
5.4.1	Canonical and variational ROKS energies of small organic dyes	107
5.4.2	ROKS vertical excitation energies of large organic dyes	110
5.4.3	Comparison of potential energy surfaces from ROKS, Δ SCF and TDDFT	111
5.5	Conclusion	113
6	Conclusion	115
A	Energies of key structures	119
A.1	ZP1 vertical excitation energies	119
A.2	ROKS excitation energies: small dye test set	121
B	Optimized geometries of key structures	123
B.1	Protonation and zinc-binding states of ZP1	123
B.2	Test set of large organic dyes	141

List of Figures

1-1	Marcus parabolas depicting free energy as a function of an ET reaction coordinate in different kinetic regimes	20
1-2	Frontier orbitals for the ground state and CT excited state involved in a prototypical ET reaction	26
1-3	Schematic of solvent reorganization associated with an ET event, highlighting electronic and orientational solvent polarization	28
2-1	Structure of the FAAQ dyad in its <i>cis</i> and <i>trans</i> conformations, with the employed donor–acceptor partitioning indicated	37
2-2	Construction of ET free energy curves for FAAQ from molecular dynamics simulations by binning of the energy gap distribution	42
2-3	Quartic parameterization of the neutral and CT free energy profiles, with Marcus profiles included for comparison	45
2-4	Scatterplot of the energy gap and dihedral angle for snapshots of FAAQ from all trajectories, with activation energies for transitions between the four free energy wells	50
2-5	Correlation between the diabatic energy gap and a simplified electrostatic energy gap	53
2-6	Illustration of the reference frames used for ensemble-averaging of the FAAQ dipole.	58
3-1	Energy level diagrams illustrating PET from the frontier molecular orbital and electronic state perspectives	62

3-2	Schematic of Zn^{2+} binding to ZP1 in aqueous solution, and summary of ZP1 structures employed in this study	65
3-3	ZP1 attachment-detachment densities for the two lowest-lying CT excitations and the lowest valence excitation	69
3-4	Net charge transfer by functional group upon excitation to the lowest CT state of ZP1, with and without bound Zn^{2+}	75
4-1	Test set, molecules 1–8 : chemical structure, absorption maximum and HOMO \rightarrow LUMO character of the S_1 state	83
4-2	Test set, molecules 9–16 : chemical structure, absorption maximum and HOMO \rightarrow LUMO character of the S_1 state	84
5-1	Schematic of Kohn-Sham orbital relaxation in ΔSCF and in ROKS .	101
5-2	Two-layer SCF algorithm for obtaining an ROKS energy which is variational with respect to both the density matrix and the open-shell mixing angle	105
5-3	Dependence of the exchange and XC contributions to the ROKS energy on θ for the lowest $n \rightarrow \pi^*$ excitation in formaldehyde and the lowest $\pi \rightarrow \pi^*$ excitation in cyclopentadiene	109
5-4	Potential energy curves for the S_0 and S_1 states of formalimine along two independent isomerization pathways	112

List of Tables

2.1	ET parameters obtained from MD simulations, assuming Gaussian statistics for the energy gap.	44
2.2	CR parameters obtained under the linear response approximation and under the quartic fits	46
2.3	Mean electronic couplings and deviations for neutral and CT configurations of FAAQ in the gas phase and in DMSO solution	47
2.4	Force field parameters for the polarizable DMSO model	60
3.1	TDDFT vertical excitation energies of the lowest valence and two lowest CT states of ZP1	70
3.2	Lowest gas-phase valence and CT excitation energies of neutral ZP1 predicted by long-range corrected TDDFT, as a function of the range-separation parameter	73
3.3	Valence excitation energies from TDDFT and CT excitation energies from CDFT as a function of number of Zn ²⁺ ions bound	76
4.1	Test set statistics for the three different excited state methods	87
4.2	PBE0 energies and spin multiplicities for the test set	88
5.1	Dependence of ROKS excitation energy on the prescription for the open-shell mixing angle for a collection of small organic dyes	107
5.2	Deviations of ROKS excitation energies from experiment for the test set of larger organic dyes	110

A.1	Lowest vertical excitation energies for ZP1 structures 2 and 4–11 obtained with several DFT models	120
A.2	Dependence of long-range corrected ROKS excitation energies on the prescription for the open-shell mixing angle	122

Chapter 1

Introduction

The flow of energy that sustains our industrialized way of life operates on a global scale, yet the efficiency with which we burn fuels and generate electrical current is determined by processes at the molecular level. As our energy needs threaten to outstrip the supply of hydrocarbon deposits, efforts to harvest nuclear, solar, wind and geothermal energy in an optimally efficient manner will become increasingly urgent. In meeting these demands, we stand to benefit substantially from a mechanistic understanding of energy conversion processes at the nanoscale.

For harnessing electrical work from solar energy, organic semiconductors (OSCs) — extended chromophores composed of main-group elements — offer a rich diversity of structural and electronic properties,¹⁻³ making them promising targets for rational design and optimization. These properties, together with the lower manufacturing costs associated with OSC materials relative to traditional semiconductors, have driven a significant and growing body of fundamental and applied research built around these materials. Furthermore, strategies from organic synthesis can be exploited to construct single-molecule electronic devices, such as donor-bridge-acceptor polyads⁴ and dendrimers,^{5,6} from conjugated subunits. These structures exhibit complex photophysical behaviors that are of fundamental interest in their own right.

In an OSC-based solar cell, the fundamental molecular processes at work are: (1) absorption of light by a material, resulting in an electronically excited state (or exciton); (2) separation of the exciton into an electron and a positive ion (or hole);

and (3) transport of the ions to their respective electrodes. Each of these basic steps influences device operation and efficiency. The charge separation (CS) process (2) is often in kinetic competition with a variety of alternative relaxation pathways which vary depending on the chemical composition of the material and its environment.⁷

Theoretical modeling and simulations are playing a key role in contemporary energy research, alongside experimental efforts. Mechanistic investigations of oxygen- and hydrogen-evolving catalysts are guiding next-generation catalyst design.^{8,9} Simulations of chemical and morphological changes in battery materials promise to lead to higher capacity, more durable batteries.¹⁰ Meanwhile, new metal oxide and OSC materials are already being screened and characterized for desirable electronic properties before a practical synthetic route is ever outlined,^{11,12} greatly narrowing the combinatorial space of structures that need to be characterized experimentally. Theory and simulation also have a role to play in our evolving understanding of the electronic properties of organic chromophores in condensed phases; this context provides a unified motivation for all of the studies presented here.

This thesis addresses quantum chemical modeling of two varieties of electronically excited states regularly encountered in photovoltaic applications: “bright” valence excited states formed through visible-light absorption, and charge-transfer (CT) excited states obtained from valence excited states through a CS process. These states play important roles in many areas of chemistry beyond solar energy conversion: many of the methods applied and refined in this work could be used to design dyes for fluorescent tagging and bio-imaging protocols;¹³ to predict the isomerization kinetics of photochemically-driven molecular rotors;¹⁴ or to characterize the spectral density influencing the possibility of quantum coherence in photosynthetic complexes,¹⁵ among other uses.

In this introductory chapter, we first review the standard theoretical framework for understanding electron transfer in solution, Marcus theory. Next we introduce the computational models we will be using and refining throughout the investigation. These models are rooted in the quantum mechanical approach of density functional theory, but we also introduce some quasi-classical methods for addressing solvent

effects. Finally, we provide an overview of the structure and contents of the remainder of this thesis.

1.1 Marcus theory of electron transfer

Electron transfer (ET) lies at the heart of chemical reactivity, as captured by the “arrow-pushing” formalism in organic chemistry textbooks. Intermolecular ET reactions that proceed without bond breaking or bond formation are among the simplest chemical transformations; yet the kinetics of these reactions remain difficult to predict from first principles. ET can also occur within a molecule, from one functional group to another, as a consequence of thermal or photoinduced excitation. The quest for a quantitative understanding of ET kinetics has been ongoing for well over 50 years and continues to gain practical significance as demand for solar energy conversion accelerates.

The standard theoretical framework for ET reactions has been established for quite some time and is referred to as Marcus theory.¹⁶ Several existing reviews detail the physical foundations,^{17–19} applications,^{18,20,21} and extensions^{19,22,23} of Marcus theory, so we provide only a brief summary here. Marcus theory is a classical transition state theory of ET which assumes that the reactant and product electronic states are weakly coupled. Furthermore, Marcus theory assumes that the molecule(s) undergoing ET are surrounded by an environment that responds linearly to the ET event (linear response approximation). In this limit, the free energy profiles of the two ET states can be represented by a pair of crossing parabolas with identical curvature, illustrated in Figure 1-1.

Two parameters suffice to characterize the relative displacement and curvature of the reactant and product free energy curves: the driving force $-\Delta G$, which constitutes the free energy difference between reactant and product states, and the reorganization energy λ , which quantifies the free energy penalty associated with forcing the reactant into an equilibrium configuration of the product or vice-versa. The Marcus expression for the ET rate is the classical transition-state theoretical rate obtained from the free

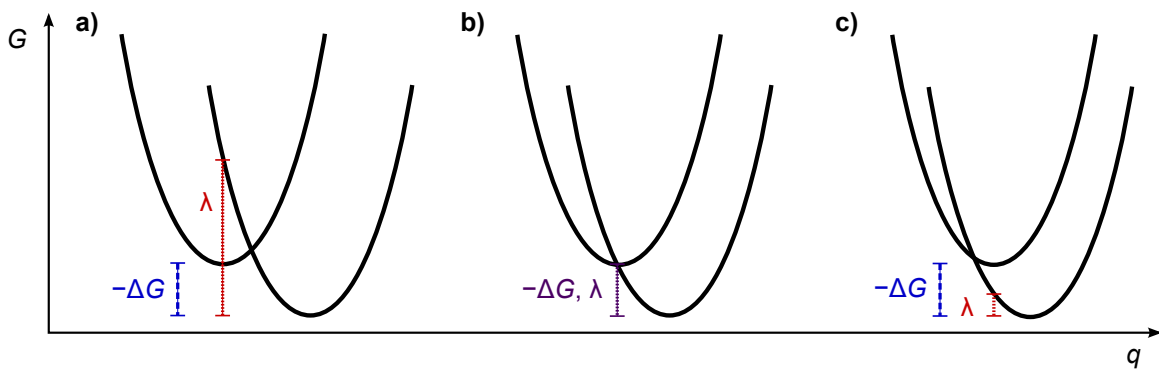


Figure 1-1: Marcus parabolas depicting free energy as a function of an ET reaction coordinate in different kinetic regimes. (a) The normal region, $-\Delta G < \lambda$. (b) The top region, $-\Delta G \approx \lambda$. (c) The inverted region, $-\Delta G > \lambda$.

energy profiles in Figure 1-1,

$$k_{\text{ET}} = \frac{2\pi}{\hbar} \frac{|V_{ab}|^2}{\sqrt{4\pi\lambda k_{\text{B}}T}} \exp \left[-\frac{(\lambda + \Delta G)^2}{4\lambda k_{\text{B}}T} \right] \quad (1.1)$$

Here T is the temperature, k_{B} is the Boltzmann constant, \hbar is the reduced Planck constant, and the pre-exponential factor is expressed in terms of thermodynamic quantities plus the electronic coupling term V_{ab} . According to Eq. 1.1, the ET activation energy ΔG^\ddagger is given by

$$\Delta G^\ddagger = \frac{(\lambda + \Delta G)^2}{4\lambda} \quad (1.2)$$

ET reactions are classified according to the relative magnitudes of $-\Delta G$ and λ . Reactions satisfying $-\Delta G < \lambda$ are said to occur in the “normal” regime, while those in the Marcus “inverted” regime satisfy $-\Delta G > \lambda$. Representative free energy curves for these two cases are shown in Figures 1-1a and 1-1c. In the intermediate “top” region of Figure 1-1b, a negligible activation free energy barrier results in the maximum ET rate for a given driving force. In the inverted regime, the Marcus theory predicts a decrease of the ET rate with increasing driving force; experimental evidence of Marcus inverted effects²⁴ has reinforced the value of the theory.

Given the demonstrated utility of the Marcus model, methods to predict Marcus ET parameters for real systems from first principles have proliferated in recent years.

These predictions are challenging because they call for a *diabatic* representation of the ET states, whereas conventional electronic structure methods produce adiabatic states. In the adiabatic representation, one of the ET states is often an excited state. It is possible to estimate the driving force in the adiabatic representation from the energy difference of the ground and excited states at their respective equilibrium geometries, but this calculation requires optimization of the excited state geometry, which hampers its applicability to larger systems.

The reorganization energy λ presents further challenges to computation. It is fundamentally a nonequilibrium property because it requires the energy of one ET state at the equilibrium geometry of the other state.²⁵ The reorganization energy is often partitioned into two contributions: an inner-sphere reorganization energy associated with distortion of the molecular geometry and an outer-sphere reorganization energy reflecting the rearrangement of solvent to accommodate the new charge distribution. The outer-sphere reorganization energy often comprises the dominant contribution to the total λ ,^{26,27} so a proper description of solvent effects is crucial.

Still, significant progress has been made towards prediction of reorganization energies. A straightforward and popular approach is the four-point method,²⁸ which treats reorganization of the donor to its radical cation and of the acceptor to its radical anion independently. This approach can be used with high-level electronic structure methods but does not account for interactions between donor and acceptor, which cannot be neglected for intramolecular ET. Alternatively, one can employ a diabaticization scheme²⁹ to compute energies for the two ET states at either state's equilibrium geometry. Adiabatic-to-diabatic transformations such as the generalized Mulliken-Hush approach³⁰ can be used for this purpose, or one can directly construct approximate diabats using tools such as empirical valence-bond methods,³¹ frozen density functional theory,³² or constrained density functional theory.³³

1.2 Computational models for excited states and ET in solution

As is often the case in physical chemistry, we are concerned with a system of primary interest (the electronically excited chromophore) interacting with an environment (the surrounding solvent) whose intrinsic properties are of little interest to us but whose influence on the system is paramount. Hence we can adopt a Hamiltonian of the form

$$\hat{H} = \hat{H}_S + \hat{H}_B + \hat{H}_{SB} \quad (1.3)$$

where S and B denote the system and bath (environment) degrees of freedom, respectively. In this thesis, the system degrees of freedom include the electronic and nuclear coordinates of the chromophore. Thus, the system Hamiltonian is of the form $\hat{H}_S(\{\mathbf{r}_i\}, \{\mathbf{R}_A\})$, where \mathbf{r}_i (\mathbf{R}_A) denotes an electronic (nuclear) position. We will treat system electrons quantum mechanically, but nuclei will be described classically, i.e. all electronic structure calculations assume the Born-Oppenheimer approximation. Despite this mixed quantum-classical description of the system, this system Hamiltonian is often denoted \hat{H}_{QM} in the literature to distinguish it from the purely classical description of the bath.

In what follows, we treat the system Hamiltonian with an electronic structure method, in particular, with density functional theory or its various extensions for excited states, which are briefly reviewed in Section 1.2.1. For the environment, we consider two strategies. Implicit (or continuum) models are parameterized by bulk properties of the solvent and the shape of the solute. They generally capture the important electronic effects of solvation at little computational expense. Alternatively, explicit (or atomistic) solvation models employ an empirical force field to describe the solvent and its interactions with the solute. Both approaches are reviewed in Section 1.2.2.

1.2.1 Density functional methods for the chromophore

Kohn–Sham density functional theory

In density functional theory (DFT), the search for the wavefunction $\psi(\mathbf{r}_1, \dots, \mathbf{r}_N)$ describing the ground state electronic configuration for N electrons interacting with an external potential (i.e. a set of fixed classical nuclei) is recast in terms of a one-electron density $\rho(\mathbf{r}) = \int \psi^*(\mathbf{r}, \mathbf{r}_2, \dots, \mathbf{r}_N) \psi(\mathbf{r}, \mathbf{r}_2, \dots, \mathbf{r}_N) d\mathbf{r}_2 \dots d\mathbf{r}_N$. The Hohenberg–Kohn theorems established the existence of a universal functional of the density, $F[\rho(\mathbf{r})]$, which determines the energy associated with the density in any given external potential,³⁴

$$E[\rho(\mathbf{r})] = \int (v_{\text{ext}}(\mathbf{r})\rho(\mathbf{r}) + F[\rho(\mathbf{r})]) d\mathbf{r} \quad (1.4)$$

Furthermore, Hohenberg and Kohn showed that the energy functional in Eq. 1.4 is minimized for the ground state density in the external potential v_{ext} . However, the universal functional $F[\rho]$ is not known and must be approximated in practice.

While approximations to the universal functional involving only the density have made significant advances in recent years,³⁵ the vast majority of DFT calculations are carried out within the Kohn–Sham (KS) formalism.³⁶ The KS approach introduces a fictitious “non-interacting” system of electrons which feel only the external potential and are associated with a set of one-electron orbitals (KS orbitals), $\{\phi_i^{\text{KS}}(\mathbf{r})\}$ chosen to reproduce the ground-state density of the real interacting system,

$$\rho(\mathbf{r}) = \sum_{i=1}^N |\phi_i^{\text{KS}}(\mathbf{r})|^2$$

The KS approach circumvents the difficult problem of defining a kinetic energy functional $T[\rho]$ by replacing it with the kinetic energy of the non-interacting system $T_s[\rho]$ — which is easily calculated from the KS orbitals — plus a small correction. This correction is grouped together with the effects of Pauli exchange and electron correlation in the exchange-correlation (XC) functional, $E_{\text{xc}}[\rho]$. In contrast with wavefunction based techniques for electron correlation,³⁷ KS-DFT captures a significant fraction of dynamical correlation at modest computational cost. An important trade-off for this

advantage is that KS-DFT lacks the systematic improvability available under, e.g. coupled cluster and configuration interaction calculations.

An enormous amount of effort has been expended to develop accurate approximations to the XC functional, leading to a hierarchy of approximations known as “Jacob’s ladder” of density functionals.³⁸ Without getting bogged down by the detailed machinery of modern XC functionals, we note that the calculations in this thesis regularly make use of hybrid approximations for exchange, wherein both exact (Hartree-Fock) and approximate density-based descriptions of exchange figure into the expression for the exchange energy.³⁹ Several of our studies also make use of a more general framework for exchange, the range-separation technique.^{40,41} Here, the fraction of exact exchange included in the functional depends explicitly on interelectronic distance.

Time-dependent density functional theory

KS-DFT is purely a ground-state theory of electronic structure. To obtain information about excited states strictly within the KS formalism, one can turn (perhaps somewhat unexpectedly) to its time-dependent analogue, established by the Runge–Gross theorem.⁴² Time-dependent density functional theory (TDDFT) is a very general theory amenable to a wide range of applications in chemical physics,⁴³ but here we focus exclusively on its use for excited state electronic structure calculations. By and large, these calculations are based on a linear response (LR) formalism^{44,45} in which electronic excitation frequencies ω_i are obtained as poles in the density response function $\chi(\mathbf{r}, \mathbf{r}', \omega)$. The machinery of LR-TDDFT will be outlined in more detail in Chapter 4, where we will also have reason to consider a direct search for excited state densities in TDDFT.

For ET applications, it is important to note that many commonly used XC functionals perform notoriously poorly in predicting the energy of CT excited states via TDDFT.⁴⁶ While range-separated functionals can often mitigate these effects, the alternative DFT methods for excited states presented below avoid this problem.

Constrained density functional theory

In contrast to TDDFT, constrained density functional theory (CDFT) is not designed to provide exact excitation energies given the true ground-state XC functional. Nevertheless, it provides indirect access to the energies and properties of CT excited states and other electronic states that are well described by weakly-interacting electronic subsystems.

In CDFT, we seek the ground-state energy subject to one or more constraints on the electron density. The energy of the constrained state is obtained by extremizing a modified functional

$$W[\rho, V_c] = E[\rho] + V_c \left(\int w_c(\mathbf{r})\rho(\mathbf{r}) d\mathbf{r} - N_c \right) \quad (1.5)$$

where $w_c(\mathbf{r})$ is a weight operator defining the shape of the constraining potential, N_c is the value of the constraint, and V_c is a Lagrange multiplier enforcing the constraint. The weight operator is typically defined in terms of atomic populations such as the Mulliken,⁴⁷ Löwdin,⁴⁸ Becke⁴⁹ or Hirshfeld⁵⁰ populations, although simpler constraining potentials have also proven useful in some related methods for studying charge transfer.⁵¹

CDFT can be used to construct diabatic states for any ET reaction whose electron donor and acceptor moieties are known in advance. In ET systems with a neutral ground state, the frontier orbitals of the ground and CT states are of the general form illustrated in Figure 1-2. In the ground state, both the donor and acceptor have closed shells. The transfer of one electron from the donor HOMO to the acceptor LUMO defines the CT state. Considered as isolated species, the donor and acceptor are both charged radicals after ET; hence the CT state is also known as a radical ion-pair state.

To obtain diabatic ET states from CDFT, one first defines which regions of the system are to be associated with the donor or with the acceptor. Net charges are then assigned to the donor and acceptor in accordance with the character of the target state. For example, to define the CT diabatic state in Figure 1-2, one constrains

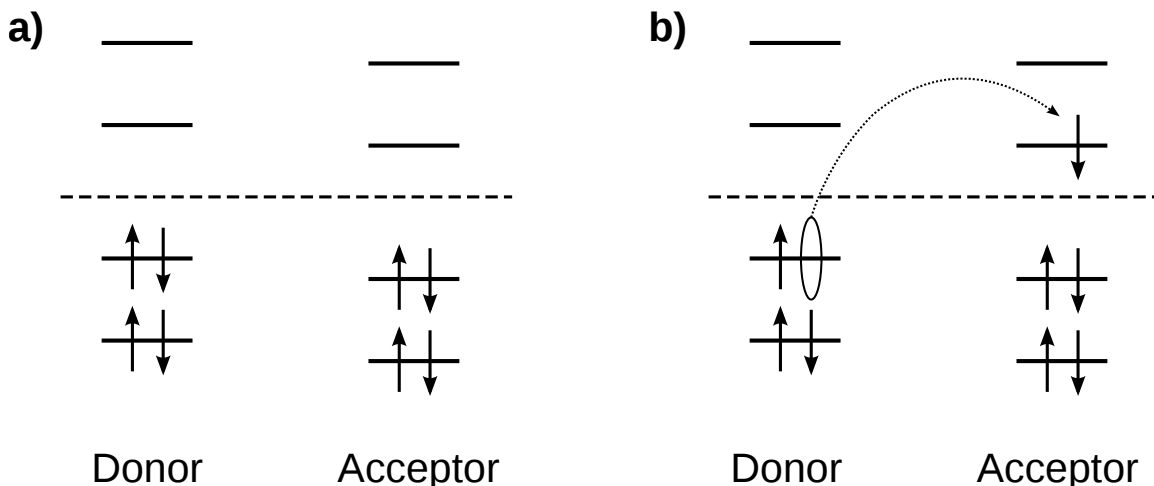


Figure 1-2: Frontier orbitals for the ground state (a) and the CT excited state (b) involved in a prototypical ET reaction. Adapted with permission from Ref. 33.

the donor (acceptor) to have one fewer (more) electron than it would possess as an isolated, neutral system. Alternatively, one can define the CT state by constraining the difference in net charge between the donor and acceptor to two electrons. A diabatic representation of the neutral ground state is obtained analogously by constraining the net charges on the donor and acceptor regions to zero. In practice, the constrained neutral state usually differs negligibly from the adiabatic ground state, so a ground state calculation can suffice for this purpose.

In certain systems it may be reasonable on chemical grounds to exclude some regions of space from either the donor or the acceptor; examples include bridges in donor-bridge-acceptor architectures and explicit solvent molecules. However, existing evidence suggests that these regions should also typically be added to the donor and/or acceptor domains because the enhanced variational freedom tends to produce a more accurate energy without sacrificing the state's diabatic character.³³

Δ SCF density functional theory

Instead of obtaining excitation energies from density functional response theory or by applying density constraints, an appealing alternative is to relate higher-energy solutions of the KS equations to excited states. These higher-energy solutions can be obtained in practice by converging the KS orbitals self-consistently with non-Aufbau

orbital occupation patterns, amounting to a constraint on orbital occupations rather than a constraint on the density. This is the Δ SCF approach to excited states in DFT.

Δ SCF lacks the firm theoretical underpinning associated with TDDFT: there is no excited-state analogue of the Hohenberg–Kohn theorem,⁵² nor can it be taken for granted that approximate functionals for the ground-state energy will return the correct excited-state energy for a given excited-state density.^{53,54} The analogous strategy within Hartree-Fock theory presents convergence difficulties and returns poor excitation energies when it does converge. Nevertheless, as we show in Chapter 4, Δ SCF-DFT is surprisingly accurate for singlet-singlet transitions that are well described by a single-orbital excitation (e.g. HOMO \rightarrow LUMO). Some reasons for the relative success of Δ SCF will be provided in Chapter 4.

1.2.2 Classical models for the solvent

The role of the environment in modulating ET properties is an essential feature of Marcus theory.¹⁶ Figure 1-3 provides a schematic for nonadiabatic ET in polar media. Solvent polarization, on average, acts to stabilize an electron localized on an electron donor. However, thermal fluctuations of the solvent can bring the two diabatic states into a transient energetic degeneracy, at which point the electron can hop to the acceptor with probability proportional to the square of the electronic coupling.

Implicit solvation models

At first glance, the mechanism illustrated in Figure 1-3 appears well-suited for a dielectric continuum model of the solvent.^{55,56} In the continuum models, the solute is placed in a cavity carved out of a continuous dielectric medium characterized by its dielectric constant ϵ , and the solvation free energy is obtained by solving the Poisson-Boltzmann equation for the surface charge on the cavity induced by the dielectric response of the solvent to the solute electron density. These continuum models typically make the approximation that the solvent can be characterized by a frequency-independent

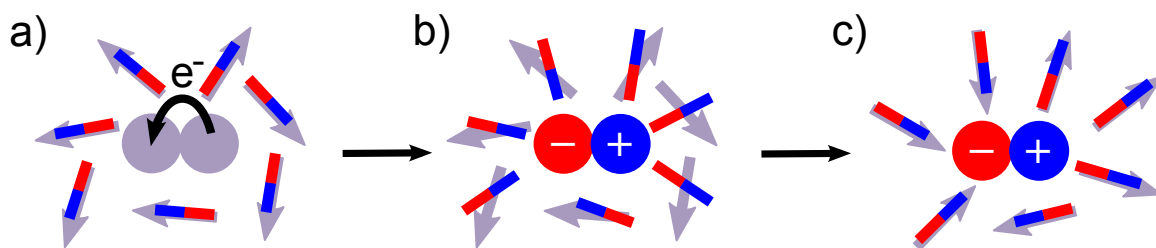


Figure 1-3: Schematic of solvent reorganization associated with an ET event, highlighting electronic and orientational solvent polarization. Conjoined spheres represent the ET dyad; arrows represent the orientation of individual solvent molecules. (a) A spontaneous fluctuation of the solvent away from equilibrium facilitates an ET event. (b) Electronic polarization (red and blue bars) of the solvent in response to ET occurs much faster than (c) orientational polarization, eventually establishing equilibrium in the CT state.

dielectric constant ϵ . This approximation is often quite good for ground-state solvation energies, especially in solvents lacking significant nonelectrostatic interactions, e.g. hydrogen bonding or π -stacking.

However, the approximation of a single dielectric constant breaks down immediately after electronic excitation of the solute, especially for CT states. The underlying reason is that vertically excited states are out of equilibrium: the solvent electron density equilibrates with the CT density of the solute, but the larger mass of the solvent nuclei causes orientational polarization to take place on a slower timescale. Immediately after electronic excitation, the solvent nuclear degrees of freedom remain in equilibrium with the ground state of the solute. Rather than introduce a fully frequency-dependent dielectric $\epsilon(\omega)$ to model this behavior, it is convenient and practical to separate the solvent polarization response into fast and slow components in accordance with solvent electronic and nuclear relaxation.^{57,58} Electronic response is characterized by the optical dielectric constant ϵ_∞ , which is the square of the refractive index of the dielectric, while nuclear response is characterized by the zero-frequency dielectric constant ϵ_0 .

Explicit solvation models

Despite the computational advantages of dielectric continuum solvation models, it is often the case in complex chemical systems that specific solute-solvent interactions

have a profound influence on the dynamics. Commonly encountered examples include hydrogen bonding interactions and interfacial effects in heterogeneous environments. In these situations, it may be advantageous to resort to an atomistic solvent model which treats each solvent atom explicitly, typically by a less computationally demanding scheme such as a semiempirical method or molecular mechanics (MM).⁵⁹ MM models define the energy of a solvent configuration in terms of the internal energy of each solvent molecule, Coulomb interactions among atomic sites of different molecules, and van der Waals interactions between molecules (this defines \hat{H}_B in Eq. 1.3). The collection of parameters defining these interactions constitutes the force field. These parameters are often obtained from experimental data but can also be fit to quantum chemistry calculations.⁶⁰

A variety of strategies exist for treating the interaction of an electronic density with a solvent described by MM (the \hat{H}_{SB} term in Eq. 1.3),⁶¹ but we will exclusively use the electronic embedding strategy here. In electronic embedding, the point charges of the MM solvent generate an electric field which is included in the KS Hamiltonian, thus allowing the density to relax self-consistently with respect to the charge distribution of the solvent.

By including an explicit description of the solvent in the calculation of ET parameters, one no longer needs to rely on assumptions such as linear response to attain a tractable model of solvent effects; instead, one may sample the configuration space of the system through Monte Carlo or molecular dynamics (MD) simulations to obtain a statistical description of the ET energetics. However, the introduction of so many solvent degrees of freedom can obscure the notion of an ET reaction coordinate describing collective solvent motions. An elegant solution to this problem is to choose the energy gap ΔE between the diabatic states as a reaction coordinate;⁶² this choice of reaction coordinate condenses all important solvent motions onto a single quantity in which the free energy is quadratic in the limit of linear response.⁶³

1.3 Structure of this thesis

This body of this thesis encompasses two broad research themes spanning four chapters. The first theme, computational modeling of ET in solution, is covered in Chapters 2 and 3. The second theme, assessment and refinement of time-independent approaches to DFT excited states, forms the basis of Chapters 4 and 5.

In Chapter 2, we present a QM/MM protocol for ET simulations and use it to characterize CR in a small donor-acceptor dyad. Our atomistic model facilitates construction of free energy curves without the need to assume linear response of the solvent, permitting a critical assessment of the Marcus picture for this system. Furthermore, by using CDFT to model the electronic states of the dyad, we can obtain statistical information about the electronic coupling between the diabatic states. We find that these couplings show a clear dependence on whether the geometric configuration is more stabilizing for the ground state or for the CT state. We explore the role of *cis-trans* isomerization on the CR kinetics, and we find a strong correlation between the vertical energy gaps of the full simulations and a collective solvent polarization coordinate. The method constitutes a unified approach to the characterization of driving forces, reorganization energies, electronic couplings and nonlinear solvent effects in light-harvesting systems. To our knowledge, these simulations represent the first CDFT-based characterization of electronic couplings in an asymmetric ET system in solution.

We turn to a different application of ET in Chapter 3: the selective detection and measurement of an analyte by ET-induced fluorescence quenching. In this study, a two-pronged approach employing both TDDFT and CDFT is used to characterize low-lying electronically excited states of the aqueous zinc sensor Zinpyr-1 (ZP1). The calculations indicate that fluorescence activation in ZP1 is governed by a photoinduced ET mechanism in which the energy level ordering of the excited states is altered by binding Zn^{2+} . Although the tertiary amine groups of ZP1 serve as the primary electron donor, we show that the pyridyl nitrogens on each Zn^{2+} -chelating arm of the molecule each contribute some electron density to the xanthone chromophore

upon ET. The calculations highlight the importance of carefully tuning the receptor site pK_a to avoid complex protonation equilibria which could otherwise hamper ratiometric sensing efforts.

The focus of Chapter 4 shifts from ET applications of CDFT to an assessment of an alternative DFT approach to excited states, Δ SCF, for organic dyes. Over a test set of vertical excitation energies of 16 chromophores, we observe surprisingly similar accuracy for the Δ SCF and TDDFT approaches with commonly used XC functionals. In light of this performance, we revisit the approximations inherent to the Δ SCF prescription and demonstrate that the method formally obtains exact stationary densities within the adiabatic approximation, partially justifying its use. The relative merits and future prospects of Δ SCF for simulating individual excited states are discussed in light of these findings.

In Chapter 5, we consider the restricted open-shell Kohn-Sham (ROKS) approach, an excited state strategy related to Δ SCF. Despite the promising performance of Δ SCF documented in Chapter 4, convergence difficulties and the need for an energy correction due to spin motivate us to evaluate the ROKS method — which in principle does not suffer from these drawbacks — as an alternative to Δ SCF for excited state simulations. We identify and resolve an ambiguity in the density-matrix based formulation of the ROKS equations by building control over the mixing between the two open shells into our ROKS algorithm. Pilot calculations with different prescriptions for the mixing angle suggest that a single prescription for the mixing angle can provide reasonable ROKS excitation energies for transitions of arbitrary symmetry. We also provide some evidence that potential energy surfaces for formalimine isomerization predicted by Δ SCF, ROKS and TDDFT are quite parallel.

Finally, in Chapter 6, we collect key findings and frame them in the broader context of computational models for fundamental chemistry in solution and for solar energy conversion in particular. Directions of ongoing and future work are also discussed.

1.4 Acknowledgment

Portions of this introductory chapter were published in our review of CDFT, Ref. 64, of which Ben Kaduk is a co-author.

Chapter 2

Simulation of Solution Phase

Electron Transfer in a Compact

Donor-Acceptor Dyad

2.1 Introduction

Electron transfer (ET) reactions are crucial steps in the storage of solar energy in chemical bonds. Whether in biological or bio-inspired light-harvesting systems^{65,66} or in advanced semiconductor materials,⁶⁷⁻⁶⁹ the same three-step mechanism underlies the conversion of incident photon flux into photocurrent. Absorption of visible light by a photosensitive structure, such as a dye molecule or a semiconductor, generates a localized excited state. The availability of lower-energy electronic states with enhanced charge separation drives an ET process, resulting in an intermediate, charge-transfer (CT) excited state. The CT state can further separate into free charges, completing the photovoltaic process.

Synthetic light-harvesting systems have very high standards to meet: in natural photosynthesis, electrons and holes are generated from the initial CT state with near unit efficiency due to rapid charge separation (CS) versus extremely slow (~ 1 s) charge recombination (CR).⁷⁰ The critical role of the CS-to-CR ratio in light-

harvesting complexes^{71,72} has inspired a substantial body of experimental and theoretical work on condensed phase CS and CR in small-molecule prototypes.^{18,73,74}

Molecular polyads — consisting of a chromophore and one or several electron donors and acceptors — are a popular architecture for artificial light-harvesting because they offer the potential for long-lived photoinduced CS in a small, chemically tunable package.^{75–77} Triads,^{78,79} tetrads⁸⁰ and higher polyads, including dendrimeric structures,⁵ exploit spatial separation of the terminal donor and acceptor to reduce the donor-acceptor electronic coupling, obtaining long-lived CT states at the expense of low yields of the CT state. Conversely, smaller dyads present high initial CT state yields, but fast geminate CR limits the overall efficiency of charge carrier generation.⁷ How small the dyad can be while maintaining a capacity for photoinduced CS is an open and important question.

Given the daunting task of striking a favorable balance between CS and CR in these polyads, we anticipate further rational design and optimization to be contingent upon a mechanistic understanding of the underlying ET processes. The Marcus theory of ET^{16,17} outlined in Chapter 1 is an excellent guide in this respect. To briefly recapitulate, in Marcus theory the ET rate is expressed in terms of three system-dependent parameters: the driving force ΔG , which is the free energy difference between the reactant and product states at equilibrium; the reorganization energy λ , which is the free energy cost to distort the configuration of the reactant to an equilibrium configuration of the product; and the donor-acceptor electronic coupling V_{DA} ,

$$k_{\text{ET}} = \frac{2\pi}{\hbar} \frac{V_{\text{DA}}^2}{\sqrt{4\pi\lambda k_{\text{B}}T}} \exp \left[-\frac{(\lambda + \Delta G)^2}{4\lambda k_{\text{B}}T} \right] \quad (2.1)$$

The validity of the Marcus model has been thoroughly investigated and confirmed over a wide range of conditions,^{81,82} including the inverted region, $-\Delta G > \lambda$, where the ET rate is predicted to decrease with increasing driving force. The model assumes linear response of the bulk solvent polarization to the electric field. Several extensions have been proposed to account for situations where the model breaks down, for example, in systems with strong vibronic effects⁸³ or electronic state-dependent po-

larizabilities.⁸⁴ Marcus theory and its extensions provide a framework for correlating molecular structure with ET properties; thus, Marcus ET parameters are important for the analysis and refinement of molecular light-harvesting architectures.

Because of the experimental challenges associated with measuring ET parameters, especially the reorganization energy,^{85,86} computer simulations have played an important role in developing an understanding of ET at the molecular level. These simulations present their own set of challenges. The role of the environment as a facilitator of ET has long been appreciated,^{87,88} but the computational cost of modeling the environment from first-principles is often prohibitive. Instead, it is common to adopt a hybrid QM/MM model^{89,90} in which the solute is described by a high-level electronic structure method while the solvent is treated with a classical force field. Furthermore, diabatic reactant and product states form a more suitable basis for studying ET than the adiabatic states obtained from traditional electronic structure methods.²⁹ Empirical valence-bond methods,³¹ frozen-density functional theory⁹¹ and constrained density functional theory (CDFT)⁹²⁻⁹⁴ have all been used to define diabatic states for ET simulations. While the complexity of these simulations has increased substantially over time, the accurate prediction of ET rates in solution remains unfinished business.

In this article, we characterize CR in the small molecular dyad formanilide-anthraquinone (FAAQ) in dimethylsulfoxide (DMSO) solution using a new QM/MM scheme for ET simulations. An unusually long-lived CT state was postulated for FAAQ in DMSO⁹⁵ on the basis of spectroscopic signatures which were later reassigned to a side reaction with the DMSO solvent.⁹⁶ The CT state is much shorter-lived in other solvents, so we naively expect fast CR in DMSO as well. Our simulations harnesses the power of CDFT to compute accurate diabatic states on the fly and the computational efficiency of polarizable force fields, achieving high-quality molecular dynamics (MD) sampling of the ET free energy surfaces. The simulations provide a detailed picture of the CR mechanism and confirm that CR in FAAQ is fast.

The rest of this chapter is organized as follows. First we introduce the compact donor-acceptor dyad FAAQ and review its experimental characterization in some

detail. After highlighting the features we consider to be essential for a quantitative computational model of condensed phase ET free energies, we lay out the details of the simulations and present free energy profiles and ET parameters for the dyad in solution. Our model predicts ET parameters in line with experimental data and provides the first qualitatively correct prediction of the FAAQ reorganization energy in DMSO. Next we identify and characterize deviations from linear response in the simulations, and we show that torsional flexibility does not strongly modulate the CR rate in FAAQ. We then show that the energy gaps from the full simulations can be mapped quite well onto a simple electrostatic model of solvent polarization. Finally, we summarize strengths and weaknesses of our approach and suggest avenues for further applications and improvements.

2.2 Model system: the FAAQ dyad

Solution phase ET in the FAAQ dyad,^{95–98} shown in Figure 2-1, has been the subject of some controversy. The report of a CT excited state in FAAQ with a lifetime of nearly 1 millisecond⁹⁵ in DMSO contrasted sharply with the empirical rule-of-thumb that CR from singlet CT states in compact dyads generally takes place on picosecond timescales.⁴ Later efforts to reproduce the long-lived CT state of FAAQ and to explore the dependence of its lifetime on solvent⁹⁶ concluded that the long-lived transient absorption signal previously assigned to the intramolecular CT state arises instead from intermolecular ET following photo-oxidation of DMSO. Femtosecond transient absorption studies on FAAQ in acetonitrile yielded more conventional CR rates of approximately 2 ps for the singlet CT state and 130 ns for the triplet CT state.⁹⁶

Happily, the controversy has generated a wealth of experimental data for FAAQ. Electrochemical studies on FAAQ and related derivatives produced an estimate for the CR driving force,⁹⁵ $-\Delta G_{\text{CR}} = 2.24$ eV, later revised⁹⁶ to $-\Delta G_{\text{CR}} = 2.68$ eV. Both estimates are indirect deductions with unclear error bars, so we consider them useful qualitative guides, rather than absolute benchmarks, for comparison to our simulations. A rough estimate for the reorganization energy λ can also be found

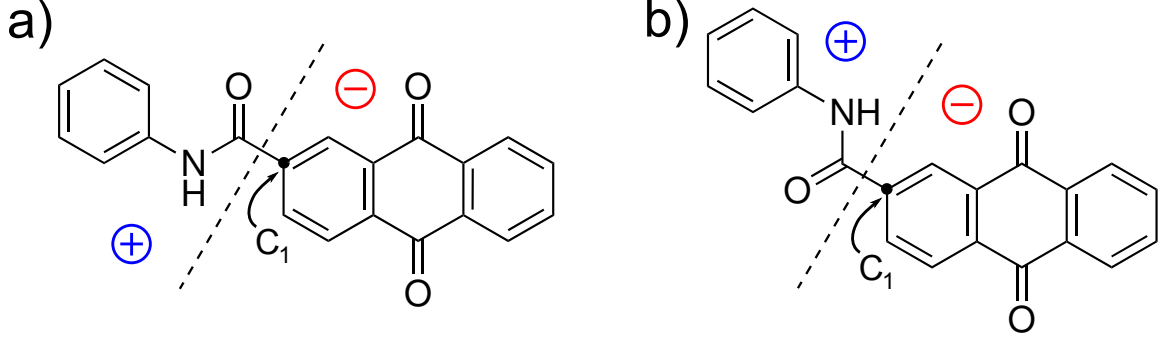


Figure 2-1: Structure of the FAAQ dyad in its (a) *trans* and (b) *cis* conformations. The dashed line indicates the location of the partition employed in this study between the donor (+) and acceptor (-).

by comparing CT state lifetimes of FAAQ and its derivatives.⁹⁹ We first make the assumption that the difference in lifetimes τ of two polyads **A** and **B** is controlled by the difference in their activation free energies rather than the difference in their pre-exponential factors. This assumption is valid to the extent that the donor-acceptor coupling is similar for **A** and **B**; this may not be the case in the long-range ET regime where the coupling decays exponentially with donor-acceptor distance, but it is a more reasonable assumption for the modestly separated polyads considered here. Then the ratio of the CR lifetimes of **A** and **B** satisfies

$$\ln \left[\frac{\tau_{\text{CR}}(\mathbf{B})}{\tau_{\text{CR}}(\mathbf{A})} \right] = -\frac{\Delta G_{\text{CR}}^{\ddagger}(\mathbf{A}) - \Delta G_{\text{CR}}^{\ddagger}(\mathbf{B})}{k_{\text{B}}T} \equiv -\frac{\Delta \Delta G_{\text{CR}}^{\ddagger}}{k_{\text{B}}T} \quad (2.2)$$

where $\Delta G_{\text{CR}}^{\ddagger} = (\lambda + \Delta G_{\text{CR}})^2 / (4\lambda)$ is the activation free energy for CR. Further assuming a negligible difference in the reorganization energy $\lambda(\mathbf{A}) = \lambda(\mathbf{B}) = \lambda$, we find

$$\lambda = \frac{\Delta (\Delta G_{\text{CR}})^2}{4\Delta \Delta G_{\text{CR}}^{\ddagger} - 2\Delta \Delta G_{\text{CR}}} \quad (2.3)$$

We use experimentally determined lifetimes and driving forces for FAAQ and its ferrocenated derivative FcFAAQ ($\tau_{\text{CR}} = 20$ ps, $-\Delta G_{\text{CR}} = 1.16$ eV)⁹⁵ to estimate the reorganization energy. Depending on the chosen estimate for $-\Delta G_{\text{CR}}$ in FAAQ, we obtain estimates of $\lambda = 1.53$ eV or $\lambda = 1.78$ eV. Finally, given the CT state lifetime of FAAQ and the estimates of ΔG_{CR} and λ , we can solve Eq. 2.1 for the electronic

coupling to determine an estimated V_{DA} between 30 and 60 meV. These estimates provide a qualitative gauge for the integrity of our simulations within the framework of Marcus theory.

2.3 Computational model for electron transfer

Any simulation of ET reactions requires a suitable definition of the reactant and product states. Among the many available definitions of diabatic states,^{29,100} the CDFT approach is convenient because it retains the many advantages of Kohn-Sham DFT while also treating both diabatic states on the same footing.³³ This even-handed treatment is important because one of the diabatic states is often an excited state; it is especially crucial for CT excited states, which are often poorly described¹⁰¹ by linear response time-dependent DFT (LR-TDDFT), the *de facto* standard tool for excited states in DFT.¹⁰² CDFT avoids these complications by treating both diabatic states as ground states of modified potentials which constrain the net charge on the donor and acceptor to appropriate fixed values for each state.⁹²

An appropriate solvent model is also crucial for accurate ET simulations. Unlike conventional chemical bond-breaking and bond-forming reactions, intramolecular ET in solution often proceeds from reactant to product state with negligible internal rearrangement; instead, the reaction is driven by solvent fluctuations,¹⁰³ as depicted in Figure 1-3. In the nonadiabatic limit (small V_{DA}), when a fluctuation brings the system to a configuration in which the reactant and product states have the same energy, an electron is transferred with probability proportional to V_{DA}^2 .

In order to adequately characterize the solvent fluctuations, we require a solvent model which can capture both orientational and electronic polarization. These two effects operate on different timescales: the solvent electrons respond essentially instantaneously to changes in the electronic structure of the solute, while orientational and internal nuclear rearrangements of the solvent lag behind.^{57,104} Dielectric continuum models offer a computationally efficient means of describing the dynamic solvent response, but these are typically limited to the linear response regime. Beyond linear

response, atomistic models are the method of choice;^{105,106} these models can capture nonlinear effects due to dependence of the solvent polarization on solute conformation or on the effective charge separation distance in the CT state. Previous simulations on model systems have indicated that these effects can modify nonequilibrium properties like reorganization energies significantly.^{107,108}

Based on the preceding considerations, we adopt a polarizable molecular mechanics (MMpol) model in which selected atoms in the solvent are endowed with isotropic polarizability by means of a charged particle (Drude oscillator) affixed by a fictitious spring.¹⁰⁹ Charges on the polarizable atoms are rescaled to compensate for the charges of the associated Drude oscillators. The solute, described with CDFT, is electronically embedded in the MMpol solvent, and the solute and solvent are allowed to polarize one another self-consistently. This CDFT/MMpol approach is designed to capture important solute/solvent interactions while remaining scalable to systems far beyond the computational capacity of a complete density functional approach. This scalability enables the simulation of asymmetrical ET reactions of flexible donor-acceptor systems in polar solvents, such as the FAAQ/DMSO system studied here.

2.4 Computational Details

All QM/MM calculations were carried out within the framework of the CHARMM/Q-Chem interface.^{110–112} The QM subsystem, a single FAAQ molecule, was electronically embedded in a $34\text{\AA} \times 34\text{\AA} \times 34\text{\AA}$ box of 314 DMSO molecules comprising the MM subsystem. The neutral (N) and charge transfer (CT) states of FAAQ were modeled using CDFT⁹² with the B3LYP functional.³⁹ Energy gaps were computed with the 3-21G and 6-31G* basis sets, while the 3-21G basis was used exclusively for MD simulations in an effort to balance the conflicting goals of accurate energetics and long MD trajectories. The DMSO solvent was modeled using the all-atom force field of Strader and Feller,¹¹³ modified to include electronic polarizability using Drude oscillators¹⁰⁹ bound to each heavy atom (C, O, S) of DMSO. The Drude particle polarizabilities were chosen to reproduce the dielectric constant of DMSO at optical

frequencies ($\epsilon_\infty = 2.19$), and the electrostatic point charges were scaled to 65% of their original values such that the zero-frequency dielectric constant was also reproduced ($\epsilon_0 = 46.7$). The DMSO force field parameters can be found in Appendix 2.C.

For MD simulations, all CH bonds in the DMSO solvent were constrained at their equilibrium length using the SHAKE algorithm¹¹⁴ to help ensure energy conservation with a 2 fs timestep. After an initial energy minimization, the FAAQ/DMSO system was equilibrated with *NPT* dynamics at 300 K and 1 atm. For the sake of efficiency, the system was first equilibrated using an all-MM model with customized force fields⁶⁰ for each of the two diabatic states of FAAQ, followed by further equilibration with the full polarizable QM/MM model. Several *NVT* polarizable QM/MM trajectories were then obtained, each multiple picoseconds in length, with FAAQ in either the neutral or CT electronic state. A simulation temperature of 300 K was enforced by a Nosé-Hoover thermostat. Data were collected only after 2 ps of equilibration for each trajectory. Equilibrium dynamics in the *NVT* ensemble samples the Helmholtz free energy A ; however, the difference in the work term PV between the two diabatic states is expected to be negligible. Furthermore, the zero of free energy is arbitrary; therefore we use the notation G for all simulated free energies to emphasize comparison with experiment.

In order to achieve mutual polarization of the solute and solvent, the QM/MM calculations necessitate a two-layer SCF procedure in which the Kohn-Sham orbitals of the QM subsystem and the Drude particle positions in the MM subsystem are optimized self-consistently. There is an algorithmic choice to be made here regarding when to alternate between optimization of the Kohn-Sham orbitals and optimization of the Drude particle positions: this alternation can be performed after each SCF step, or instead only after convergence of the current optimization. These approaches have been termed “microiterative SCF” and “direct SCF”, respectively.¹¹⁵

We determined empirically that an intermediate approach, in which the Kohn-Sham orbitals and Drude particle positions were separately optimized to within gradually narrower tolerances, achieves faster convergence than direct SCF, whereas a fully microiterative approach would require substantial modification of the existing

CHARMM/Q-Chem interface. Therefore, the intermediate approach was employed in all polarizable QM/MM calculations reported here.

Diabatic couplings were evaluated within the framework of CDFT,¹¹⁶ both in the gas phase and in DMSO solvent. The solution phase couplings take into account the different solvation environments of the neutral and CT states by self-consistently polarizing each state’s density with its own set of Drude particles prior to the coupling calculation. Solvent effects on CDFT couplings at the ET transition state were recently studied in the mixed-valence Q-TTF-Q anion in aqueous solution;¹¹⁷ here we obtain complementary information about solvent effects on couplings for equilibrium configurations of both diabatic states. This data can be used to assess the validity of the Condon approximation in the FAAQ/DMSO system.¹¹⁸

2.5 Results

2.5.1 Construction of free energy profiles

As a first step towards determination of the ET free energy profiles, we obtained 30 ps of equilibrium polarizable QM/MM dynamics in each diabatic state (neutral or CT). A representative trajectory for each diabatic state is presented in parts (a) and (b) of Figure 2-2. Each plot also shows the energy of the other diabatic state at the various configurations visited along the trajectory.

We sample the vertical energy gap $\Delta E_\alpha = E_\alpha^{\text{CT}} - E_\alpha^{\text{N}}$ of configurations α at regular intervals of 40 fs along these trajectories to build up a statistical picture of the distribution of energy gaps, as illustrated in the histograms in Figure 2-2, parts (c) and (d). The probability distribution of the energy gap in diabatic state X , $P_X(\Delta E)$, is related to the free energy G_X by

$$G_X(\Delta E) = -k_{\text{B}}T \ln P_X(\Delta E) \quad (2.4)$$

where $P_X(\Delta E)$ is to be inferred from the energy gap histograms.

There are several reasonable ways to parametrize $P_X(\Delta E)$ from the sampled en-

ergy gaps. A Gaussian fit to the energy gap distribution will result in a parabolic free energy profile, in keeping with Marcus theory. However, there is no formal restriction on the functional form of the fit, provided it reasonably captures the statistical distribution of energy gaps. First, we explore the Marcus picture, which facilitates comparison to the experimental ET parameters derived under the assumption of linear response. We then consider a more flexible model for the free energy and show that the predicted deviations from the Marcus model favor fast recombination of the CT state.

The Marcus picture

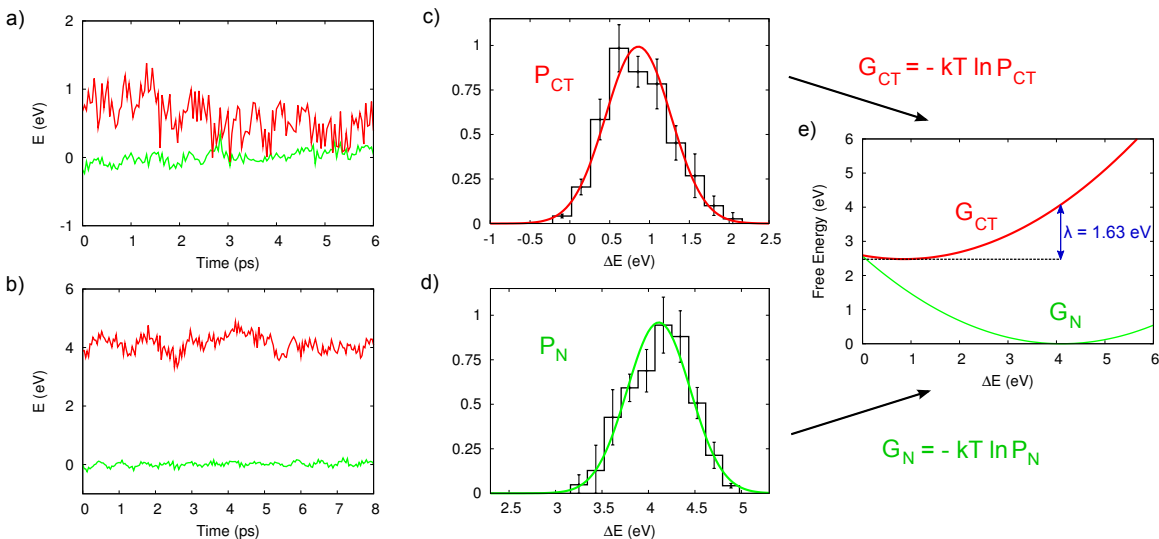


Figure 2-2: Construction of ET free energy curves for FAAQ. All energies are in eV. Several MD trajectories are computed with FAAQ either in the CT state (a) or the neutral state (b). Along each trajectory, the energy gap ΔE is sampled in order to generate probability distributions for the energy gap $P(\Delta E)$ for the (c) CT and (d) neutral trajectories. The histograms show the relative frequency of each energy gap window, while the curves are a Gaussian fit. (e) Free energy curves for the neutral and CT states are computed as the logarithm of the probability distributions.

Gaussian fits to the neutral and CT energy gap distributions are shown in Figure 2-2(c) and 2-2(d). The error bars in the histograms indicate the standard error in the bar heights obtained separately for each MD trajectory. Applying Eq. 2.4 to the Gaussian fits, we obtain the Marcus free energy curves in Figure 2-2(e). The

nested parabolas confirm that the simulations place CR in the Marcus inverted region, $-\Delta G_{\text{CR}} > \lambda$.

Within the linear response approximation, the driving force and reorganization energy can be obtained directly from the mean energy gaps of the neutral and CT configurations,⁸⁵

$$\Delta G_{\text{CR}} = \frac{1}{2} (\langle \Delta E \rangle_{\text{N}} + \langle \Delta E \rangle_{\text{CT}}) \quad (2.5)$$

$$\lambda = \frac{1}{2} (\langle \Delta E \rangle_{\text{N}} - \langle \Delta E \rangle_{\text{CT}}) \quad (2.6)$$

The mean energy gaps and corresponding ET parameters are presented in Table 2.1. Our ET parameters $\Delta G_{\text{CR}} = 2.38$ eV and $\lambda = 1.64$ eV fall between the two estimates inferred from experimental data, $-\Delta G_{\text{CR}} \approx 2.24 - 2.68$ eV and $\lambda \approx 1.53 - 1.78$ eV. From the standard error of the mean energy gap for each state, we estimate uncertainties of roughly 0.2 eV for both $-\Delta G_{\text{CR}}$ and λ due to the limited MD sampling. Nevertheless, the calculated $-\Delta G_{\text{CR}}$ and λ demonstrate that the experimental ET properties, interpreted within the Marcus picture, are borne out by the microscopic details of the CDFT/MMpol simulations. The agreement of our calculated λ with experiment is especially encouraging because it indicates that our simulations achieve a realistic picture of both equilibrium and nonequilibrium solvation regimes. Previous work has demonstrated that 0.2 eV of the reorganization energy arises directly from solute reorganization,⁹⁹ while an additional 0.6 eV can be attributed to bulk electrostatic effects.²⁹ The larger reorganization energy found here suggests that solvent configurations at equilibrium with either diabatic state are further stabilized, relative to nonequilibrium configurations, by conformation-specific solute-solvent interactions such as hydrogen bonding that are not captured by conventional continuum solvent approaches.¹¹⁹

Beyond linear response

Having validated the Marcus picture obtained through the CDFT/MMpol approach, we can investigate the degree to which the simulations predict deviations from the

Basis set	$\langle \Delta E \rangle_N$	$\langle \Delta E \rangle_{CT}$	$-\Delta G_{CR}$	λ_{CR}	ΔG_{CR}^\ddagger
3-21G	4.13	0.86	2.49	1.63	0.11
6-31G*	4.03	0.74	2.38	1.64	0.08

Table 2.1: ET parameters obtained from MD simulations, assuming Gaussian statistics for the energy gap. All energies are in eV.

linear response regime in the FAAQ/DMSO ET reaction. The linear response assumption is built into most implicit solvent models,⁵⁶ so CDFT/MMpol is specially poised to probe this question.

We begin by observing that our simulations do not provide a statistically even-handed description of the entire reaction coordinate: the sampling is most complete in the vicinity of the neutral and CT free energy minima. An umbrella sampling approach could overcome this limitation¹²⁰ and should provide an interesting avenue for further investigation. Here, we focus on the statistics of the energy gap near the free energy minima.

In the last section, ensemble-averaged energy gaps were used to compute ET parameters via Eqs. 2.5 and 2.6. However, in addition to the average energy gaps, our simulations provide an estimate of typical *fluctuations* σ_X of the energy gap. Linear response dictates that both diabatic states experience the same energy gap fluctuations, but the simulations do not fully bear out this assumption. We find markedly larger energy gap fluctuations for the CT state, $\sigma_{CT} = 0.43$ eV, compared to the neutral state fluctuations $\sigma_N = 0.35$ eV. We performed two statistical tests of the hypothesis that the collection of energy gaps for the neutral and CT diabatic states came from distributions with the same variance. The traditional F-test and Levene’s test¹²¹ both reject the null hypothesis of equal variances ($p < 0.01$).

What are the mechanistic and kinetic consequences of the nonlinear solvent response? To address this key question, we used the four statistics — energy gap averages and fluctuations for each state — to obtain a unique quartic parametrization of the neutral free energy curve (up to an arbitrary choice of the zero of free energy),

$$G_N(q) = G_0 + G_1 q + \frac{1}{2}G_2 q^2 + \frac{1}{6}G_3 q^3 + \frac{1}{24}G_4 q^4 \quad (2.7)$$

where $q = \Delta E - \langle \Delta E \rangle_N$. From Eq. 2.7, a quartic expression for G_{CT} is uniquely obtained via the linear free energy relation,¹²² $G_{CT}(\Delta E) = G_N(\Delta E) + \Delta E$. The same overall fit is obtained regardless of which state is parameterized first. Expressions for the coefficients G_i in terms of $\langle \Delta E \rangle_N$, $\langle \Delta E \rangle_{CT}$, σ_N and σ_{CT} can be found in Appendix 2.A.

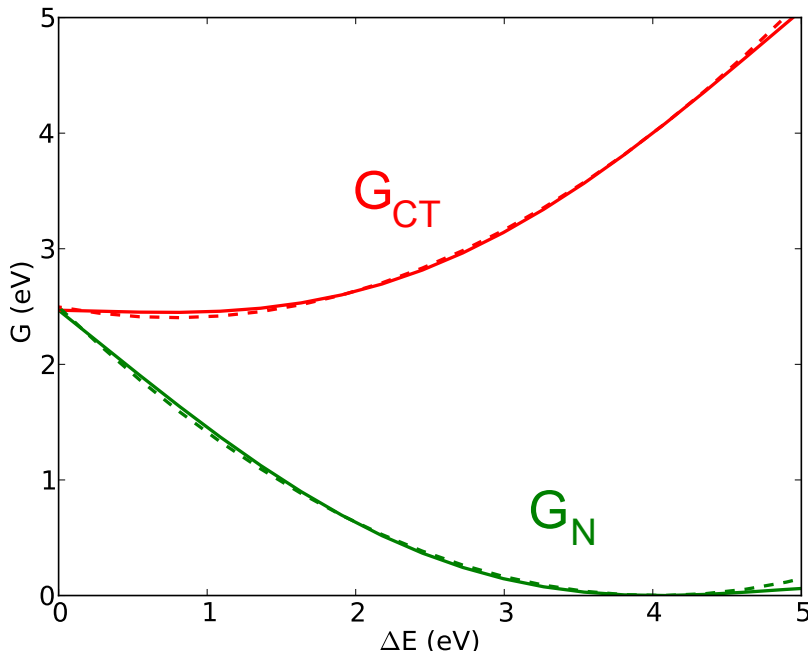


Figure 2-3: Quartic parameterization of the neutral and CT free energy profiles (solid lines). Marcus free energy profiles (dashed lines) are shown for comparison.

The quartic free energy model is displayed in Figure 2-3. Qualitatively, the quartic fit is strikingly similar to the Marcus picture. Nevertheless, the nonlinear solvent response raises the driving force by 0.07 eV to $-\Delta G_{CR} = 2.45$ eV and lowers the reorganization energy by 0.06 eV to $\lambda_{CR} = 1.58$ eV. As shown in Table 2.2, the activation barrier to CR is significantly reduced in the quartic model to $\Delta G_{CR}^\ddagger = 0.02$ eV. From the ratio of ΔG_{CR}^\ddagger for the Marcus and quartic models, the quartic model predicts an order-of-magnitude enhancement of k_{CR} relative to the Marcus picture. This finding emphasizes that slight nonlinearities in the solvent response — which have been characterized experimentally in other examples of condensed phase

ET^{123,124} — can fundamentally alter the kinetics of CR and CS.

Approximation	σ_N	σ_{CT}	$-\Delta G_{CR}$	λ_{CR}	ΔG_{CR}^\ddagger
Linear response	0.29	0.29	2.38	1.64	0.08
Nonlinear correction	0.35	0.43	2.45	1.58	0.02

Table 2.2: CR parameters obtained under the linear response approximation and under the quartic fits. All energies are in eV.

2.5.2 Characterization of the electronic coupling

The Marcus expression, Eq. 2.1, has a standard interpretation from the perspective of classical transition-state theory:¹²⁵ the exponential term, parameterized by the reorganization energy and driving force for ET, embodies the likelihood of visiting the transition state region where an ET event becomes maximally probable; then the pre-exponential term, controlled by the electronic coupling, characterizes the inherent probability of ET at the isoenergetic point. In the last section, we used the diagonal elements of the diabatic two-state Hamiltonian to compute energy gap fluctuations and parameterize the exponential term in the rate expression; here, we use CDFT to characterize V_{DA} as well as its fluctuations in the neutral and CT ensembles.

The magnitude of the CDFT couplings, presented in Table 2.3, is in excess of most experimentally determined couplings for compact donor-acceptor dyads.⁴ The couplings also exceed our previously described estimate $V_{DA} \approx 0.03 - 0.06$ eV by an order of magnitude. We anticipate that much of the discrepancy between the computed and experimentally inferred couplings can be attributed to the short-range character of intramolecular ET in FAAQ. In most systems for which the CDFT coupling prescription has been tested and validated, the relevant ET process is either intermolecular³ or bridge-mediated.^{126,127} In FAAQ, the donor-acceptor “bridge” is effectively a single C-C bond; this feature makes the CDFT coupling especially sensitive to the size and shape of the constraints. Nevertheless, these errors should be largely systematic across the sampled configurations because the same partitioning strategy was used for all configurations. Therefore we can still gain mechanistic insights by studying trends in the CDFT couplings.

Configurations	$\langle V_{\text{DA}} \rangle$	σ_V
Gas phase		
Neutral	0.90	0.15
CT	0.73	0.18
DMSO		
Neutral	0.61	0.12
CT	0.25	0.06

Table 2.3: Mean electronic couplings and deviations for neutral and CT configurations of FAAQ in the gas phase and in DMSO solution. All energies are in eV.

The distribution of electronic couplings presented in Table 2.3 reveals several interesting trends. First, the neutral configurations exhibit a substantially larger coupling than the CT configurations, indicative of a modest non-Condon effect.^{118,128} In particular, the observation of increased electronic coupling for configurations exhibiting a larger energy gap indicates that the mean electronic coupling at the transition state $\Delta E = 0$, where its magnitude matters most, may be smaller than the values predicted here.

Another striking feature of the couplings is the substantial difference between the gas phase and solution phase values, both for mean couplings and for deviations. Other recent simulations of solvent effects on electronic couplings^{117,126,129,130} have been at odds regarding the magnitude of these effects; here we find a significant reduction of the coupling matrix element upon incorporation of solvent. Fluctuations in the coupling are also damped by the solvent, as was also observed in a computational study where the time-dependence of V_{DA} was monitored explicitly.¹³¹

Finally, we note that the ET parameters obtained from our simulations correspond to CT state lifetimes on the fs to ps timescale, in qualitative agreement with the experimental refutation⁹⁶ of the previously claimed long-lived CT state in FAAQ.⁹⁵ Future fine-tuning of the CDFT coupling prescription should lead to improved estimates of the coupling, thereby enabling quantitative ET rate calculations within the CDFT/MMpol model.

2.6 Discussion

The use of the diabatic energy gap as a reaction coordinate for solution phase ET has a long history rooted in Warshel’s semiclassical trajectory approach.^{62,132} This particular choice of reaction coordinate is convenient because it collapses the full complexity of the solvent dynamics onto a single degree of freedom, while still providing a quadratic free energy profile in the limit of linear response.¹³³ The energy gap is also easier to control for the purposes of umbrella sampling than other more physically appealing choices such as a solvent polarization reaction coordinate, motivated by the original work of Marcus.¹⁶

But the physical content of ΔE as a reaction coordinate is limited. How does the reaction proceed? First we consider the extent to which a key internal degree of freedom in FAAQ, the dihedral angle between the donor and acceptor, influences the ET free energy profiles. Could excited state isomerization have a measurable effect on k_{CR} ? We then turn our attention to the role of the solvent and to the notion of a collective solvent coordinate for ET in particular. Towards this end, we map the diabatic energy gaps from our simulations onto a classical polarization coordinate. The correlation between the energy gap and the polarization coordinate provides another measure of how successfully the Marcus model captures the atomistic details of our simulations.

2.6.1 Role of solute flexibility in ET kinetics

The FAAQ molecule is highly conjugated, with the amide bridge providing the only practical means of breaking planarity. The torsional barrier between the FA and AQ groups is expected to be large compared to $k_{\text{B}}T$, prohibiting any substantial population of the *cis* configurations illustrated in Figure 2-1b. Nevertheless, the possibility of photoinduced isomerization prompted us to examine whether the *cis* and *trans* configurations have different ET kinetics, and if so, to quantify the difference.

We obtained 750 snapshots of *cis* configurations for each diabatic state, following the same procedure outlined for the *trans* configurations. To obtain a rough estimate

of the free energy of activation for isomerization, we take the linear response approach and fit the statistics of the dihedral angle ϕ to a pair of parabolas,

$$G_{cis}(\phi) = \frac{1}{2\sigma_{cis}^2} (\phi - \langle\phi\rangle_{cis})^2 \quad (2.8)$$

$$G_{trans}(\phi) = \frac{1}{2\sigma_{trans}^2} (\phi - \langle\phi\rangle_{trans})^2 + \Delta G_{cis-trans} \quad (2.9)$$

The free energy difference $\Delta G_{cis-trans} = G_{cis}(\langle\phi\rangle_{cis}) - G_{trans}(\langle\phi\rangle_{trans})$ was approximated from the free energy of optimized *cis* and *trans* FAAQ structures obtained at the B3LYP/6-31G* level with DMSO modeled by the SM8 model,¹³⁴ yielding $\Delta G_{cis-trans} = 3.8$ meV. Then we estimate the free energy barrier to isomerization by computing the free energy at the curve-crossing.

Activation free energies for isomerization and for CR within the linear response approximation are shown in Figure 2-4, superimposed over the distribution of all 3000 snapshots in the $(\Delta E, \phi)$ plane. The isomerization barrier heights range from 0.52 – 0.71 eV (12 – 16 kcal mol⁻¹); given the short lifetime of the CT state, these barriers preclude any substantial degree of excited state isomerization. We therefore expect that any influence of the *cis* isomer on the overall CR rate in experiments can be safely neglected. Furthermore, the barrier heights for CR within the Marcus picture are quite similar for the two isomers: 0.08 (0.09) eV for CR in the *cis* (*trans*) conformation. Thus, even if isomerization were more facile, it would have only a minor influence on k_{CR} .

In summary, the linear response assumption leads to a model for the ET mechanism in which CR is largely decoupled from *cis-trans* isomerization. The rigidity of the donor and acceptor units precludes any further dependence of the CR rate on the details of solute conformation. These insights raise the possibility of constructing an ET reaction coordinate that captures the key solute-solvent interactions while averaging out all of the internal degrees of freedom in FAAQ. We explore this possibility next.

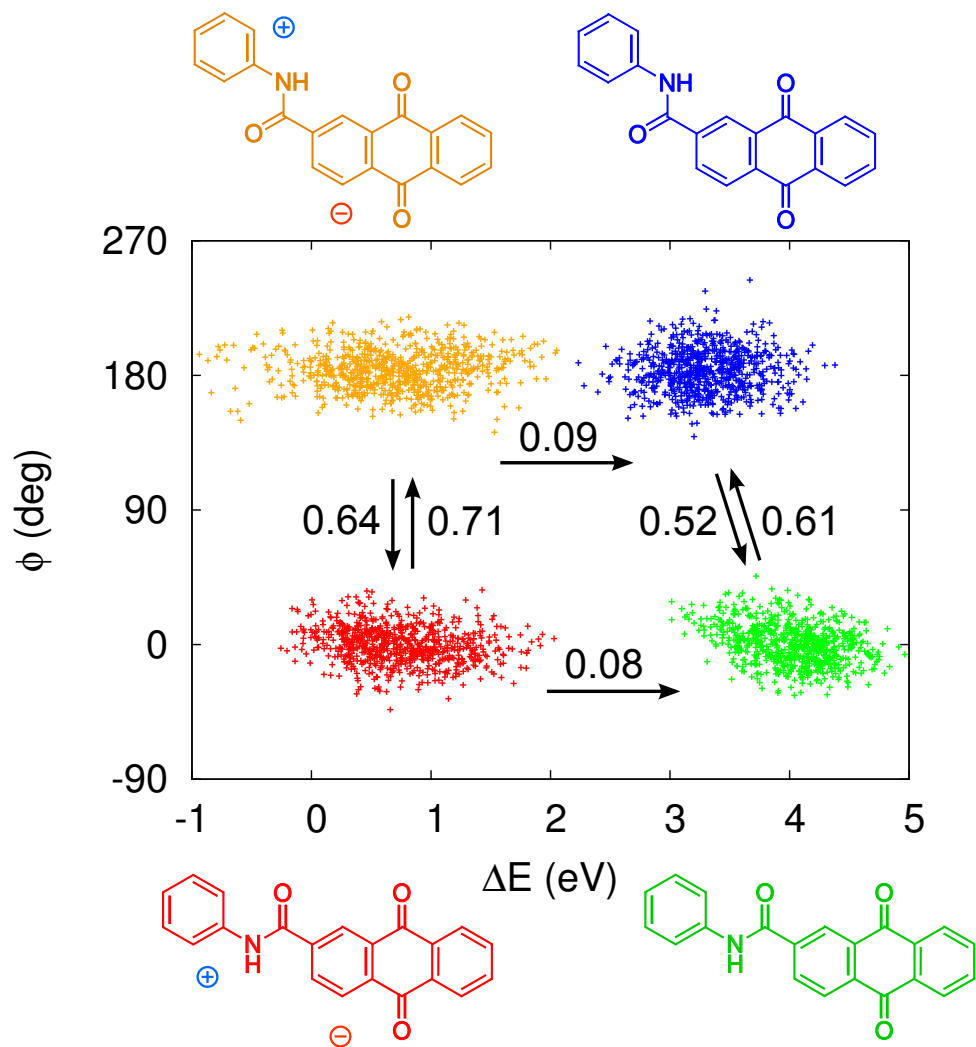


Figure 2-4: Scatterplot of the energy gap ΔE and dihedral angle ϕ for snapshots from all MD trajectories. Colors represent the type of snapshot: green = neutral, *trans*; red = CT, *trans*; blue = neutral, *cis*; orange = CT, *cis*. The labeled arrows indicate activation energies ΔG^\ddagger (in eV) for transitions between the four wells (\uparrow, \downarrow : *cis-trans* isomerization; \rightarrow : charge recombination).

2.6.2 Reaction coordinate based on a simplified electrostatic model

How well can a classical solvent polarization coordinate capture the atomistic details of the ET simulations? To provide a quantitative answer, we construct a plausible polarization coordinate and study its correlation with the energy gap reaction coordinate.

We express the collective solvent polarization in terms of an *electrostatic* energy gap possessing the general form $\Delta E_{\text{el}} = \Delta(\mu_X \cdot \mathbf{E}_X)$, where μ_X is the electric dipole moment of FAAQ in diabatic state X , and \mathbf{E}_X is the electric field generated by the particular solvent configuration around the solute dipole. The construction of ΔE_{el} is outlined below; further details are provided in Appendix 2.B.

First we replace the FAAQ dyad with a point electric dipole μ_X whose magnitude and direction are fixed to reproduce the ensemble-averaged dipole moment of FAAQ in diabatic state X , as obtained from our simulations. The DMSO solvent is treated as a collection of point charges, taken directly from the MM model. Then the electrostatic energy gap for a given snapshot α is the difference between the interaction energies of the solute dipole and solvent electric field in the two diabatic states,

$$\Delta E_{\text{el}} = \langle \mu \rangle_{\text{CT}} \cdot \mathbf{E}_{\text{CT}} - \langle \mu \rangle_{\text{N}} \cdot \mathbf{E}_{\text{N}} \quad (2.10)$$

Given this prescription, we evaluate ΔE_{el} for snapshots α from the CDFT/MMpol simulations and consider the correlation r between ΔE_{el} and the diabatic energy gap ΔE ,

$$r \equiv \text{Corr}(\Delta E, \Delta E_{\text{el}}) = \frac{1}{N-1} \sum_{\alpha=1}^N \left(\frac{\Delta E_{\alpha} - \langle \Delta E \rangle}{\sigma_{\Delta E}} \right) \left(\frac{\Delta E_{\text{el},\alpha} - \langle \Delta E_{\text{el}} \rangle}{\sigma_{\Delta E_{\text{el}}}} \right) \quad (2.11)$$

The location of the solute dipole in the definition of ΔE_{el} remains to be determined; two possibilities are considered here. First, to set an upper bound on the correlation achievable with a single-dipole representation of FAAQ, we placed a dipole at each nucleus i of the molecule and considered the linear combination $\mu = \sum_i c_i \mu_i$. The

correlation coefficient r in this model can then be optimized with respect to the coefficients \mathbf{c} in a least-squares sense.¹³⁵ This model has 38 degrees of freedom (one per nucleus in the FAAQ model) and achieves a correlation $r = 0.97$ upon optimization of \mathbf{c} as illustrated in Figure 2-5a.

The correlation is reduced slightly when we restrict the model of the solute to a single dipole. Varying the location of the single dipole over all FAAQ nuclei, we obtained an optimal correlation $r = 0.93$ (Figure 2-5b) by placing it on the carbon atom labeled C_1 in Figure 2-1. Thus, we can account for the bulk of the energy gap fluctuations in the FAAQ/DMSO system with a simple electrostatic model of solvent polarization.

The correlation scatterplots in Figure 2-5 show some interesting trends. First, the polarization models provide a better fit for the neutral configurations than for the CT configurations, likely because of the more drastic difference in polarization between the two diabatic states at neutral configurations. Also, the *cis* and *trans* isomers are segregated in the single-dipole scatterplot in Figure 2-5b. The two isomers have different effective charge separation distances in the CT state, so it is sensible that the best-fit mappings between ΔE and ΔE_{el} for the *cis* and *trans* configurations could have different constant shifts. The inclusion of additional solute degrees of freedom can mask the distinction between the isomers, as evidenced by the lack of isomer segregation in Figure 2-5a.

Some potentially important features that our simulations cannot intrinsically capture, such as intermolecular charge transfer between the solute and the first solvation shell¹³⁶ or within the solvent,¹³⁷ are naturally absent from this analysis. Still, the scatterplots show that solvent polarization coordinates can be constructed which faithfully mirror the energy gaps obtained from the full CDFT/MMpol simulations.

2.7 Conclusion

We have explored the mechanistic and kinetic details of ET in the compact donor-acceptor dyad FAAQ solvated in DMSO. Our simulations corroborate experimental

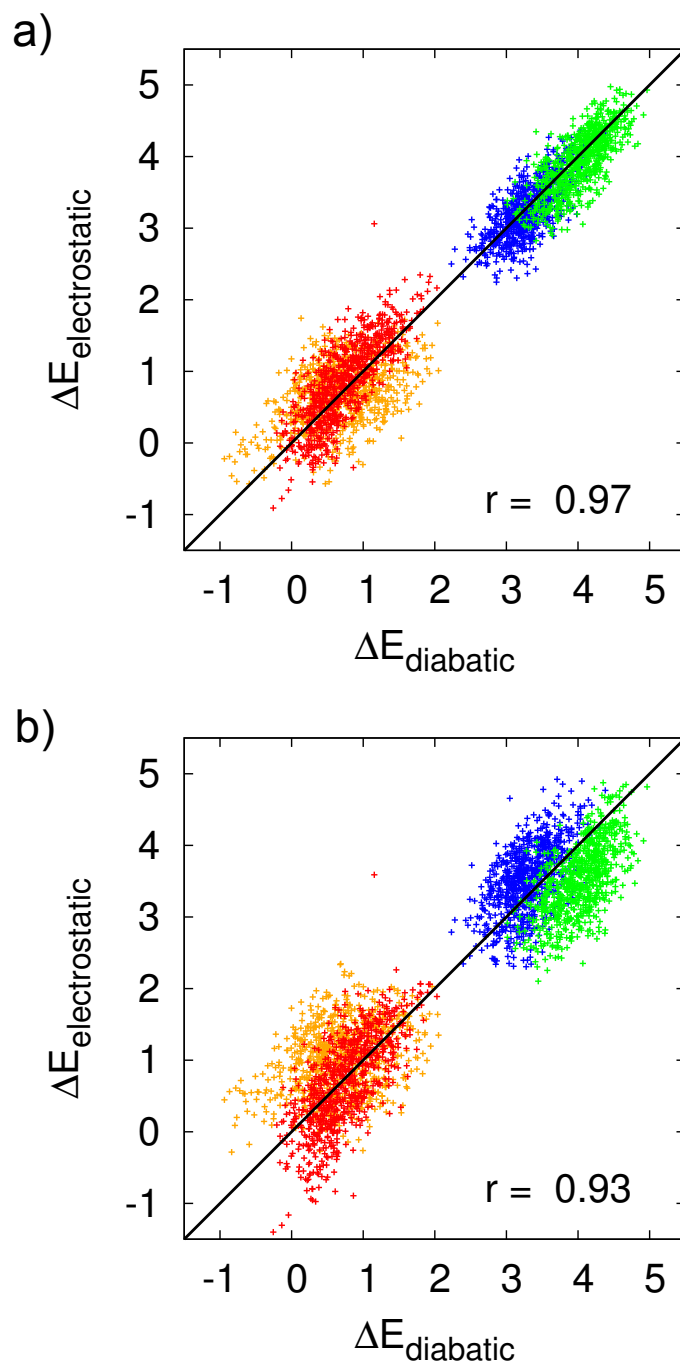


Figure 2-5: Correlation between the diabatic energy gap and electrostatic energy gap, where the latter describes the interaction between the solvent electric field and (a) a linear combination of dipoles at each FAAQ nucleus or (b) a single dipole placed at C_1 (see Figure 2-1). Colors represent the type of snapshot: green = neutral, *trans*; red = CT, *trans*; blue = neutral, *cis*; orange = CT, *cis*.

evidence that CR takes place in the Marcus inverted region. Although inverted region effects have been postulated to drastically extend the lifetimes of singlet CT excited states in compact dyads,⁹⁵ we find a small activation barrier that promotes CR on the ps timescale, in agreement with transient absorption studies.⁹⁶ A modest nonlinear solvent response further enhances the CR rate.

From the microscopic details of the simulations, we identify several mechanistic features bearing consequences for the ET kinetics. We find evidence of non-Condon effects: the electronic coupling is weaker in the equilibrium solvation environment of the CT state than in that of the ground state. *Cis-trans* isomerization does not appear to qualitatively change the ET landscape in FAAQ. Finally, we find good correlation between the diabatic energy gap and a simplified electrostatic reaction coordinate. Despite signatures of nonlinear response detected in our simulations, the Marcus picture of ET driven by collective solvent polarization captures the fundamental mechanism of CR in FAAQ.

To carry out these simulations, we have introduced a computational model dubbed CDFT/MMpol for condensed phase ET simulations. Designed for accuracy and scalability, the CDFT/MMpol approach couples diabatic states from constrained DFT with a polarizable force field to account for mutual polarization of the donor-acceptor system and surrounding solvent. A more accurate modeling of the solute-solvent interaction — for example, at a QM/QM level — would serve to shore up our evidence of a nonlinear response; but obtaining sufficient statistics to demonstrate the effect at a higher level of theory would make such an effort intractably demanding from a computational standpoint.

Looking ahead, the approach outlined here is readily adaptable to the presence of other low-lying excited states, for example, the localized S_1 state on AQ from which CS originates in FAAQ. These states can be treated with DFT methods better suited to localized excitations, such as LR-TDDFT^{45,102} or Δ SCF.^{138,139} Together with a prescription for couplings between CT and local excited states,¹⁴⁰ this approach would provide a fully self-consistent model of CR *and* CS in the condensed phase. Such a model would represent an important step towards predicting how the ratio of CS to

CR might be tuned through chemical modifications.

To extend the scope of the CDFT/MMpol approach to larger polyads such as donor-bridge-fullerene systems^{141,142} or to models of natural photosynthesis,^{143,144} it would be appealing to substitute the CDFT description of the solute with an accurate MMpol model for configurational sampling.³ Improvements in force-matching techniques are cause for optimism that MMpol force fields can rise to this challenge.⁶⁰

Finally, we anticipate that CDFT/MMpol will provide a useful starting point for real-time quantum or semiclassical dynamics simulations of condensed phase ET.^{145,146} These methods require diabatic energies and couplings along real-time trajectories; our approach can supply the necessary parameters on-the-fly for ET in complex systems. We look forward to applying CDFT/MMpol simulations to existing and nascent formulations of real-time ET dynamics such as the two-hop Langevin equation recently proposed by our group.¹⁴⁷

2.8 Acknowledgment

Lee-Ping Wang is gratefully acknowledged for preparing the force fields used in this study and for spearheading implementation of the two-layer SCF scheme. He is a co-author of Ref. 148.

2.A Appendix: Parameterization of the quartic free energy model

Here we present our strategy for parameterizing a quartic free energy model from CDFT/MMpol simulations. We use Gaussian statistics from the neutral and CT energy gap probability distributions to parameterize either of the following two curves:

$$\begin{aligned}
 G_{\text{N}}(q_{\text{N}}) &= G_0 + G_1 q_{\text{N}} + \frac{1}{2} G_2 q_{\text{N}}^2 + \frac{1}{6} G_3 q_{\text{N}}^3 + \frac{1}{24} G_4 q_{\text{N}}^4 \\
 \tilde{G}_{\text{CT}}(q_{\text{CT}}) &= \tilde{G}_0 + \tilde{G}_1 q_{\text{CT}} + \frac{1}{2} \tilde{G}_2 q_{\text{CT}}^2 + \frac{1}{6} \tilde{G}_3 q_{\text{CT}}^3 + \frac{1}{24} \tilde{G}_4 q_{\text{CT}}^4
 \end{aligned}$$

where $q_X = \Delta E - \langle \Delta E \rangle_X$. The coefficients $\{G_i\}$ can be expressed in terms of the average energy gaps $\langle \Delta E \rangle_N$, $\langle \Delta E \rangle_{CT}$ and their variances σ_N^2 , σ_{CT}^2 :

$$\begin{aligned}
G_0 &= 0 \\
G_1 &= 0 \\
G_2 &= \frac{k_B T}{\sigma_N^2} \\
G_3 &= -2 \left[\frac{k_B T}{\langle \Delta E \rangle_{CT} - \langle \Delta E \rangle_N} \left(\frac{2}{\sigma_N^2} + \frac{1}{\sigma_{CT}^2} \right) + \frac{3}{(\langle \Delta E \rangle_{CT} - \langle \Delta E \rangle_N)^2} \right] \\
G_4 &= 6 \left[\frac{k_B T}{(\langle \Delta E \rangle_{CT} - \langle \Delta E \rangle_N)^2} \left(\frac{1}{\sigma_N^2} + \frac{1}{\sigma_{CT}^2} \right) + \frac{2}{(\langle \Delta E \rangle_{CT} - \langle \Delta E \rangle_N)^3} \right]
\end{aligned}$$

The zero of energy, set by G_0 , is of course arbitrary. The equivalent expressions for the $\{\tilde{G}_i\}$ are:

$$\begin{aligned}
\tilde{G}_0 &= 0 \\
\tilde{G}_1 &= 0 \\
\tilde{G}_2 &= \frac{k_B T}{\sigma_{CT}^2} \\
\tilde{G}_3 &= -2 \left[\frac{k_B T}{\langle \Delta E \rangle_N - \langle \Delta E \rangle_{CT}} \left(\frac{2}{\sigma_{CT}^2} + \frac{1}{\sigma_N^2} \right) - \frac{3}{(\langle \Delta E \rangle_N - \langle \Delta E \rangle_{CT})^2} \right] \\
\tilde{G}_4 &= 6 \left[\frac{k_B T}{(\langle \Delta E \rangle_N - \langle \Delta E \rangle_{CT})^2} \left(\frac{1}{\sigma_N^2} + \frac{1}{\sigma_{CT}^2} \right) - \frac{2}{(\langle \Delta E \rangle_N - \langle \Delta E \rangle_{CT})^3} \right]
\end{aligned}$$

From either curve, the linear free energy relation $G_{CT}(\Delta E) = G_N(\Delta E) + \Delta E$ allows us to deduce the other curve. To make a direct comparison between the two parameterizations, one simply chooses G_0 and \tilde{G}_0 such that their difference reproduces ΔG . The quartic parameterization is unique for a given set of energy gap statistics $\{\langle \Delta E \rangle_N, \langle \Delta E \rangle_{CT}, \sigma_N^2, \sigma_{CT}^2\}$.

Note that the parameterization is only valid near the free energy minima of the neutral and CT states. For energy gaps far from these minima, the integrity of the model quickly disintegrates. This is evident from the fact that the quartic fit is actually concave down. However, the model succeeds at incorporating differences in

energy gap fluctuations between the neutral and CT states; the parabolic fit cannot make this distinction. Given that the equilibrium CT configurations occasionally sampled $\Delta E = 0$ in our simulations, we anticipate that the quartic fit is valid out to the region of the ET transition state.

2.B Appendix: Electrostatic energy gap models

As outlined in Section 2.6, we extract an electrostatic solvent polarization coordinate from the full CDFT/MMpol simulations according to the general scheme

$$\Delta E_{\text{el}} = \langle \mu \rangle_{\text{CT}} \cdot \mathbf{E}_{\text{CT}} - \langle \mu \rangle_{\text{N}} \cdot \mathbf{E}_{\text{N}}$$

where the brackets indicate that the solute dipole moment $\langle \mu \rangle_{\text{X}}$ is averaged over the equilibrium ensemble for state X, and \mathbf{E}_{X} is the solvent electric field. The substitution of the FAAQ dipole moment in lieu of the full molecule effectively removes all solute internal degrees of freedom from the model. Translational and rotational solute degrees of freedom are conserved for each snapshot by performing the ensemble average in a molecular reference frame affixed to FAAQ and defined in Figure 2-6. Then the averaged dipole moment was translated back into the local frame of each snapshot for the calculation of ΔE_{el} .

Electronic polarization of the solvent is explicitly accounted for by employing diabatic-dependent electric fields for each snapshot. This critical contribution to the solvent polarization is absent from conventional QM/MM simulations but is captured by the Drude oscillator model used in our approach.

For the scatterplot shown in Figure 2-5a, the ensemble-averaged dipole was placed at each nucleus and weighted by linear combination coefficients \mathbf{c} such that the resulting electrostatic energy gap correlated maximally with the diabatic energy gap. The \mathbf{c} were determined through a correlation optimization script written for this purpose in Python. The optimal values of the \mathbf{c} obtained from this script are shown below, along with the individual coordinate correlations.

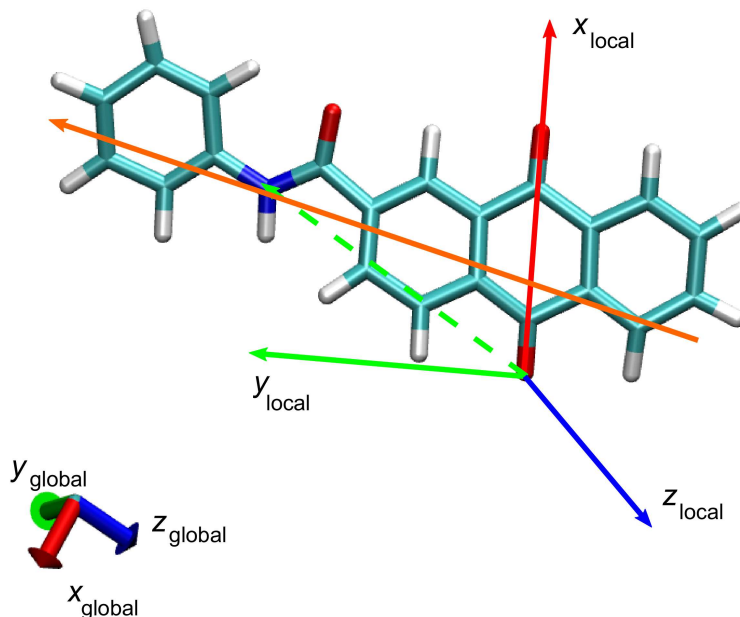


Figure 2-6: Illustration of the reference frames used for ensemble-averaging of the FAAQ dipole.

```

degrees of freedom in analysis = 38
number of data points acquired = 3000
(sorted) coordinate correlations:
[-0.92843488 -0.88943688 -0.82386172 -0.80294217 -0.7728407 -0.7130249
-0.71292998 -0.68850464 -0.66729941 -0.66435441 -0.6612397 -0.63460937
-0.60652073 -0.53854154 -0.52889835 -0.5244267 -0.51426307 -0.5044501
-0.49759608 -0.49093923 -0.480037 -0.437951 -0.4089387 -0.40662883
-0.39450954 -0.357034 -0.34087958 -0.29842242 -0.25810203 -0.22918662
-0.21254592 -0.20360583 -0.19695817 -0.13882302 -0.08884027 -0.07571224
-0.06779173 -0.01415549]
Optimal correlation = 0.969939085543
(unsorted) linear combination coefficients:
[ -4.07682592  14.04589348 -36.37414595  17.89999013 -12.70350082
-16.79748228  4.98587104 -1.58533974 -9.56749262  5.98152003
-6.77872348  5.29388316 -3.59411754 -3.91289924 -0.39765118
-0.51060502  1.87039648 -0.30202298 -1.01448651  1.32069888
 2.13285778 -5.79993433  1.05423627 -12.72663693 -3.56284780
-2.1195242  0.52961111 -4.38033486 -15.87822201  3.82525926
 2.24010551 -1.80261191  3.81939504  6.08093864 -0.15763209
-0.486439 -0.74085006 -0.84316418]

```

Note that the coordinate with 93% correlation, whose scatterplot is shown in Figure 2-5b, is the first entry in the list of “coordinate correlations”. The linear combination coefficients are not presented in the same order as the coordinate correlations,

the latter of which were sorted by magnitude. Without indicating precisely which correlations correspond to which nuclei, we note the observed trend that nuclei with larger coordinate correlations tended to be closer to the donor-acceptor boundary.

2.C Appendix: Force field parameters for polarizable DMSO

Nonbonded parameters				
atom	charge (a.u.)	polarizability (\AA^3)	ϵ (kcal/mol)	$R_{\min}/2$ (\AA)
H	0.0585	0.000	-0.024	1.34
C	-0.0962	1.963	-0.078	2.04
S	0.2028	3.234	-0.350	2.00
O	-0.3614	0.894	-0.120	1.70

Bond parameters		
bond	k_b (kcal/mol \AA^2)	b_0 (\AA)
H—C	322	1.11
C—S	240	1.80
S—O	540	1.53

Angle parameters		
angle	k_θ [kcal/(mol rad ²)]	θ_0 (deg)
H—C—H	35.5	108.4
H—C—S	46.1	111.3
C—S—O	79.0	106.75
C—S—C	34.0	95.0

Dihedral parameters			
dihedral angle	k_ϕ (kcal/mol)	n	δ (deg)
H—C—S—O	0.2	3	0
H—C—S—C	0.2	3	0

Table 2.4: Force field parameters for the polarizable DMSO model. See Ref. 113 for complete parameter definitions and functional form of the empirical force field. The effect of the polarizable Drude particles on the empirical energy expression is described in Ref. 109.

Chapter 3

Fluorescence quenching by photoinduced electron transfer in a luminescent Zn^{2+} sensor

3.1 Introduction

Photoinduced electron transfer (PET)^{149,150} is the widely accepted mechanism for the behavior of a class of “turn-on” fluorescent chemosensors which fluoresce only in the presence of targeted analytes. These sensors are electron donor-acceptor systems in which the initial photoexcitation is localized on the acceptor (Figure 3-1a). In the absence of analyte, the HOMO of the donor lies higher in energy than that of the acceptor and can transfer an electron to the acceptor’s HOMO. The electron transfer process competes favorably with radiative decay to the ground state, substantially diminishing the fluorescence quantum yield.¹⁵¹ Binding of the sensor to its particular analyte lowers the donor HOMO below that of the acceptor HOMO, preventing electron transfer and favoring fluorescence.

One may also consider PET from the perspective of electronic states (Figure 3-1b) instead of molecular orbitals. In this picture, the bare sensor possesses a charge-transfer (CT) excited state which lies energetically beneath the lowest optically active

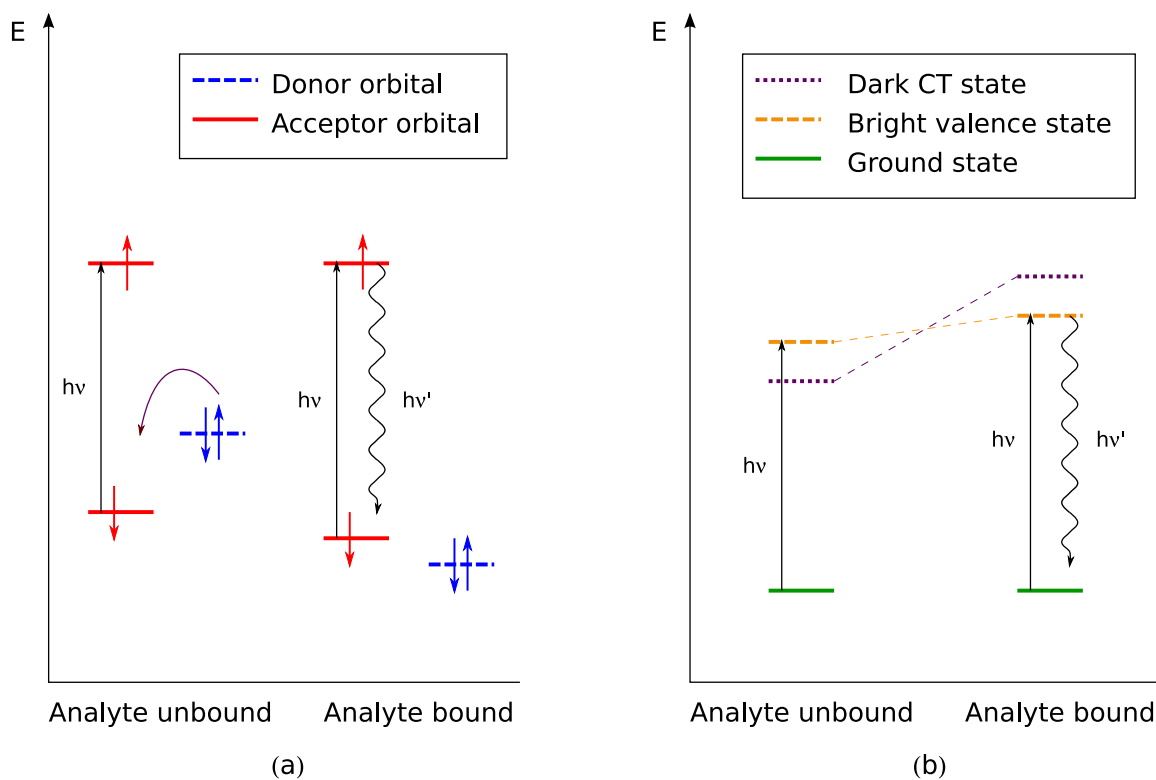


Figure 3-1: Energy level diagrams illustrating PET from (a) the frontier molecular orbital perspective and from (b) the electronic states perspective.

excited state and provides a nonradiative relaxation pathway for the photoexcited sensor. When the sensor binds its analyte, the CT state is shifted above the optically active state and can no longer quench the fluorescence.

PET and other luminescence switching mechanisms have been harnessed in the design of a variety of chemical sensors.^{152,153} Desirable properties of the sensors, such as selectivity for the analyte and intensity of the fluorescence activation, can be tuned by the addition of functional groups which modify the sensor's electronic structure. The systematic optimization of fluorescence-based chemosensors is an active area of research.^{152,154} The study described in this chapter is motivated by the conviction that rational sensor design can benefit from computational insight into the photophysics of these sensors, especially as a predictive tool for features (such as the energetics of the CT state) that are difficult to probe experimentally.

In this chapter we describe a computational investigation of the photophysics of luminescence switching in the zinc-sensing fluorophore Zinpyr-1 (ZP1, Figure 3-2).^{155,156} While PET is a likely mechanism for fluorescence quenching in ZP1, there are several alternative possibilities^{152,157} worth consideration. Among these, internal charge transfer,¹⁵⁸ excimer formation,¹⁵⁹ and resonance energy transfer¹⁶⁰ are all employed in sensor design, but these mechanisms are generally limited to molecular architectures¹⁵⁷ to which ZP1 does not conform. Proton-coupled electron transfer (PCET)¹⁶¹ has been reported in some chemical sensors¹⁶² and is a viable alternative to simple PET.

It has become somewhat routine for researchers in sensor design and synthesis to use TDDFT to calculate electronic spectra and assess whether the qualitative picture of PET holds for their sensors.¹⁶³⁻¹⁶⁵ Petsalakis and coworkers report a series of studies^{166,167} on pyrene-based fluorophores that led to a rule for predicting the strength of a PET process in terms of donor and acceptor orbital energies. Wang, Dyer and coworkers have illustrated the value of computation in sensor design by predicting the photophysical properties of a Zn^{2+} PET sensor and then assessing their predictions by synthesis and characterization of the sensor.¹⁶⁸ However, the reliance of previous computational studies on TDDFT alone is troublesome because

of its well-documented tendency to underestimate the energy of CT excited states.⁴⁶

To address concerns about the reliability of CT excited states obtained from TDDFT, in this study we supplement conventional TDDFT calculations with CDFT for the CT excited state. The CT excitation energy is given by the energy difference between the ground and CT diabatic states, each obtained via CDFT. Together, the TDDFT and CDFT calculations permit a valuable methodological cross-comparison, as they approach the problem of CT excited states from distinct perspectives.

After a review of the salient chemical and photophysical properties of ZP1 obtained from previous experiments, we describe the details of our computational approach. We report TDDFT vertical excitation energies of ZP1 with traditional hybrid and long-range corrected (LC) functionals and show that these computations are unable to clearly resolve the ordering of the low-lying excited states. CT excitation energies deduced from CDFT calculations are then compared to valence excitation energies from TDDFT. Together, the two methods are shown to support the PET fluorescence quenching hypothesis. Finally we assess the merits and shortcomings of our approach and discuss some future directions for modeling sensor photophysics.

3.2 The Zn^{2+} chemosensor ZP1

Several examples of both one- and two-arm fluorescein-based zinc sensors have emerged since ZP1 was first characterized,¹⁵⁴ featuring improvements such as diminished background fluorescence of the metal-free chromophore,^{169–171} reversible Zn^{2+} binding for monitoring zinc over time,^{172,173} and ratiometric sensing for quantifying the concentration of Zn^{2+} in solution.¹⁷⁴ We have chosen to focus our modeling efforts on ZP1 because of the volume of experimental data available for this sensor and because of its established role as a template for future fluorescein-based zinc sensor design.¹⁵⁴

ZP1 and several of its derivatives are effective probes of Zn^{2+} in biological settings and have made possible a number of important neurological and immunological studies on the bioactivity of zinc.^{175,176} The sensor consists of a pair of di(2-picolyl)amine (DPA) arms covalently bonded to a 2',7'-dichlorofluorescein (DCF) body at the 4'

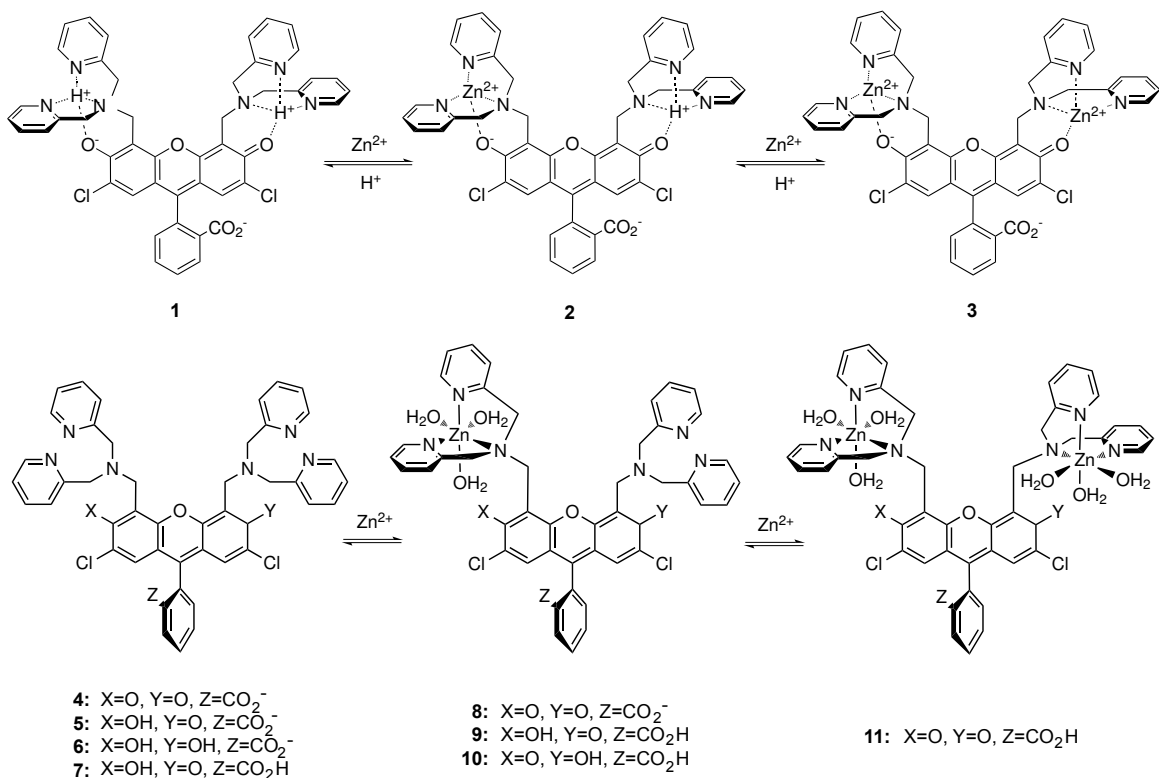


Figure 3-2: Top: schematic of Zn²⁺ binding to ZP1 in aqueous solution, with formal charges as indicated. Bottom: ZP1 structures employed in this study, including explicit coordination of water to Zn.

and 5' positions of the DCF ring (Figure 3-2). DPA is known to selectively bind Zn²⁺ over other dications encountered in physiological settings,¹⁷⁷ notably Ca²⁺ and Mg²⁺. ZP1 can bind Zn²⁺ in either of two pockets formed by the chelating nitrogens of DPA and a carbonyl oxygen on the xanthone ring. We will denote ZP1 structures binding Zn²⁺ by Zn-ZP1 or Zn₂-ZP1, according to the number of Zn²⁺ ions bound.

In the absence of Zn²⁺ and at physiological pH, the absorption spectrum of ZP1 exhibits a maximum at $\lambda = 515$ nm, and the molecule fluoresces with a modest quantum yield $\Phi = 0.17$.¹⁵⁶ In saturated Zn²⁺ solution, the maximum absorption wavelength is blueshifted to 507 nm and the quantum yield increases to $\Phi = 0.87$. This enhancement of the fluorescence is quite selective for Zn²⁺; only its *d*¹⁰ congener Cd²⁺ is known to induce a comparable fluorescence activation. This behavior is consistent with a PET mechanism in which the lowering of the donor HOMO is more pronounced upon binding to a filled *d* shell metal dication than to a dication with an

unfilled d shell.¹⁵³

A variety of protonation states are available to ZP1: four pyridyl nitrogens and the pair of ion-binding pockets are accessible for protonation, as well as the DCF carboxylate group. Accordingly, the fluorescence emission spectrum of ZP1 exhibits a complicated pH dependence, which has recently been explored in detail by potentiometric titration studies.¹⁵⁶ At neutral pH, one of the two binding pockets is protonated. Protonation of the second binding pocket corresponds to a pK_a of 6.96, indicating a mixture of occupied and free binding pockets at physiological pH. In aqueous Zn^{2+} solution, experimental evidence indicates significant fluorescence enhancement for ZP1 structures in which both coordination sites are occupied, relative to structures with at least one empty site.¹⁵⁶

3.3 Computational Details

For each metal-coordination and protonation state of ZP1 under study, the ground state geometry was optimized using Kohn-Sham DFT with the B3LYP functional^{39,178} as implemented in TURBOMOLE.¹⁷⁹ An SV(P) basis set¹⁸⁰ was employed for main group atoms, and a Stuttgart-Köln ECP was used for zinc.¹⁸¹ The optimizations were performed in aqueous solution using the COSMO solvation model.¹⁸² To account for direct coordination of the solvent to the metal, three explicit water molecules were ligated to Zn, resulting in an overall octahedral coordination.

Gas-phase TDDFT vertical excitation energies were evaluated with the B3LYP functional and SV(P) basis set, and solvation effects were studied with COSMO. Because conventional hybrid density functionals have a systematic tendency to underestimate CT excited state energies,⁴⁶ the recently developed long-range corrected LC-PBE and LC-PBE0 functionals, as implemented by Herbert and coworkers¹⁸³ were also employed for gas-phase TDDFT calculations in Q-CHEM.¹¹¹ Attachment-detachment densities¹⁸⁴ of relevant electronic transitions were computed within the Tamm-Dancoff approximation¹⁸⁵ and rendered in VMD.¹⁸⁶ The correlation-consistent cc-pVDZ and aug-cc-pVDZ basis sets¹⁸⁷ were used to gauge the adequacy of the

smaller SV(P) basis for our TDDFT calculations.

Further characterization of the CT states was carried out using CDFT with the B3LYP functional and SV(P) basis set. Ground state molecular analysis techniques such as atomic population analysis⁴⁹ are available for constrained states in CDFT and are used here to characterize changes in electron density over molecular fragments. All reported TDDFT and CDFT excitation energies are vertical excitation energies.

Some additional care must be taken to correctly capture solvent stabilization of the CT state. To account for nonequilibrium solvation effects, we employ a modified Onsager self-consistent reaction field (SCRf) model¹⁸⁸ in which the slow and fast components of the polarization response are separated according to the Pekar partition.^{57,189} We emphasize that this correction scheme only applies to vertical excitation energies, in which the solute nuclear configuration has not yet relaxed in response to the CT density. A solute radius $a_0 = 10\text{\AA}$ was chosen to ensure full electrostatic interaction between the solute density and the dielectric continuum while still encapsulating the solute density almost entirely within the cavity. The value $\epsilon = 80$ was used for the static dielectric constant of water, and the fast dielectric constant was obtained from the square of the index of refraction of water, $\epsilon_\infty = 1.77$.

3.4 Results and Discussion

3.4.1 TDDFT with a conventional hybrid functional

Based on our understanding of the chemistry of ZP1 at neutral pH,¹⁵⁶ we expect the anion and neutral ZP1 structures **5** and **6** in Figure 3-2, which each have at least one deprotonated receptor site, to be important in biological applications. However, as noted by Baik and coworkers,¹⁶⁵ geometry optimizations on fluorescein-based sensors tend to converge to the nonfluorescent lactone isomer when the carboxylate is left deprotonated. In lieu of their constrained optimization approach, we attempted geometry optimizations for the carboxylate structures with the COSMO solvation model, rejecting structures which formed the lactone during this procedure.

Optimization of structures **4** and **5** did not result in lactone formation, so we proceeded to evaluate their vertical excitation spectra with TD-B3LYP/SV(P) in the gas phase and with COSMO. The doubly-protonated structure **6** relaxed to the lactone isomer even with COSMO solvation, so we included an explicit water molecule which acts as a hydrogen bond donor to discourage ring closure. This procedure resulted in a ring-opened optimized structure for **6**.

Gas-phase TDDFT calculations on **4** through **6** at the B3LYP/SV(P) level yielded several spurious low-lying CT excited states, as identified by their absence upon inclusion of solvation effects. These spurious states are unsuitable for comparison with gas-phase excited states from other approaches. We therefore protonated the carboxylate group to obtain structure **7**, which is not expected to exist in aqueous solution, but which proved to be a useful benchmark for comparison to LC-TDDFT and CDFT excited states, as its gas-phase excitation spectrum was not contaminated with low-lying CT states.

Although **7** is not expected to fluoresce,¹⁹⁰ experimental evidence¹⁹¹ indicates that the lack of fluorescence in neutral fluorescein and its derivatives is due to fast conversion to the anion rather than to significant differences in the absorption spectra of the neutral and anionic species. Additionally, the protonation state of the benzoic acid group in fluorescein is known to have only a small effect on the location of its absorption maximum.^{191,192} Thus we anticipate that calculations on **7** will produce a vertical excitation spectrum similar to that of **6**.

Gas-phase TD-B3LYP/SV(P) predicts for **7** an optically weak transition at 2.30 eV (oscillator strength $f < 0.01$). An attachment-detachment density plot indicates substantial CT character from the proton-free DPA arm to the xanthone ring (Figure 3-3). A second CT state, in which the proton-coordinating arm acts as the electron donor, is identified at 2.97 eV ($f = 0.03$). A bright excited state at 2.81 eV ($f = 0.33$) lies between the two CT states and is attributed to excitation within the conjugated π system of the xanthone ring. We judge the SV(P) basis to be sufficiently complete for our purposes by noting that low-lying excited state energies computed with the aug-cc-pVDZ basis set differ by less than 0.03 eV from their SV(P) counterparts.

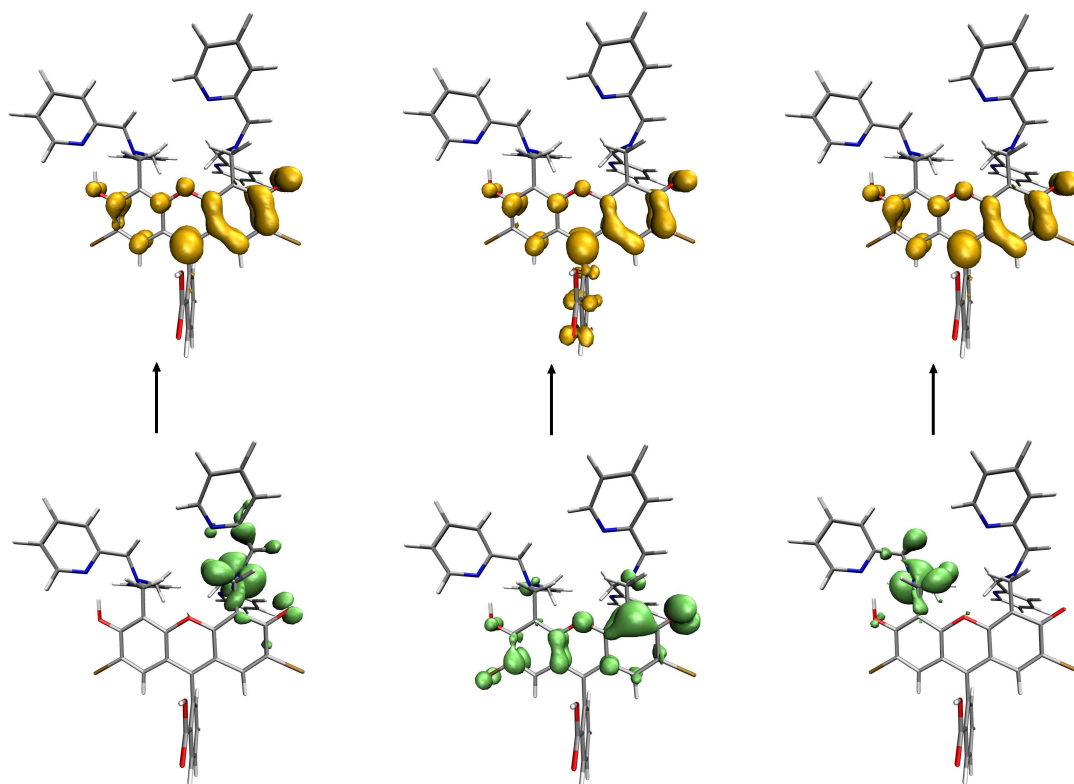


Figure 3-3: ZP1 attachment-detachment densities for low-lying excitations (from left to right): lowest CT, valence, and second-lowest CT excitation.

Structure		Excitation energy (eV)			
Label	Zn ²⁺	expt.	valence	CT ₁	CT ₂
4	0		2.86	2.89	3.20
5	0	2.41	2.92	2.44	3.13
6	0		3.02	3.24	3.27
7	0		2.85	2.21	2.90
8	1		2.92	2.84	> 4.0
9	1		2.89	2.33	> 4.0
10	1		2.92	3.14	> 4.0
11	2	2.44	2.87	> 3.0	> 4.0

Table 3.1: TDDFT vertical excitation energies of the lowest valence and two lowest CT states of ZP1, evaluated with the B3LYP functional, SV(P) basis set, and COSMO solvation model. The lowest excitation energy for each structure is indicated in boldface.

We observe a moderate solvatochromic shift in the absorption spectrum of **7** in aqueous solution. The COSMO model predicts a blueshift of less than 0.05 eV for the bright state, while the low-lying CT state is stabilized by 0.1 eV due to its larger dipole moment. COSMO solvation removes CT contamination from the spectra of structures **4** through **6**; their energies and orbital character are summarized in Table 3.1. Structure **5** with its single protonated binding pocket exhibits a CT state 0.48 eV lower in energy than the lowest bright state, while the lowest valence and CT states of structures **4** and **6** are too close in energy for us to draw any conclusions about their relative ordering.

For structures **5** and **7**, which each have one protonated and one free binding pocket, the relative ordering of the CT and bright excited states supports the claim that fluorescence in metal-free ZP1 is quenched by ET to a lower-energy dark state, and the attachment-detachment densities suggest that it is reasonable to classify the PET process in this system qualitatively as electron donation from an amino nitrogen lone pair to the xanthone ring. Furthermore, in both **5** and **7**, the protonated arm’s CT state is higher in energy than the bright state, which is consistent with the moderate fluorescence activation observed experimentally for conditions under which both binding pockets are protonated.

Next we consider changes to the vertical excitation spectrum of ZP1 upon binding

one Zn^{2+} ion. We considered three protonation states for Zn-ZP1, corresponding to structures **8** through **10** in Figure 3-2. TD-B3LYP with COSMO solvation (Table 3.1) predicts that the CT state of structures **8** and **9**, which each retain an empty binding pocket, will lie lower in energy than the valence excited state, and thus continue to quench fluorescence. On the other hand, structure **10**, in which both binding pockets are occupied by an ion, exhibits a CT excited state at $\Delta E = 3.14$ eV, 0.22 eV above the valence excited state at $\Delta E = 2.92$ eV. This pattern corroborates the hypothesis that occupation of both binding sites by any coordinating ion is sufficient to alter the energy level ordering and activate the sensor’s fluorescence.

TD-B3LYP places the bright state of $\text{Zn}_2\text{-ZP1}$ (structure **11**) at 2.84 eV, essentially unperturbed from that of metal-free ZP1. No CT states below 4.0 eV were identified in its vertical excitation spectrum, corroborating the claim that PET is unavailable for fluorescence quenching in $\text{Zn}_2\text{-ZP1}$.

The valence excitation energy predicted by TD-B3LYP with COSMO for the various ZP1 structures deviates substantially from the experimental absorption maximum at 2.41 eV. Our disagreement with experiment on the absorption maximum of ZP1 is concerning but not unprecedented; B3LYP has previously been reported to overestimate absolute valence excitation energies in some chromophores by similar magnitudes.^{193,194} Whether this error in absolute excitation energies affects the relative ordering of the excited states is uncertain. The valence excited state energy is an overestimate while the CT excited state energies are probably underestimates. It remains conceivable that the valence state actually lies beneath the CT state in ZP1, so we turn to the alternative methods described below for further investigation.

3.4.2 TDDFT with long-range corrected functionals

While B3LYP results are in line with the proposed PET mechanism, they could be considered inconclusive for at least two reasons. First, we do not know whether overestimation of the valence excited state impacts the predicted ordering of the excited states. Second, as mentioned earlier, hybrid functionals in TDDFT are known to underestimate, sometimes severely, the energy of CT excited states. Methods

which employ exact (nonlocal) exchange, such as configuration interaction singles (CIS),^{195,196} should not suffer the latter pitfall – though it should be noted that Subotnik has recently demonstrated the existence of systematic errors for CT states in CIS.¹⁹⁷ In any case, CIS greatly overestimates the excitation energy of the valence excited state (see Appendix A) and does not predict a lower-lying CT state in any of the ZP1 structures we studied. Therefore, we employed the long-range corrected ω LC-PBE and ω LC-PBE0 functionals,¹⁹⁸ which pair the success of semilocal and hybrid functionals for local excited states with a correct description of exchange at long range.

The performance of these functionals has been previously benchmarked for excited states, with values for ω between 0.2 bohr⁻¹ and 0.3 bohr⁻¹ giving the least error in excitation energies for ω LC-PBE and values in the vicinity of 0.1 bohr⁻¹ performing best for ω LC-PBE0; root-mean-square errors in these optimal parameter ranges are reported to be on the order of 0.3 eV.¹⁸³ However, ZP1 is significantly larger than any of the systems employed in the benchmarking study, so the previously determined values of ω may not be the most appropriate. We therefore decided to quantify the sensitivity of the excitation energies in ZP1 to the choice of ω .

A gas-phase LC-TDDFT calculation was carried out for metal-free ZP1 (structure **7**) and for Zn₂-ZP1 (structure **11**) at several reasonable¹⁸³ values of ω (Table 3.2). Here we find for neutral ZP1 that ω LC-PBE places the CT state above the valence state for values of ω in the “optimal” range, but the CT state slides beneath the valence state for smaller values of ω . In contrast, our ω LC-PBE0 calculations place the CT state beneath the valence state for the optimal choice of ω .

For the metal-free ZP1 anion **5**, ω LC-PBE removes the spurious CT states as ω is increased. At $\omega = 0.1$ bohr⁻¹, there are at least six CT states beneath the lowest bright state, while the spectrum at $\omega = 0.3$ bohr⁻¹ is entirely lacking in CT states beneath the bright state. The CT excitation energies are more strongly dependent on the choice of ω than the valence excitation energies because we are varying ω over distances that are beyond the characteristic length scale of the valence transition but are roughly commensurate with that of the CT transition. Still, both valence and

ZP1		$E_{ex}, \omega\text{LC-PBE}$		$E_{ex}, \omega\text{LC-PBE0}$	
ω (a.u.)	valence	CT	valence	CT	
0.10	2.63	1.79	2.96	2.78	
0.15	2.72	2.28	2.99	3.18	
0.20	2.89	2.75	3.08	3.48	
0.25	2.97	3.20	3.16	3.70	
0.30	3.07	3.47	3.23	3.86	
Zn ₂ -ZP1					
ω (a.u.)	valence	CT	valence	CT	
0.10	2.68	> 4.0	2.97	> 4.0	
0.15	2.81	> 4.0	3.04	> 4.0	
0.20	2.92	> 4.0	3.10	> 4.0	
0.25	3.01	> 4.0	3.17	> 4.0	
0.30	3.10	> 4.0	3.25	> 4.0	

Table 3.2: Lowest gas-phase valence and CT excitation energies of neutral ZP1 (in eV) predicted by long-range corrected PBE functionals, as a function of the range-separation parameter ω . The lowest excitation energy for each structure is indicated in boldface. Gas-phase TD-B3LYP/SV(P) predicts the lowest valence and CT states at 2.81 eV and 2.30 eV, respectively, for metal-free ZP1 and at 2.86 eV and > 4.0 eV for Zn₂-ZP1.

CT excited states vary significantly as a function of ω .

These LC functionals place the bright state of Zn₂-ZP1 below the first CT excited state, in agreement with TD-B3LYP and with the experimental observation of enhanced fluorescence in Zn₂-ZP1. Still, for metal-free ZP1 the optimal $\omega\text{LC-PBE}$ functional places the valence state below the CT state, while the optimal $\omega\text{LC-PBE0}$ functional places the valence state above the CT state. Hence, it appears that these functionals are unable to clearly resolve the energy level ordering of the CT and bright states in metal-free ZP1.

With semilocal functionals, CT state contamination of the spectrum may actually play an important role in the cancellation of errors that makes certain TDDFT excitation energies so accurate. By lifting this contamination, long-range corrections can throw the error cancellation out of balance. The $\omega\text{LC-PBE}$ valence excitation energies in metal-free ZP1 illustrate this trend, drifting increasingly further from the experimental value of 2.41 eV as ω is increased (Table 3.2). Given the LC functionals' ambiguous excited state ordering for ZP1, we anticipate similar problems for the more

challenging case of Zn-ZP1. Therefore, we turn to CDFT as an independent probe of the CT excited states.

3.4.3 CT excited states via CDFT

CDFT provides a wholly alternative route to the characterization of CT excited states in ZP1. We consider two definitions for the CDFT constraint regions. In one approach, one DPA arm is selected to be the donor region while the other arm comprises a spectator region with no applied constraint. In the other approach, both arms are assigned to the donor region. The DCF body of ZP1 defines the acceptor region in both cases. While the single-arm partitioning scheme is in keeping with our simple model of PET fluorescence quenching in this system, the two-arm scheme is desirable for its flexibility to permit some delocalization of the positive charge over both arms in the CT state.

Under the two-arm partitioning scheme, gas-phase CDFT with B3LYP predicts a CT state at 2.44 eV for structure **7**. Onsager solvation with the Pekar partitioning scheme stabilizes the CT state by 0.05 eV. A Becke population analysis of the constrained density (Figure 3-4a) indicates that the amine lone pair on the proton-free arm dominates the electron donation, while 31% of the donated density is attributed to the other arm. The population analysis also indicates a small contribution per pyridyl ring that cumulatively accounts for 32% of the transferred electron. These results corroborate the qualitative picture of PET in ZP1 as electron donation from the proton-free amine nitrogen to the xanthone ring; still, a quantitative understanding of the excited states requires us to consider the role of the pyridyl rings as partial electron donors.

If instead a single arm is constrained to serve as the electron donor, the predicted gas-phase CT state energy increases substantially. For example, the CT state of **7** was raised to 2.82 eV by constraining the arm near the phenolic oxygen (left side of the structure in Figure 3-2) to be the donor, while a CT excitation energy of 3.47 eV was found by treating the other arm as the donor.

The donor and acceptor regions of Zn-ZP1 and Zn₂-ZP1 are defined by analogy

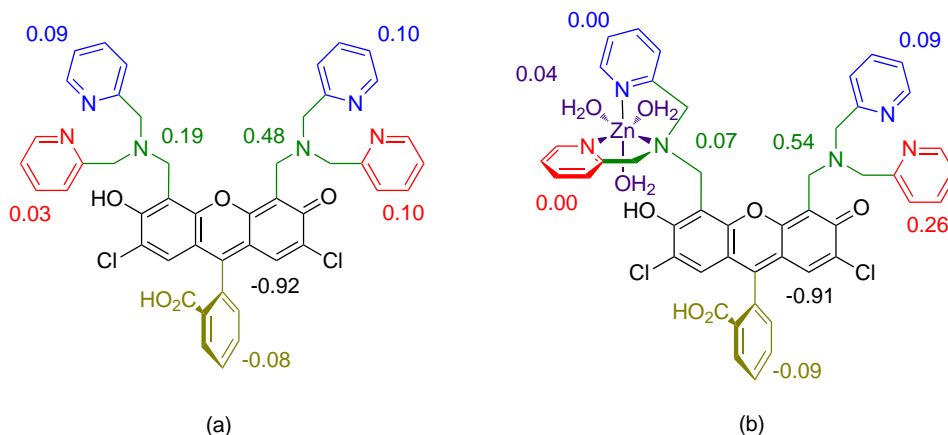


Figure 3-4: Net charge transfer by functional group upon excitation to the lowest CT state of ZP1 with (a) no zinc bound and (b) 1 zinc bound, computed using CDFT with B3LYP and Onsager solvation. The number of electrons is obtained from the Becke population on each highlighted group.

to the metal-free case, with zinc and any coordinated water assigned to the donor region. We found that this partitioning scheme led to unphysically large CT energy gaps ($\Delta E > 8$ eV) when a xanthone carbonyl oxygen is covalently bonded to zinc, as in structure **2**. Therefore we choose to focus on structures in which zinc coordinates exclusively to the chelating nitrogens and water, in spite of crystallographic evidence that Zn binds preferentially to the carbonyl oxygen near the coordinating arm.¹⁵⁶ To test whether this structural alteration could severely change the excitation spectrum, we computed low-lying TD-B3LYP/SV(P)/COSMO excitation energies of the xanthone-chelating structure **2**, with the pocket proton shown in the figure removed. These energies were found to differ by less than 0.1 eV from their counterparts in the analogous structure **8**, suggesting that the additional separation of zinc from the xanthone ring will not drastically alter the ordering of the excited states.

CDFT/B3LYP with Onsager solvation places the CT state of Zn-ZP1 above the valence state regardless of whether the metal-free arm is protonated (Table 3.3). A CT state at 3.59 eV is found if the phenolic proton is placed by the same arm as the bound Zn^{2+} (structure **9**), and this energy increases to 4.46 eV if the phenolic proton is moved to the Zn-free arm (structure **10**). Because the TDDFT bright state lies below 3 eV for each of these structures, fluorescence enhancement is possible with

Structure		Excitation energy (eV)	
Label	Zn ²⁺	valence (TDDFT)	CT (CDFT)
7	0	2.85	2.39
8	1	2.92	4.51
9	1	2.89	3.59
10	1	2.92	4.46
11	2	2.87	7.74

Table 3.3: Valence excitation energies from TDDFT and CT excitation energies from CDFT, both in eV. See Figure 3-2 for structure details. All CDFT energies are at the B3LYP/SV(P) level with Onsager solvation.

only one bound Zn²⁺ ion.

Population analysis of the CT state of Zn-ZP1 shows that the electron-donating region is more localized on a single arm than in the case of metal-free ZP1: for structure **9** (Figure 3-4b), 89% of the donated electron in Zn-ZP1 comes from one arm, compared with 68% for metal-free ZP1. The population analysis suggests that Zn²⁺ lifts the lowest CT state energy in part by reducing the coordinating arm’s participation in electron donation.

For Zn₂-ZP1, the CT state is unambiguously inaccessible as a photophysical intermediate; CDFT/B3LYP with Onsager solvation places it 7.74 eV above the ground state. The high energy of this state can be rationalized from a molecular orbital perspective by noting that the CT excited state in Zn₂-ZP1 is produced by excitation from a Zn-N bonding orbital instead of a lone pair orbital.

TDDFT and CDFT both place the lowest CT state of metal-free ZP1 beneath the bright state, and both predict a bright state beneath the lowest CT state for Zn₂-ZP1. For the more challenging case of Zn-ZP1, CDFT consistently predicts a bright state lying beneath the lowest CT state. TDDFT is at odds with this ordering for two of the three Zn-ZP1 structures we considered, but both methods show a marked increase in the CT state energy upon protonation of at least one binding pocket. These results suggest that PET fluorescence quenching in ZP1 can be deactivated by a single Zn²⁺ ion at physiological pH, where protonation of a binding pocket is common.

We caution that the limited separation of the donor and acceptor in this system makes CDFT energies sensitive to the way the atomic populations are defined and to

the choice of donor-acceptor partition. One could examine whether this sensitivity is drastic enough to alter the predicted energy level ordering in ZP1 by varying the location of the partition, but there is little flexibility in the choice of partition for the well-defined donor-acceptor structure of ZP1.

We do not have a simple guideline for determining under what conditions CDFT will provide a more reasonable CT excitation energy than conventional or long-range corrected TDDFT. The two methods are more reliable in opposite limits; that is, TDDFT is well-suited to the description of localized excited states while CDFT performs best in the limit of long-range charge transfer excitations. Hence the two methods are in some sense complementary. Intramolecular CT in small PET sensors lies somewhere in the middle of these two extremes. While TDDFT is indispensable for the determination of valence excited states in molecules with tens to hundreds of atoms, we find that CDFT provides a competitive alternative for the study of intramolecular CT excited states.

3.5 Conclusion

We have carried out a two-pronged DFT study on the viability of the photoinduced electron transfer mechanism of fluorescence quenching in ZP1. An emphasis was placed on an accurate description of the charge transfer excited state believed to be responsible for quenching the fluorescence, which we characterized by TDDFT with hybrid and LC functionals, and also by CDFT. TD-B3LYP predicts an energy level ordering consistent with the PET mechanism for zinc-free and zinc-saturated ZP1. TDDFT corroborates the experimentally motivated hypothesis that fluorescence is enhanced in ZP1 whenever both ion-binding sites are occupied. CDFT also places the CT excited states at energies consistent with PET fluorescence quenching in the zinc-free and zinc-saturated cases. Furthermore, CDFT and TDDFT both predict activation of the fluorescence upon binding of a single Zn^{2+} ion if the other binding pocket is protonated. CDFT enables population analysis on the CT excited state, which provides insight into the PET mechanism in ZP1 by reporting that the donated

electron density is largely localized on one arm’s amine nitrogen.

This study illustrates the special challenge that intramolecular ET presents for CDFT, which can largely be traced to the definition of the donor and acceptor fragment densities. CDFT is naturally better suited for intermolecular CT because the partition between donor and acceptor densities in such cases is more clearly defined. For intramolecular CT, it is important to be aware of the increased sensitivity of the computed energy to the location of the partition and to the partitioning scheme in use. Furthermore, a non-integer charge constraint might be more appropriate than an integer constraint for molecules with limited donor-acceptor separation like ZP1. Several proposals for reducing the sensitivity of CDFT energies to these details are currently under investigation.¹⁹⁹

Looking forward, we would like to apply the methods described in this study to next-generation fluorescein-based sensors. In particular, we are interested in the evaluation and development of ratiometric sensors such as ZPP1, in which the fluorescence intensity of the sensor depends strongly on whether one or two Zn^{2+} ions are bound, enabling quantitation of zinc.¹⁷⁴

It would also be useful to model the binding affinities of ZP1 and its derivatives for other transition metal ions. While experimental binding affinities are available for ZP1 with several transition metal ions, a computational approach would enable us to study metal ion affinities for a wide variety of ZP1 derivatives without having to synthesize each derivative.

Finally, it would be very desirable to have a method for predicting the degree of fluorescence activation conferred by the binding of a particular ion to ZP1. The fluorescence quantum yield of a molecule in dilute solution is a complicated function of the various decay pathways available to the molecule upon light absorption, and the rate constants of these processes are very sensitive to the molecular environment. We are not aware of any systematic approach in the literature for the *ab initio* computation of fluorescence quantum yields of luminescent molecules, but we believe that it would be an interesting and fruitful avenue to explore.

Chapter 4

Assessment of Δ SCF density functional theory for electronic excitations in organic dyes

4.1 Introduction

Conjugated organic dyes have found widespread use: from lasers, paints, and inks to more exotic technologies such as dye-sensitized solar cells,^{71,200,201} organic light-emitting devices,^{202–205} organic transistors,²⁰⁶ and organic solar cells.^{76,207} The performance of these materials relies heavily on the careful tuning of their electronic properties. Consequently, there is growing interest in the development and application of computational methods for characterizing electronic excitations in condensed-phase organic materials.^{208,209}

Among the earliest approaches to this challenge were semiempirical molecular orbital methods such as complete neglect of differential overlap²¹⁰ and the Pariser-Parr-Pople approach.²¹¹ As computational resources expanded, *ab initio* methods such as time-dependent Hartree-Fock and configuration interaction singles became feasible for molecules of moderate size.¹⁰² None of these methods are expected to give quantitative results, but often they are sufficient to predict trends. More recently,

methods such as complete active space self-consistent field²¹² and equation-of-motion coupled cluster²¹³ have been developed, which promise quantitative results for excited states. Unfortunately, at present, these are too expensive for routine use on organic dyes that typically have 50–100 atoms. A modern method that offers a good compromise between accuracy and efficiency is time-dependent density functional theory (TDDFT).^{42,102,214}

TDDFT within the adiabatic approximation (AA) (Refs. 215 and 216) has been the workhorse method for computing excitation energies in organic molecules over the last decade. TDDFT excitation energies with commonly employed exchange-correlation functionals are usually accurate to within 0.3 eV for localized valence excitations in organic molecules.²¹⁷ However, TDDFT is less reliable for excitations with long-range character, such as Rydberg^{218,219} and charge transfer excitations^{101,220} as well as excitations in large conjugated molecules.^{193,221,222} Recently developed long-range corrected functionals have addressed these issues with promising success.^{41,183,223,224} Several time-independent alternatives for computing excitation energies within a density functional theory (DFT) framework have been proposed,^{53,225,226} but many of these methods pose significant implementation challenges²²⁷ or are too computationally expensive compared to TDDFT.

The Δ SCF-DFT (or simply Δ SCF) method, one of the earliest such time-independent methods,¹³⁸ is straightforward to implement and offers low computational cost. This method is also known in the literature as excited state DFT²²⁸ or constrained DFT²²⁹ (not to be mistaken for the method of the same name⁹² in which constraints are applied to the density). The Δ SCF procedure employs non-Aufbau occupations of the Kohn–Sham orbitals to converge the SCF equations to an excited state that might have other states of the same symmetry beneath it. Because SCF algorithms are geared toward energy minimization, they can sometimes cause a collapse to these lower energy states during the SCF iterations. Techniques such as the maximum overlap method²³⁰ have been developed to address these convergence issues, thereby rendering the Δ SCF method an efficient potential alternative to TDDFT for excited state geometry optimizations and molecular dynamics. Analytical excited state Hes-

sians, which are needed to obtain infrared or vibrationally resolved electronic spectra, are also readily accessible from the Δ SCF approach, in contrast to the current situation for TDDFT — though progress in this area has been rapid in recent years.²³¹ Δ SCF was recently associated with the fourth-order correction to a “constricted” variational approach to TDDFT,²³² but here we focus on its use as a stand-alone method.

Although Δ SCF has gained some traction recently as a DFT-based alternative to TDDFT for excited states,^{219,230,233–235} the performance and range of validity of the method remain poorly understood. This paper addresses this gap in understanding in two ways: first, by comparing excitation energies computed by TDDFT and Δ SCF with experimental values for a representative set of conjugated organic molecules; and second, by providing new insight into the approximations that are made when computing excitation energies from Δ SCF.

The rest of the chapter is arranged as follows. First, we construct a set of organic dye molecules that we use as a benchmark test set. Next, we present TDDFT and Δ SCF excitation energies and discuss the performance of the two methods relative to experiment. We find that the two approaches are quite comparable, which we find surprising given the lack of formal justification for Δ SCF. We therefore spend some time in the discussion examining the theoretical underpinnings of TDDFT and Δ SCF in order to determine if there might not be a deeper reason for the success of Δ SCF. Finally, we conclude our analysis and suggest some potential future directions.

4.2 Test Set

It is of course impossible to construct a single test set that characterizes the quality of a given functional for excited states. The wide variety of behaviors of different functionals for Rydberg states,²¹⁸ charge transfer states,²²⁰ excited states of conjugated organic molecules^{193,220,222,223,236} and core excitations²³⁰ suggests a more modest goal: to design a test set that assesses a functional’s utility for a given purpose. Because of our interest in organic electronics, we are most keenly interested in testing TDDFT

and Δ SCF for the low-lying singlet excited states of common dye molecules. Other test sets consisting of small conjugated organic molecules have been constructed to assess the performance of TDDFT, with typical errors of roughly 0.2–0.3 eV for the best-performing functionals.^{224,237,238} Our chosen test set is tabulated in Tables 4-1 and 4-2. In each case, E_{ex} is the energy of the lowest maximum in the experimental absorption spectrum.

There were a number of criteria that we used to select the molecules in the test set. First, they were required to have a significant absorption in the visible region. This typically requires extensive π conjugation over most of the molecule, resulting in low-lying $\pi \rightarrow \pi^*$ transitions. Further, as can be seen in Tables 4-1 and 4-2, all of the excitations are predominantly HOMO \rightarrow LUMO. This restriction is not essential, but leads to more robust SCF convergence than, say, HOMO \rightarrow LUMO + 1 would. The single-reference character of the excited states helps us circumvent the general problem that some excited states require a multireference approach. We make no restriction on the degree of charge transfer present in the excited state. However, in order to control for solvatochromic effects, we selected molecules for which experimental absorption spectra are available in gas phase, thin film, or nonpolar solvent. Ideally, all of the experimental results would be in gas phase, but this restriction would only leave us with five molecules in our test set, which would be insufficient. We therefore must accept some degree of inequivalence between the experimental observable (absorption maximum in a weak environment) and the calculated quantity (vertical excitation in the gas phase). We should note that methods exist to attempt to correct theoretical gas phase excitation energies for dielectric²³⁹ and vibrational²³⁸ effects to obtain solvent-corrected 0 – 0 excitation energies, but such shifts will in any case be smaller than the errors due to the approximate nature of the density functional.

Despite the fact that all of the molecules satisfy the criteria given above, our test set includes molecules covering a wide range of current applications. Some molecules are found in biological systems (**1**, **8**, **9**, **13**, **14**), others are used for organic electronics (**2**, **3**, **4**, **15**, **16**), and some as synthetic organic dyes (**5**, **6**, **7**, **10**, **11**, **12**). Thus, we

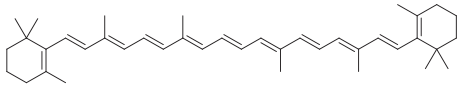
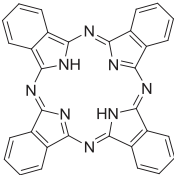
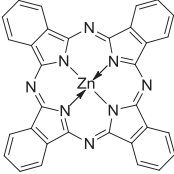
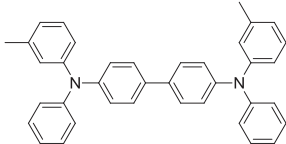
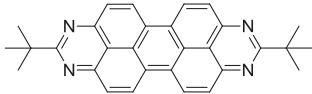
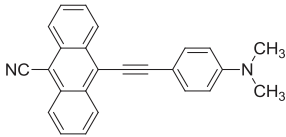
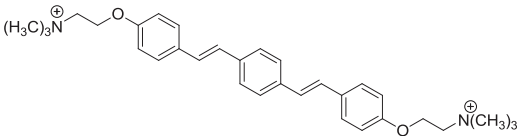
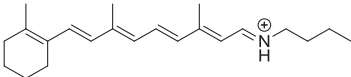
dye	structure	environment	E_{ex} (eV)	% H \rightarrow L
1		pentanes	2.50 ^a	100.0
2		gas phase	1.82 ^b	95.3
3		gas phase	1.88 ^b	91.9
4		thin film	3.46 ^c	97.5
5		toluene	2.87 ^d	95.7
6		thin film	2.59 ^e	99.5
7		thin film	3.55 ^f	99.6
8		gas phase	2.01 ^g	95.2

Figure 4-1: Test set, molecules **1–8**: chemical structure, absorption maximum measured in the specified environment, and TD-B3YLP HOMO \rightarrow LUMO character of the lowest singlet excited state. Experimental excitation energies: ^aRef. 240; ^bRef. 241; ^cRef. 242; ^dRef. 243; ^eRef. 244; ^fRef. 245; ^gRef. 246.

have made an effort to select a structurally diverse set of molecules that can answer

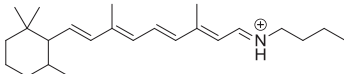
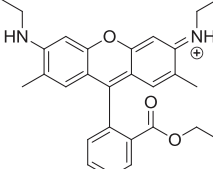
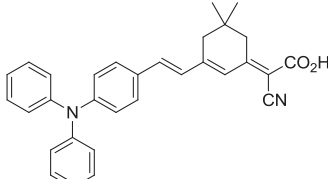
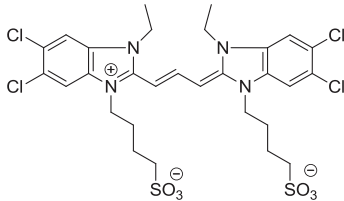
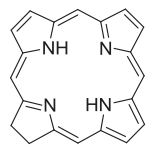
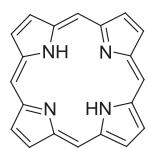
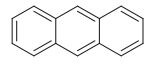
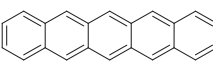
dye	structure	environment	E_{ex} (eV)	% H \rightarrow L
9		gas phase	2.36 ^a	99.7
10		thin film	2.26 ^b	98.0
11		thin film	2.58 ^c	98.6
12		thin film	2.11 ^d	74.6
13		benzene	1.94 ^e	72.1
14		gas phase	2.01 ^f	57.0
15		trichlorobenzene	3.21 ^g	98.0
16		trichlorobenzene	2.06 ^g	100.0

Figure 4-2: Test set, molecules **9–16**: chemical structure, absorption maximum measured in the specified environment, and TD-B3YLP HOMO \rightarrow LUMO character of the lowest singlet excited state. Experimental excitation energies: ^aRef. 246; ^bRef. 247; ^cRef. 248; ^dRef. 249; ^eRef. 250; ^fRef. 251; ^gRef. 252.

the question: how accurate are Δ SCF and TDDFT for organic dyes?

4.3 Computational Methods

All geometries were optimized at the B3LYP/6-31G* level in the gas phase; these geometries are provided in Appendix B. TDDFT and SCF excitation energies were computed in the 6-311+G* basis set with an array of exchange-correlation functionals. An SRSC pseudopotential was employed for Zn.²⁵³ The functionals were chosen because of their widespread use, and the hybrid functionals intentionally represent a wide variation in the fraction of exact (Hartree–Fock) exchange. The SCF calculations include two additional M06 functionals²⁵⁴ for which TDDFT excitation energies were unavailable. An additional functional consists of 60% PBE exchange and 40% Hartree–Fock exchange with PBE correlation and will be denoted PBE4.

The Δ SCF procedure was carried out as follows. Starting with the molecular orbital coefficients of the ground state as an initial guess, the Kohn–Sham equations were solved using a modified SCF procedure in which the lowest $N - 1$ orbitals and the $(N + 1)$ th orbital were occupied at each update of the density matrix. The shifting of orbital energies during this procedure occasionally caused the density to collapse to the ground state. In these cases, the maximum overlap method²³⁰ provided a way to retain the target configuration through convergence.

The non-Aufbau electronic state obtained from this procedure is not a spin eigenfunction. To obtain the energy of the singlet excited state, we use the common spin purification formula,¹³⁸

$$E_S = 2E_{\uparrow\downarrow} - E_{\uparrow\uparrow}$$

Both the spin-mixed ($\uparrow\downarrow$) and spin-pure energies are of interest, so we include both in our analysis. All computations were performed with a modified version of the Q-CHEM 3.2 software package.¹¹¹

4.4 Results

Deviations of computed TDDFT and Δ SCF vertical excitation energies from experiment are presented in Table 4.1, with a more detailed description of the PBE0 results

in Table 4.2. Typical mean absolute errors (MAEs) in TDDFT excitation energies are 0.3 eV, with B3LYP and PBE0 outperforming their counterparts with greater or lesser exact exchange. The magnitude of these deviations is in line with that observed in previous TDDFT benchmarking studies.^{217,255}

For Δ SCF with spin purification, the results parallel the TDDFT results quite closely for all functionals: B3LYP and PBE0 perform best, with MAE and RMSD similar to those of the corresponding functionals in the TDDFT approach. This similarity suggests an argument in favor of applying the spin purification procedure. In keeping with Beckes assertion that the fraction of exact exchange reflects the independent-particle character of the system,³⁹ the appropriate fraction of exact exchange in Kohn–Sham DFT should be a characteristic of the system, not of the method (TDDFT, Δ SCF, or another approach) chosen to compute excitation energies. Of course, it is also convenient from a practical standpoint that TDDFT and spin-purified Δ SCF perform similarly for the same functionals.

The energy of the mixed state in Δ SCF systematically underestimates experimental energies when the employed functional possesses a conventional fraction of exact exchange (20%–30%). Functionals with twice as much exact exchange (BH&H and M06-2X) give mixed states that are more accurate, performing comparably to the best functionals for TDDFT excitation energies. The satisfactory performance of spin-contaminated Δ SCF with a larger fraction of exact exchange can be interpreted as a convenient cancellation of errors. The energy of the mixed state underestimates the singlet energy by half the singlet–triplet splitting. The addition of surplus exact exchange systematically increases the singlet–triplet gap. Therefore, the energy of the mixed state tends to increase with increasing exact exchange. At least on average, one can thus raise the fraction of exact exchange such that the energy of the mixed state with surplus exact exchange matches the energy of the pure singlet with the original functional. Functionals with roughly 50% exact exchange achieve this cancellation in our test set.

The functional LC- ω PBE0 ($\omega = 0.1 \text{ bohr}^{-1}$, $c_{\text{HF}} = 0.25$) was included in our study to assess the performance of long-range corrected density functionals. Given that

Mean error			
Functional	TDDFT	$\Delta\text{SCF}_{\text{mixed}}$	$\Delta\text{SCF}_{\text{pure}}$
PBE	-0.23	-0.72	-0.56
B3LYP	0.08	-0.47	-0.16
PBE0	0.15	-0.42	-0.05
LC- ω PBE0	0.23	-0.26	0.24
PBE4	0.28	-0.26	0.26
BH&H	0.33	-0.14	0.45
M06-2X		-0.08	0.41
M06-HF		0.52	1.47
MAE			
Functional	TDDFT	$\Delta\text{SCF}_{\text{mixed}}$	$\Delta\text{SCF}_{\text{pure}}$
PBE	0.39	0.72	0.58
B3LYP	0.27	0.49	0.25
PBE0	0.27	0.45	0.21
LC- ω PBE0	0.27	0.32	0.26
PBE4	0.31	0.33	0.30
BH&H	0.35	0.27	0.45
M06-2X		0.27	0.42
M06-HF		0.52	1.47
RMSD			
Functional	TDDFT	$\Delta\text{SCF}_{\text{mixed}}$	$\Delta\text{SCF}_{\text{pure}}$
PBE	0.46	0.81	0.66
B3LYP	0.32	0.57	0.32
PBE0	0.32	0.52	0.28
LC- ω PBE0	0.33	0.38	0.32
PBE4	0.38	0.38	0.37
BH&H	0.42	0.31	0.50
M06-2X		0.30	0.48
M06-HF		0.74	1.69

Table 4.1: Test set statistics for the three different excited state methods. All values are in eV.

Molecule	Exp.	TDDFT	$\Delta\text{SCF}_{\text{mixed}}$	Mixed $\langle S^2 \rangle$	$\Delta\text{SCF}_{\text{pure}}$	Triplet $\langle S^2 \rangle$
1	2.50	2.25	1.64	1.015	2.08	2.088
2	1.82	2.08	1.55	1.029	1.91	2.021
3	1.88	2.08	1.54	1.029	1.96	2.047
4	3.46	3.40	3.16	1.017	3.37	2.017
5	2.87	2.96	2.34	1.009	2.84	2.067
6	2.59	2.51	2.01	1.009	2.47	2.027
7	3.55	3.15	2.61	1.008	3.00	2.034
8	2.01	2.42	1.41	1.062	1.72	2.023
9	2.36	2.71	1.68	1.048	2.05	2.020
10	2.26	2.89	2.08	1.056	2.28	2.014
11	2.58	2.49	2.05	1.024	2.38	2.022
12	2.11	2.75	2.06	1.055	2.16	2.009
13	1.94	2.29	1.93	1.046	2.21	2.015
14	2.01	2.30	2.26	1.019	2.63	2.050
15	3.21	3.29	2.71	1.008	3.32	2.024
16	2.06	1.96	1.49	1.009	2.02	2.037

Table 4.2: PBE0 energies and spin multiplicities for the test set. All energies are in eV.

these functionals are optimized (in part) to give accurate TDDFT vertical excitation energies,¹⁸³ it is somewhat surprising to note that LC- ω PBE0 performs best neither for TDDFT nor for ΔSCF . We suspect this arises from the fact that these excited states are bright, which selects against the charge transfer excitations (which tend to be dark) for which LC- ω PBE0 would outperform all other tested functionals.

It is important to note that while ΔSCF and TDDFT have statistically similar accuracy for the singlet states, it does not follow that ΔSCF and TDDFT predict similar results for a given molecule. For example, as illustrated in Table 4.2, the ΔSCF and TDDFT vertical excitation energies with PBE0 can often differ by as much as 0.6 eV for the same molecule. These fluctuations cancel out, on average, and the MAEs of ΔSCF and TDDFT excitation energies differ by only 0.06 eV over the whole set. Further, the $\langle S^2 \rangle$ values from the table clearly justify the use of spin purification for these states.

4.5 Discussion and Analysis

Based on the results of Section 4.4, it would appear that Δ SCF and TDDFT predict vertical excitation energies of organic dyes with approximately equal accuracy, with Δ SCF being perhaps slightly better when the best functionals are used. If we combine this information with existing evidence that Δ SCF is effective for Rydberg states²²⁸ core excitations,^{230,256} solvent effects²⁵⁷ and double excitations²⁵⁸ we are led to the pragmatic conclusion that SCF is a powerful tool for excited states. Is this just a coincidence? Or are there deeper reasons why SCF is so effective? To answer these questions, we must unpack the approximations inherent to TDDFT and Δ SCF calculations.

4.5.1 Linear response TDDFT

According to the Runge–Gross theorem,⁴² there exists a one-to-one correspondence between the time-dependent density, $\rho(x, t)$, and the time-dependent potential, $v_{\text{ext}}(x, t)$. Thus, one can formulate an equation of motion that involves $\rho(x, t)$ alone, where x contains spatial and spin coordinates, $x \equiv (r, \sigma)$:

$$\dot{\rho}(x, t) = F[\rho]$$

where F must be defined. In the Kohn–Sham (KS) formulation of TDDFT, the exact density is constructed out of a set of time-dependent orbitals,

$$\rho(x, t) = \sum_{i=1}^{\text{occ}} |\phi_i(x, t)|^2$$

The KS orbitals, in turn, obey a Schrödinger equation,

$$i\dot{\phi}_i(x, t) = \left(-\frac{1}{2}\nabla^2 + v_{\text{ext}}(x, t) + \int \frac{\rho(x', t)}{|\mathbf{r} - \mathbf{r}'|} dx' + v_{\text{xc}}[\rho](x, t) \right) \phi_i(x, t) \equiv \hat{H}_{\text{KS}}\phi_i(x, t)$$

where the external potential, v_{ext} , is augmented by the classical Coulomb potential and the unknown exchange–correlation potential, $v_{\text{xc}}[\rho]$. According to the Runge–

Gross theorem, v_{xc} exists and is uniquely determined by the density. Thus, $v_{xc}(x, t)$ is a functional of $\rho(x, t)$, justifying the notation $v_{xc}[\rho]$. The major challenge in TDDFT is determining accurate approximations to the exchange-correlation potential.^{41, 43, 45, 259–263}

Now, in principle, $v_{xc}(x, t)$ can depend on $\rho(x, t)$ at any point r in space and any time t in the past. In practice, it is very difficult to obtain approximations to $v_{xc}(x, t)$ that obey causality and possess all the proper time translation invariance properties.^{264, 265} As a result, nearly all existing approximations to $v_{xc}(x, t)$ are strictly local in time — $v_{xc}(x, t)$ depends only on the density of the system at time t . This approximation is known as the adiabatic approximation (AA). It greatly simplifies the construction of approximate potentials, and from this point forward, our manipulations will assume the AA.

In order to obtain excitation energies from TDDFT, the most common route is to employ linear response (LR).^{216, 266} Here, one first performs a traditional DFT calculation to obtain the ground state density. Next, one subjects the system to a small time-dependent external potential, $\delta v(x, t)$, that induces a small change in the density, $\delta\rho(x, t)$, and a corresponding small change in the exchange correlation potential, $\delta v_{xc}(x, t)$. One then uses the time-dependent KS equations to connect the different linear variations and computes excitation energies as the poles in the frequency-dependent response function.²¹⁴ The resulting equations can be cast as a generalized eigenvalue problem:

$$\begin{pmatrix} \mathbf{A} & \mathbf{B} \\ -\mathbf{B} & -\mathbf{A} \end{pmatrix} \begin{pmatrix} \mathbf{X}_M \\ \mathbf{Y}_M \end{pmatrix} = \omega_M \begin{pmatrix} \mathbf{X}_M \\ \mathbf{Y}_M \end{pmatrix}$$

Here, \mathbf{X}_M and \mathbf{Y}_M are vectors of length (occupied) \times (unoccupied) that represent the density response and the \mathbf{A} and \mathbf{B} matrices are given by

$$\begin{aligned} A_{ia;jb} &\equiv (\epsilon_a - \epsilon_i)\delta_{ij}\delta_{ab} + B_{ia;jb} \\ B_{ia;jb} &\equiv \int \phi_i(x_1)\phi_j(x_2) \left(\frac{1}{r_{12}} + \frac{\delta v_{xc}(x_1)}{\delta\rho(x_2)} \right) \phi_a(x_1)\phi_b(x_2) dx_1 dx_2 \end{aligned}$$

where i, j (a, b) index occupied (unoccupied) orbitals. In principle, the eigenvalues ω_M are the exact (within the AA) transition energies between the ground electronic state and the various excited states: $\omega_M = E_i - E_0$. Meanwhile the eigenvectors, \mathbf{X}_M and \mathbf{Y}_M contain information about the intensity of the transition.

4.5.2 Δ SCF densities

Now, because quantum mechanics is linear, linear response in Hilbert space starting from any two different reference states will give equivalent transition energies. However, since most density functionals have a nonlinear dependence on the density, the excitation energy obtained from LR-TDDFT depends on the reference state one chooses. Thus, for example, in certain cases it is advantageous to choose a reference state with a different spin multiplicity.^{267–271}

Instead of sifting for excitations in the density response, an alternative approach is to search directly for the excited state density in TDDFT. Here, one recognizes that every eigenstate Ψ_i of the Hamiltonian is a stationary state. Hence, $\rho_i(x, t)$ is constant in time and

$$\dot{\rho}(x, t) = F[\rho] = 0 \quad (4.1)$$

Within the KS formulation, the density is invariant if each KS orbital changes by a phase factor

$$\phi_j(x, t) = e^{-i\epsilon_j t} \phi_j(x)$$

so that

$$\begin{aligned} i\dot{\phi}_j(x, t) &= \epsilon_j \phi_j(x, t) \\ \hat{H}_{\text{KS}}\phi_j(x, t) &= \epsilon_j \phi_j(x, t) \end{aligned}$$

Thus, the equations obeyed by stationary densities within TDDFT are *exactly the same as the SCF equations for traditional KS-DFT*. Viewed in this light, it is clear that Δ SCF states — which solve the traditional KS-DFT equations with non-Aufbau occupations of the orbitals — have a rigorous meaning in TDDFT: they correspond

to stationary densities of the interacting system. Further, these stationary densities have a clear connection with excited states of the molecule. This connection between TDDFT and Δ SCF comes tantalizingly close to rigorously justifying the use of Δ SCF-DFT for excited states: Δ SCF-DFT gives stationary densities that are exact within the AA.

Before moving on, we note how the AA is expected to influence Eq. 4.1. The above derivation is so concise that it almost seems as if no approximation has been made at all. However, we note that in Eq. 4.1 the density is constant at all times. Thus, the system must have been *prepared* in the desired eigenstate. This assumption violates the terms of the Runge–Gross theorem, which applies only to different densities that originate from the same state (usually assumed to be the ground state at $t = -\infty$). Only within the AA can different initial densities be justified.²⁷²

The Δ SCF scheme implied by Eq. 4.1 is exact within the AA because the system has no memory of how it was prepared. If our functional has memory, Eq. 4.1 states that $F[\rho_i(x, t)] = 0$ when applied to a particular density, $\rho_i(x, t)$, that is constant in time. To put it another way, Eq. 4.1 depends only on the zero frequency ($\omega = 0$) part of F . In many ways, this is the ideal scenario within the AA. Any adiabatic functional is time-local and thus frequency independent. However, it is trivial for a frequency-independent kernel to be correct at one frequency (i.e. $\omega = 0$) and so one suspects that the AA could be well-suited to the Δ SCF approach. In contrast, within linear response one relies on the ω -independent kernel being a good approximation to the true kernel at every excitation energy. It is clear that, except in special cases, the latter condition cannot hold and thus LR-TDDFT would seem more limited by the AA.

4.5.3 Δ SCF energy expressions

Δ SCF gives us a rigorous route to obtain a stationary density in TDDFT. But how should we associate an energy with this density? Since there is no Hohenberg–Kohn theorem for excited states,⁵² there can be no single density functional that gives the correct energy for all excited states. Instead, one must tackle the problem of defining

different functionals for different excited states^{53,225} or else make the functional depend on more than just the density.^{273,274} The simplest procedure is to evaluate the ground state energy expression using the Δ SCF orbitals

$$E^{\text{ex}} = E[\phi_i^{\text{ex}}(x)] \quad (4.2)$$

and this is the “mixed” Δ SCF energy used above. It should be noted that this energy expression is not a functional of the density, but rather an explicit functional of the orbitals. If we used the excited state density (rather than the orbitals), we would need to derive a corresponding set of KS orbitals to compute the kinetic energy, $T_s[\rho]$. By definition, these orbitals would be obtained by constrained search²⁷⁵ and the resulting orbitals would give a different energy than the excited state orbitals. The orbital dependence lends some measure of robustness to the Δ SCF predictions.

In practice, it is necessary to correct Eq. 4.2 because Eq. 4.1 is necessary but not sufficient: not all stationary densities correspond to excited states even though all excited states give stationary densities. To see this, suppose you have a state that is a linear combination of two eigenstates:

$$|\Psi\rangle \propto |\Psi_1\rangle + |\Psi_2\rangle$$

Then the time evolving wavefunction is

$$|\Psi(t)\rangle \propto e^{-iE_1t} |\Psi_1\rangle + e^{-iE_2t} |\Psi_2\rangle$$

and the density is

$$\begin{aligned} \rho(\mathbf{r}) &\equiv \langle \Psi(t) | \delta(\mathbf{r} - \hat{\mathbf{r}}) | \Psi(t) \rangle \\ &\propto \langle \Psi_1 | \delta(\mathbf{r} - \hat{\mathbf{r}}) | \Psi_1 \rangle + \langle \Psi_2 | \delta(\mathbf{r} - \hat{\mathbf{r}}) | \Psi_2 \rangle \\ &\quad + e^{-i\Delta Et} \langle \Psi_1 | \delta(\mathbf{r} - \hat{\mathbf{r}}) | \Psi_2 \rangle + e^{i\Delta Et} \langle \Psi_2 | \delta(\mathbf{r} - \hat{\mathbf{r}}) | \Psi_1 \rangle \end{aligned}$$

where $\Delta E = E_1 - E_2$. If ΔE is not zero, we do not have an eigenstate and in general

the density is not stationary. However, suppose the transition density between the two excited states is zero everywhere. That is, suppose that

$$\rho_{12} \equiv \langle \Psi_1 | \delta(\mathbf{r} - \hat{\mathbf{r}}) | \Psi_2 \rangle = 0$$

In this situation, the oscillating piece of the density is zero and the density is stationary even though the wavefunction is not an eigenstate. Thus, it is, in principle, possible for Eq. 4.1 to locate densities that do not correspond to eigenstates.

How does this affect Δ SCF in practice? Note that ρ_{12} is zero only if no one particle potential can drive the $1 \rightarrow 2$ transition. The most common situation where this occurs is if the eigenstates have different total spin (e.g. the transition density for singlet–triplet transitions is always rigorously zero in the absence of spin-orbit coupling). Thus, any linear combination

$$|\Psi\rangle \propto c_S |\Psi_S\rangle + c_T |\Psi_T\rangle$$

of a singlet eigenstate (Ψ_S) and a triplet eigenstate (Ψ_T) will have a stationary density and could lead to spurious Δ SCF solutions. In practice, this indeterminacy leads to spin contamination of the KS eigenstates in the following way. Suppose we have a singlet ground state and we are interested in the HOMO \rightarrow LUMO transition. The singlet and one of the triplet states require two determinants:

$$\begin{aligned} |\Psi_S\rangle &\propto \left| \dots \psi_{\text{HOMO}}^\uparrow \psi_{\text{LUMO}}^\downarrow \right\rangle - \left| \dots \psi_{\text{HOMO}}^\downarrow \psi_{\text{LUMO}}^\uparrow \right\rangle \\ |\Psi_T\rangle &\propto \left| \dots \psi_{\text{HOMO}}^\uparrow \psi_{\text{LUMO}}^\downarrow \right\rangle + \left| \dots \psi_{\text{HOMO}}^\downarrow \psi_{\text{LUMO}}^\uparrow \right\rangle \end{aligned}$$

but KS-DFT biases us toward states that are well-represented by a single determinant.²⁷⁶ Thus, rather than obtaining a pure singlet or a pure triplet we obtain a broken symmetry solution like

$$|\uparrow\downarrow\rangle = \left| \dots \psi_{\text{HOMO}}^\uparrow \psi_{\text{LUMO}}^\downarrow \right\rangle \propto |\Psi_S\rangle + |\Psi_T\rangle$$

When employed in Eq. 4.2, this mixed spin state gives an energy somewhere between the singlet and triplet excitation energies. Thus, we are led to the purification formula

$$E_S = 2E_{\uparrow\downarrow} - E_{\uparrow\uparrow}$$

This scheme has a long history in predicting exchange couplings,^{277,278} and the results above suggest that it predicts singlet HOMO→LUMO transitions in line with intuition. We thus see that the projection of excited state energies arises directly from the indeterminacy of the Δ SCF equations in the presence of spin degeneracy. We can also explicitly solve the case of three unpaired electrons to obtain two doublet energies:

$$E_D^\pm = \frac{1}{2}(E_{\downarrow\uparrow\uparrow} + E_{\uparrow\downarrow\uparrow} + E_{\uparrow\uparrow\downarrow} - E_{\uparrow\uparrow\uparrow}) \\ \pm \sqrt{\frac{1}{2}(E_{\downarrow\uparrow\uparrow} - E_{\uparrow\uparrow\downarrow})^2 + \frac{1}{2}(E_{\uparrow\downarrow\uparrow} - E_{\uparrow\uparrow\downarrow})^2 + \frac{1}{2}(E_{\downarrow\uparrow\uparrow} - E_{\uparrow\downarrow\uparrow})^2}$$

The projection scheme can be further generalized to an arbitrary number of unpaired electrons,²⁷⁹ although the ensuing equations are overdetermined.²⁸⁰

A more sophisticated scheme for dealing with spin would involve introducing a multideterminant reference state into the KS calculation. This is the idea behind the ROKS and REKS methods^{281–283} which will be addressed in the next chapter. As we will see, techniques of this sort are certainly more elegant than *post facto* energy projection, but they also fundamentally change the equations being solved.

4.6 Conclusion

We have revisited the approximations that define the Δ SCF approach to excited states in DFT. The performance of the method was assessed by comparing Δ SCF excitation energies for several organic dyes with TDDFT and experimental excitation energies. We found that deviations of spin-purified Δ SCF excitation energies from experimental values are comparable to those of TDDFT for all functionals tested.

Spin-contaminated Δ SCF energies were found to require more exact exchange to achieve similar accuracy. As a partial justification of these results, we demonstrated that Δ SCF densities are precisely the stationary densities of TDDFT within the adiabatic approximation, and the necessity of purifying the energies arises from the indeterminacy of the stationary equations with respect to different spin states.

While this study establishes some expectations regarding the range of applicability of the Δ SCF approach, there remain several unanswered questions to be explored in future work. We have shown that Δ SCF performs well for HOMO \rightarrow LUMO excitations, but it remains to be determined how it performs for higher energy excitations. It will also be interesting to compare and contrast the performance of a spin-adapted approach such as ROKS with the spin purification approach presented here.

Several possible extensions and applications of Δ SCF methodology also deserve attention. Δ SCF gradients are readily available from ground-state SCF codes. Therefore, if the excited state potential energy surface (PES) obtained from Δ SCF is reasonably parallel to the true Born–Oppenheimer PES, Δ SCF could provide an efficient alternative to TDDFT and other wavefunction based methods for geometry optimization and molecular dynamics on excited states.^{284–286} Furthermore, Δ SCF also provides an affordable route to the excited state Hessian, from which one could construct vibrationally resolved absorption and emission spectra.^{287,288} It is also a simple matter to incorporate solvation effects in Δ SCF.^{3,257} Together, these features could provide an affordable way to calculate full absorption and emission spectra in different environments for large molecules such as phthalocyanines. It will be intriguing to see if the robustness of Δ SCF for low-lying excited states extends across a wide enough range of excited state properties to make these simulations worthwhile.

4.7 Acknowledgment

The work described in this chapter was carried out jointly with Shane Yost, who is a co-author of Ref. 139.

Chapter 5

Self-consistent implementation of restricted open-shell Kohn-Sham methods for excited states

5.1 Introduction

As organic semiconductors and related materials move from the laboratory to commercialization, accurate methods for modeling their electronic structure and dynamics are becoming increasingly in demand.^{11,289} Many existing techniques rooted in DFT — including TDDFT, CDFT and Δ SCF — have been discussed and applied in the preceding chapters. In particular, for low-lying excited states in organic dyes, we showed that the Δ SCF approach is as reliable a predictor of excitation energies as linear response TDDFT, while also possessing certain practical advantages such as readily available gradients and Hessians.¹³⁹

Each established electronic structure method, from semiempirical techniques to full CI, presents a unique set of strengths and weaknesses, and Δ SCF is no exception. Despite its often-tolerable accuracy of roughly 0.3 eV with commonly employed functionals and the simplicity of its energy derivatives, Δ SCF possesses several drawbacks for practical applications. First, accurate Δ SCF excited states require the use of the

spin purification procedure¹³⁸ described in Chapter 4, which makes it necessary to carry out two SCF calculations for every computed excitation energy. The second difficulty — and perhaps also the more significant one — is that the Δ SCF orbital relaxation procedure is prone to “variational collapse”, in which the SCF convergence procedure for an excited state leads back to the ground state determinant. Variational collapse is often instigated by changes in the relative energies of frontier KS orbitals during the SCF procedure, and the maximum overlap method (MOM)^{230,256} is designed to address this issue by occupying orbitals at each SCF step in order of their overlap with the span of the occupied KS orbitals from the previous SCF step. Nevertheless, neither a non-Aufbau rule nor a maximum overlap rule for orbital occupation can guarantee SCF convergence to the target state. This state of affairs makes Δ SCF less appealing for the potential energy scans and molecular dynamics simulations for which it is otherwise computationally well-suited, because the necessary convergence strategy can vary unpredictably from one geometry to the next.

Both of these shortcomings of Δ SCF can be avoided, in principle, if the spin adaptation takes place at the level of the KS orbital optimization, in lieu of a *post facto* energy correction. The restricted open-shell Kohn-Sham (ROKS) approach to excited states,^{281,282,290} summarized in Section 5.2, offers a straightforward means of optimizing the KS orbitals to minimize any linear combination of single-determinant energies,²⁹¹ although we are primarily concerned with the case of the lowest singlet excited state. There exist more sophisticated techniques for obtaining static excited states in DFT while avoiding variational collapse;²⁹² particularly noteworthy in this regard is the hierarchy of constricted variational methods (CV-(n)-DFT) recently established by Ziegler, Cullen and coworkers.^{232,293,294} However, the relative simplicity of ROKS makes it appealing for computationally demanding applications.

Despite more than a decade of quantum chemical modeling with ROKS, both practical and fundamental questions about this strategy linger. The majority of ROKS studies have involved codes that use a plane-wave basis,^{285,295–297} thereby precluding a thorough assessment of the performance of ROKS with hybrid XC functionals and with other recent advancements in XC functional design, such as range-separation.⁴⁰

On the more fundamental side, despite the clear analogy between the Δ SCF and ROKS ansatz, the working equations of the two methods are very distinct. Thus it merits investigation whether the excitation energies obtained by these two methods are in rough mutual agreement, and to what extent their results may be expected to differ. Furthermore, there exists a well-documented complication in ROKS in which rotations between the open-shell orbitals in ROKS can artificially lower the energy of the S_1 state.^{283,297,298} Efforts to address this concern have either accompanied a reformulation of the entire ROKS ansatz²⁹⁷ or resulted in a set of possible solutions which must be tested on a case-by-case basis.²⁹⁹ Thus, this investigation is also motivated by the search for a simple, robust resolution to the open-shell mixing problem in ROKS.

The remainder of this chapter is organized as follows. After a brief review of established ROKS theory, we discuss the issue of indeterminacy of the ROKS equations for open-shell singlets with respect to mixing between the two open-shell orbitals. In the absence of a formal argument for adopting a particular treatment for this mixing, we propose and implement two strategies: a “canonical” approach where the orbital mixing is determined by the SCF procedure, and a “variational” approach in which the mixing is chosen to extremize the ROKS energy. After outlining computational details, we analyze ROKS energies for a set of small organic dyes as a function of the prescription for orbital-mixing. Settling on a satisfactory strategy, we then present ROKS vertical excitation energies of the large organic chromophores introduced in Chapter 4 for comparison with Δ SCF and TDDFT results. We also compare potential energy surfaces (PES) for isomerization of the formaldimine molecule — a minimal model for the retinal chromophore — as obtained via ROKS, Δ SCF and TDDFT. Finally, we conclude with our perspective on the practical utility of ROKS for excited state simulations, as well as some targets for future work.

5.2 Theory

Our implementation of ROKS closely follows the formulation due to Filatov and Shaik,²⁸¹ which is itself rooted in Roothaan’s vector-coupling approach to restricted open-shell Hartree-Fock (ROHF) theory.³⁰⁰ We specialize immediately to the case of singlet excited states constructed from two determinants. In this formulation, the energy of a two-determinantal singlet excited state is given by the sum rule

$$E_s^{\text{ROKS}} = 2E_m [\{\phi_i\}] - E_t [\{\phi_i\}] \quad (5.1)$$

where s , m and t denote the singlet excited state, mixed-spin determinant and triplet determinant, respectively. This energy expression bears similarity to the expression used for singlet excited states in ΔSCF ,¹³⁸ with the key distinction that in ROKS the mixed- and triplet-state determinants are constructed from the *same set of orbitals* $\{\phi\}$, while in ΔSCF the orbitals are separately optimized for each determinant,

$$E_s^{\Delta\text{SCF}} = 2E_m [\{\phi_i^m\}] - E_t [\{\phi_i^t\}] \quad (5.2)$$

This fundamental difference in philosophy between the ΔSCF and ROKS approaches is illustrated schematically in Figure 5-1. Following precedent, we refer to the mixed and triplet determinants collectively as the microstates entering the ROKS energy expression.

Variational minimization of the ROKS energy with respect to the KS orbitals leads to the complication of different Fock operators for each shell.^{281,299} Nevertheless, through the vector-coupling technique²⁸¹ it is possible to derive a unified eigenvalue equation for closed- and open-shell orbitals in the molecular orbital (MO) basis,

$$\mathbf{FC} = \epsilon\mathbf{C} \quad (5.3)$$

The effective Fock matrix \mathbf{F} in Eq. 5.3 has a natural block structure defined by the different shells (closed, open and virtual), and it takes a different form in each of these

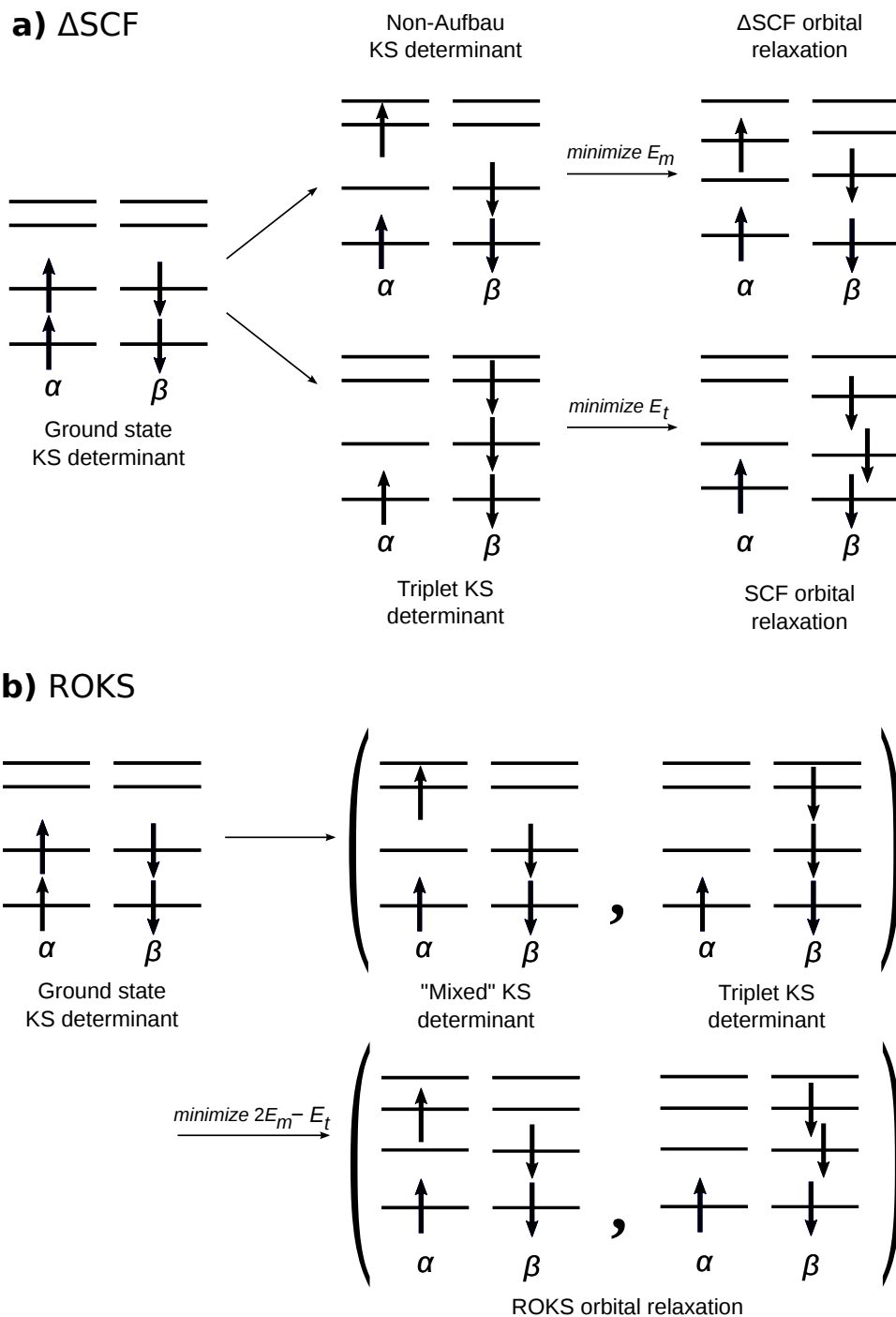


Figure 5-1: Relaxation of Kohn-Sham orbitals (a) in Δ SCF, and (b) in ROKS. Note that the converged mixed and triplet determinants in Δ SCF are constructed from different KS orbitals, whereas in ROKS both determinants are built from a common set of orbitals. Furthermore, the α and β orbital sets are identical in ROKS.

blocks. Expressed in terms of Fock matrices for the mixed and triplet determinants, the ROKS Fock matrix for the S_1 state is

$$\begin{pmatrix} \mathbf{F}_m^\alpha + \mathbf{F}_m^\beta - \frac{1}{2}\mathbf{F}_t^\alpha - \frac{1}{2}\mathbf{F}_t^\beta & 2\mathbf{F}_m^\alpha - \mathbf{F}_t^\beta & 2\mathbf{F}_m^\beta - \mathbf{F}_t^\beta & \mathbf{F}_m^\alpha + \mathbf{F}_m^\beta - \frac{1}{2}\mathbf{F}_t^\alpha - \frac{1}{2}\mathbf{F}_t^\beta \\ 2\mathbf{F}_m^\alpha - \mathbf{F}_t^\beta & 2\mathbf{F}_m^\beta - \mathbf{F}_t^\alpha & \mathbf{F}_m^\alpha + \mathbf{F}_m^\beta - \mathbf{F}_t^\alpha & 2\mathbf{F}_m^\beta - \mathbf{F}_t^\alpha \\ 2\mathbf{F}_m^\beta - \mathbf{F}_t^\beta & \mathbf{F}_m^\alpha + \mathbf{F}_m^\beta - \mathbf{F}_t^\alpha & 2\mathbf{F}_m^\alpha - \mathbf{F}_t^\alpha & 2\mathbf{F}_m^\alpha - \mathbf{F}_t^\alpha \\ \mathbf{F}_m^\alpha + \mathbf{F}_m^\beta - \frac{1}{2}\mathbf{F}_t^\alpha - \frac{1}{2}\mathbf{F}_t^\beta & 2\mathbf{F}_m^\beta - \mathbf{F}_t^\alpha & 2\mathbf{F}_m^\alpha - \mathbf{F}_t^\alpha & \mathbf{F}_m^\alpha + \mathbf{F}_m^\beta - \frac{1}{2}\mathbf{F}_t^\alpha - \frac{1}{2}\mathbf{F}_t^\beta \end{pmatrix}$$

where the four rows (and columns) indicate, in order, closed-shell, first open shell, second open shell, and virtual orbitals. The corresponding expression for the T_1 state is

$$\begin{pmatrix} \frac{1}{2}\mathbf{F}_t^\alpha + \frac{1}{2}\mathbf{F}_t^\beta & \mathbf{F}_t^\beta & \frac{1}{2}\mathbf{F}_t^\alpha + \frac{1}{2}\mathbf{F}_t^\beta \\ \mathbf{F}_t^\beta & \frac{1}{2}\mathbf{F}_t^\alpha + \frac{1}{2}\mathbf{F}_t^\beta & \mathbf{F}_t^\alpha \\ \frac{1}{2}\mathbf{F}_t^\alpha + \frac{1}{2}\mathbf{F}_t^\beta & \mathbf{F}_t^\alpha & \frac{1}{2}\mathbf{F}_t^\alpha + \frac{1}{2}\mathbf{F}_t^\beta \end{pmatrix}$$

We construct the effective Fock matrix in three steps:

1. Build mixed and triplet density matrices from the unified set of KS orbitals.
2. Build Fock matrices for the mixed and triplet determinants from the mixed and triplet densities.
3. Project linear combinations of the single-determinant Fock matrices in the MO basis onto the appropriate blocks to create the effective Fock matrix.

Using this effective Fock matrix, we solve Eq. 5.3 self-consistently using the standard machinery of quantum chemical SCF algorithms. The single-determinant ener-

gies are then determined from the converged KS orbitals and substituted into Eq. 5.1 to obtain the ROKS energy of the S_1 state.

5.2.1 The influence of orbital mixing between open shells

Several authors have identified, in their pilot ROKS calculations, a complication that arises when solving the ROKS equations for the lowest singlet excited state.^{283,295,297–299} When the excited state possesses the same symmetry as the ground state, the ROKS algorithm formulated above permits mixing between the two open shell orbitals. This orbital mixing can artificially lower the energy of the excited state, typically by an amount commensurate with twice the singlet-triplet splitting,^{297,298} potentially delivering an S_1 excitation energy that would actually make a better estimate for the triplet energy. This instability is not unexpected:²⁸¹ in fact, it was already established that a proper description of excited states of the same symmetry as the ground state requires a symmetry-dependent XC functional.^{53,301,302}

To illustrate how mixing of the open-shell orbitals affects ROKS in practice, let $|a\rangle$ and $|b\rangle$ represent the two open-shell orbitals. The matrix elements of the density matrix \mathbf{P} for the mixed determinant in the atomic orbital (AO) basis are:

$$P_{\mu\nu} = 2 \sum_{k \in \text{occ}} C_{\mu k} C_{\nu k}^\dagger + C_{\mu a} C_{\nu a}^\dagger + C_{\mu b} C_{\nu b}^\dagger \quad (5.4)$$

Now we rotate $|a\rangle$ relative to $|b\rangle$ by an angle θ , which modifies the open-shell MO coefficients:

$$\begin{aligned} \tilde{C}_{\mu a} &= C_{\mu a} \cos \theta + C_{\mu b} \sin \theta \\ \tilde{C}_{\mu b} &= -C_{\mu a} \sin \theta + C_{\mu b} \cos \theta \end{aligned}$$

Inserting the rotated MO coefficients into Eq. 5.4, one finds that $\tilde{P}_{\mu\nu} = P_{\mu\nu}$, so the rotation does not affect the density matrix. However, the ROKS energy expression is properly a function of *the KS orbitals* rather than of the density matrix, and in practice the ROKS energy depends on the choice of θ through the XC (including

exact exchange) contributions.

In applications, the indeterminacy of the open-shell mixing angle leads to a pair of solutions to the ROKS equations which have been termed “localized” and “delocalized” solutions.^{283,298} Frank and coworkers found that a particular ROKS solution (localized or delocalized), once identified as the physically correct solution for a given system, could be selectively enforced through modification of the Goedecker-Umrigar algorithm used in their calculations.^{299,303} This algorithm was originally designed to converge SCF equations for self-interaction-corrected XC functionals,³⁰⁴ but is applicable to any scenario involving an orbital-dependent Fock operator. Billeter and Egli circumvented the open-shell mixing problem by introducing a more general Slater transition state reference.²⁹⁷ Here we consider a strategy for controlling the open-shell mixing without a complete reformulation of the ROKS approach.

For geometry optimizations and molecular dynamics simulations, previous implementations of ROKS have employed the Hellmann-Feynman theorem to compute forces. However, since the ROKS energy expression is not strictly variational with respect to the open-shell mixing angle, the Hellmann-Feynman theorem may not hold for certain ROKS states, depending on how this state was obtained. Below we outline a simple modification to the ROKS algorithm which guarantees that this energy is variational with respect to θ .

5.2.2 Variational treatment of open-shell mixing

As explained in Section 5.2.1, minimization of the ROKS energy as a functional of the density matrix alone cannot guarantee that the energy is variational with respect to the open-shell mixing angle θ . However, we can enforce this condition directly by requiring at each SCF step that θ is chosen to extremize the energy,

$$\left. \frac{\partial E[\mathbf{P}, \theta]}{\partial \theta} \right|_{\theta^*} = 0$$

Then a rotation by the θ^* which extremizes E is applied to the open-shell MO coefficients, permitting construction of the proper θ -dependent XC contributions to the

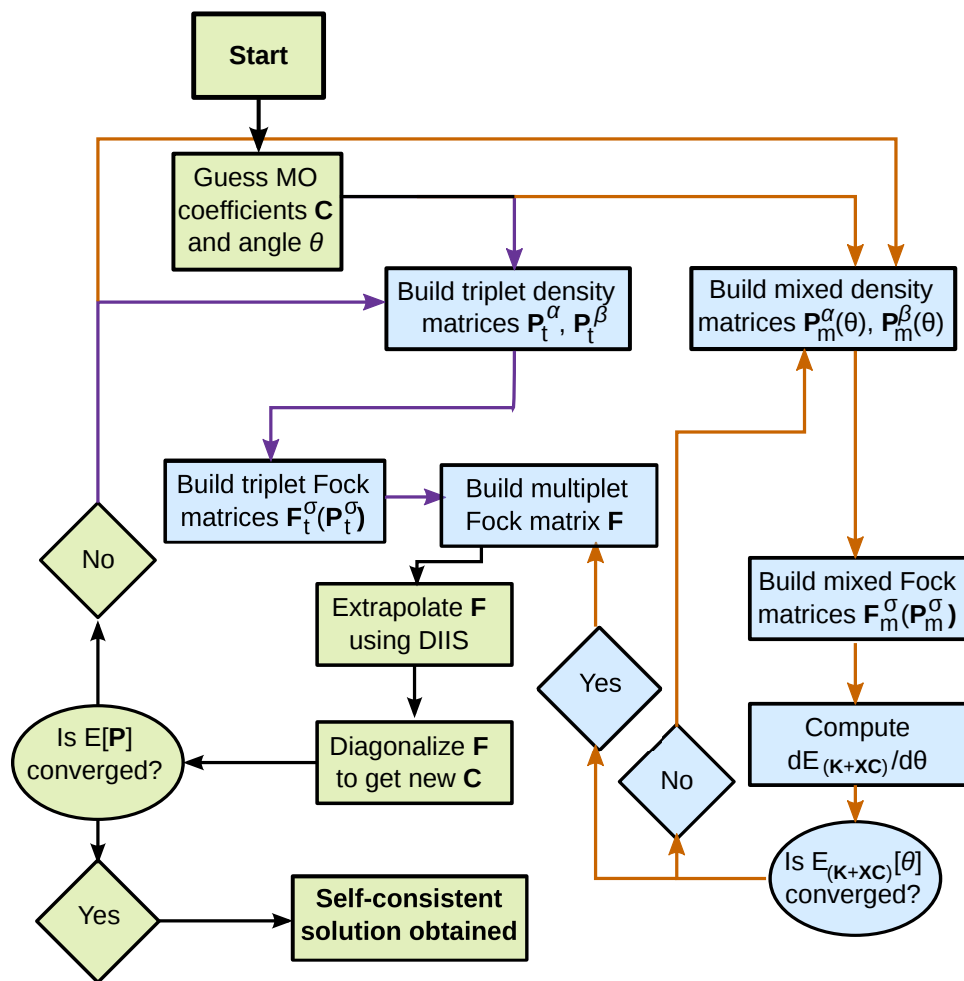


Figure 5-2: Two-layer SCF algorithm for obtaining an ROKS energy which is variational with respect to both the density matrix and the open-shell mixing angle.

Fock matrix.

Lacking an analytical expression for $E[\theta]$, we perform the one-dimensional optimization of $E[\theta]$ numerically within each SCF cycle. The resulting two-layer SCF procedure for ROKS is summarized in Figure 5-2. We use a simple Newton-Raphson scheme for the θ -optimization. As we will see in Section 5.4, a Fourier series approximation to $E[\theta]$ may potentially be more expedient for this one-dimensional optimization than a quadratic approximation; but in practice we find that these θ -microiterations converge quite rapidly (typically 3-10 microiterations during the first SCF iteration, and only 1-3 corrective microiterations per SCF cycle afterward).

It is trivial to modify our algorithm to enforce a fixed θ throughout the calculation.

We will refer to ROKS orbitals with fixed $\theta = 0$, equivalent to not applying any θ -dependent correction, as “canonical” ROKS orbitals.

5.3 Computational details

The ROKS algorithm outlined above was implemented in a development version of the Q-CHEM 4.0 software package¹¹¹ for S_1 and T_1 excited states of molecules with closed-shell singlet ground states. A standard DIIS procedure was used to accelerate convergence.³⁰⁵ Occasionally for the larger systems, virtual orbitals crossed into the energy domain of the open shell orbitals. To converge the orbitals in these cases, we introduced a level shift procedure³⁰⁶ to force the virtual orbitals away from the open-shell orbitals energetically. Fortunately, these level shifts did not significantly increase the number of SCF cycles necessary to achieve convergence.

Geometries for the small-dye test set of Schreiber *et al.* at the MP2/6-31G* level were obtained directly from Ref. 236. ROPBE0 vertical excitation energies were also computed with the 6-31G* basis set. The basis set sensitivity of ROKS will be addressed in more detail in Section 5.4.

For the large-dye test set, the same B3LYP/6-31G* optimized geometries employed in Chapter 4 and included in Appendix B were used here. Due to computational constraints, the 6-31G* basis set was also used for ROKS excited state calculations on the large-dye test set.

ROKS, Δ SCF and TDDFT calculations on formalimine were carried out at selected geometries with the PBE0 hybrid functional and the 6-31G* basis set. Bond distances were held fixed at their ground-state values, so the resulting one-dimensional projections of the PES do not represent minimum energy paths; nevertheless, they provide a useful first assessment of how parallel the S_1 PES obtained by these three excited state methods should be.

5.4 Results and Discussion

5.4.1 Canonical and variational ROKS energies of small organic dyes

Molecule	Symmetry	$\theta = 0$	$\theta = \frac{\pi}{4}$	θ_{\min}	θ_{\max}	Best estimate
ethene	$\pi \rightarrow \pi^*$	7.68	4.54	4.54	7.68	7.80
butadiene	$\pi \rightarrow \pi^*$	5.37	3.31	3.31	5.37	6.18
hexatriene	$\pi \rightarrow \pi^*$	4.23	2.67	2.67	4.23	5.10
octatetraene	$\pi \rightarrow \pi^*$	3.54	2.26	2.26	3.54	4.47
cyclopropene	$\pi \rightarrow \pi^*$	6.75	4.35	4.35	6.75	7.06
cyclopentadiene	$\pi \rightarrow \pi^*$	4.97	3.24	3.24	4.97	5.55
norbornadiene	$\pi \rightarrow \pi^*$	4.99	3.93	3.93	4.99	5.34
benzene	$\pi \rightarrow \pi^*$	6.51	4.69	4.69	6.51	5.08
naphthalene	$\pi \rightarrow \pi^*$	4.40	3.27	3.27	4.40	4.24
furan	$\pi \rightarrow \pi^*$	6.09	4.29	4.29	6.09	6.32
pyrrole	$\pi \rightarrow \pi^*$	6.37	4.66	4.66	6.37	6.37
imidazole	$\pi \rightarrow \pi^*$	6.43	4.86	4.86	6.43	6.19
pyridine	$n \rightarrow \pi^*$	4.80	5.34	4.80	5.34	4.59
pyrazine	$\pi \rightarrow \pi^*$	3.98	3.92	3.92	3.98	3.95
pyrimidine	$n \rightarrow \pi^*$	4.34	4.86	4.34	4.86	4.55
pyridazine	$n \rightarrow \pi^*$	3.63	3.80	3.63	3.80	3.78
triazine	$n \rightarrow \pi^*$	4.64	5.51	4.60	5.21	4.60
tetrazine	$\pi \rightarrow \pi^*$	2.22	2.18	2.18	2.22	2.24
formaldehyde	$n \rightarrow \pi^*$	3.67	4.71	3.67	4.71	3.88
acetone	$n \rightarrow \pi^*$	4.10	5.07	4.10	5.07	4.40
benzoquinone	$n \rightarrow \pi^*$	2.46	2.57	2.46	2.57	2.80
formamide	$n \rightarrow \pi^*$	5.48	6.90	5.48	6.90	5.63
acetamide	$n \rightarrow \pi^*$	5.46	6.77	5.46	6.77	5.80
propanamide	$n \rightarrow \pi^*$	5.51	6.74	5.51	6.74	5.72
cytosine	$\pi \rightarrow \pi^*$	4.63	4.20	4.19	4.74	4.66
thymine	$\pi \rightarrow \pi^*$	4.96	3.87	3.87	4.96	4.82
uracil	$\pi \rightarrow \pi^*$	5.06	4.10	4.10	5.10	4.80
adenine	$\pi \rightarrow \pi^*$	4.94	4.03	4.03	4.94	5.25

Table 5.1: Dependence of the ROPBE0/6-31G* excitation energy (in eV) on the prescription for the open-shell mixing angle for a collection of small organic dyes.

First we consider how the different prescriptions for the open-shell mixing angle affect vertical excitation energies. For this purpose we introduce the set of 28 small organic dyes for which low-lying excited state energies were recently benchmarked

by Schreiber *et al.* with high-level wavefunction methods.²³⁶ Four prescriptions for the mixing angle are assessed: two fixed-angle prescriptions ($\theta = 0$, no mixing; and $\theta = \pi/4$, complete mixing) and two variational prescriptions (minimization and maximization of the energy with respect to θ). ROKS vertical excitation energies for the $S_0 \rightarrow S_1$ transition in each dye are collected in Table 5.1. Note that the ordering of excited states in ROKS may differ from that of the wavefunction methods used to obtain the “best estimates” in Table 5.1; in all cases the best estimate for the state most closely representative of the ROKS S_1 state was used.

It is clear from Table 5.1 that each variational approach coincides (or nearly coincides) with one of the fixed-angle approaches. However, the particular pairing depends on the symmetry of the electronic transition: for $\pi \rightarrow \pi^*$ transitions, the canonical choice $\theta = 0$ maximizes the ROKS energy along the mixing angle, while for $n \rightarrow \pi^*$ transitions, $\theta = 0$ minimizes the ROKS energy. These results corroborate the observations of Hutter and coworkers for a related set of organic dyes;²⁹⁸ however, it is interesting to note that the fixed-angle excitation energy and the corresponding variational excitation energy can vary by up to about 0.1 eV. This disagreement seems to be more common in the larger dyes, where minimization and maximization of $E[\theta]$ give optimal θ slightly different from 0 and $\pi/4$. These differences are on the order of 0.01–0.1 radians.

Rather unexpectedly, we find that the canonical ROKS orbitals always provide the more accurate excitation energy, regardless of the symmetry of the transition and regardless of whether these orbitals represent a minimum or a maximum along the mixing angle. This is very encouraging from a practical perspective, as it suggests that within the density-matrix approach to ROKS, a single convergence strategy will work for any system (provided, of course, that the $S_0 \rightarrow S_1$ transition is well-described by a single-orbital excitation).

Regarding accuracy, ROPBE0 tends to underestimate the excitation energy of $\pi \rightarrow \pi^*$ transitions and to overestimate that of $n \rightarrow \pi^*$ transitions. This trend is weakly evident in Table 5.1 but is more exaggerated for $\pi \rightarrow \pi^*$ transitions in the more complete 6-311+G* basis set (see Appendix A): adding diffuse functions tends

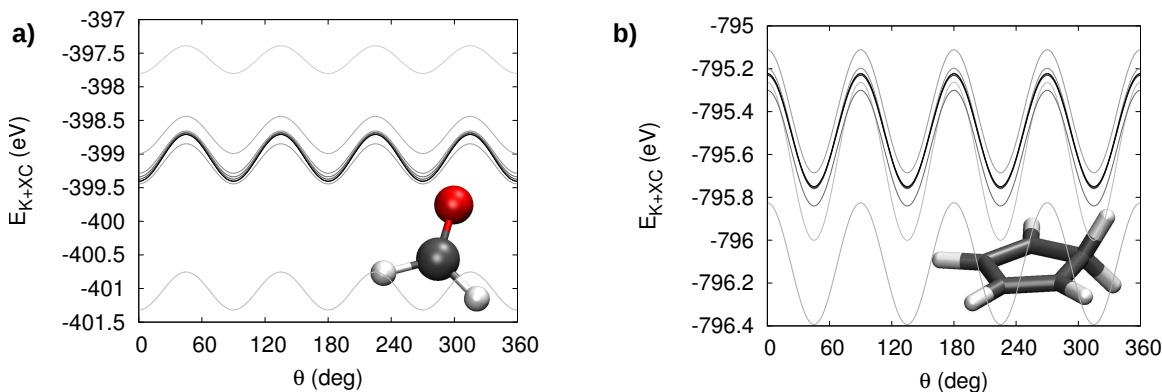


Figure 5-3: Dependence of the exchange and XC contributions to the ROKS energy on θ for (a) the lowest $n \rightarrow \pi^*$ excitation in formaldehyde and (b) the lowest $\pi \rightarrow \pi^*$ excitation in cyclopentadiene. The darkness of each curve indicates the SCF iteration at which the scan took place, with darker curves representing later SCF iterations.

to lower the ROKS excitation energy for these transitions. Others have suggested that the underestimation of $\pi \rightarrow \pi^*$ excitation energies in ROKS may be largely due to the use of LDA and GGA functionals,²⁹⁵ but our results suggest that hybrid functionals do not substantially correct this behavior. We also studied these transitions with the long-range corrected LC- ω PBE functional and found that this underestimation persists (see Appendix A).

Given that $E[\theta]$ must be periodic with period $\pi/2$ — and given that $\theta = 0$ and $\theta = \pi/4$ tend to represent its critical points in the $[0, \pi/2]$ interval — it is worth examining $E[\theta]$ in more detail to confirm the presence or absence of other local extrema. In Figure 5-3, we plot the explicit dependence of the ROKS energy on the mixing angle for the $n \rightarrow \pi^*$ transition in formaldehyde and for the $\pi \rightarrow \pi^*$ transition in cyclopentadiene. The energy is indeed a sinusoidal function of θ with period $\pi/2$, in agreement with the results of Hutter and coworkers.²⁹⁸ To better understand whether the angular dependence of the energy changes according to the quality of the current set of KS orbitals, Figure 5-3 shows $E[\theta]$ at every SCF macroiteration from the ground-state orbital guess through convergence. For both test cases, we see no variation in the shape of $E[\theta]$, only in its energetic offset.

Having established the efficacy of using canonical orbitals to obtain ROKS excitation energies, we proceed to benchmark ROKS for the test set of larger dyes

introduced in Chapter 4.

5.4.2 ROKS vertical excitation energies of large organic dyes

We evaluated ROKS vertical excitation energies for the large dye test set of Chapter 4 using a variety of XC functionals, many of which were also used in the Δ SCF benchmarking study.¹³⁹ We also include results obtained within the local density approximation (LDA) to facilitate comparison with previous ROKS studies which have relied heavily on this functional. The Minnesota functionals M06-2X and M06-HF were excluded from this study because our current implementation of ROKS does not support kinetic energy density-dependent functionals.

Functional	Mean Error	MAE	RMSD
LDA	-0.56	0.57	0.66
BLYP	-0.55	0.56	0.65
PBE	-0.53	0.55	0.64
B3LYP	-0.16	0.29	0.35
PBE0	-0.04	0.26	0.32
BH&HLYP	0.43	0.43	0.51
LC- ω PBE	0.08	0.23	0.28
LC- ω PBE0	0.40	0.40	0.47
ω B97	0.91	0.91	0.94
ω B97-X	0.79	0.79	0.82

Table 5.2: Deviations of ROKS excitation energies from experiment for the test set of larger organic dyes (in eV). The canonical open-shell mixing angle ($\theta = 0$) and 6-31G* basis set were used for each constituent calculation. Functionals are arranged in order of increasing degree of exact exchange, to the extent possible.

Performance statistics across the large-dye test set are reported in Table 5.2. In parallel with the Δ SCF results in Chapter 4, hybrid functionals with a modest fraction of exact exchange are most successful at reproducing the experimental excitation energies. In particular, ROPBE0 achieves approximately the same 0.3 eV accuracy obtained with Δ PBE0 and with TD-PBE0. Although the LC- ω PBE0 functional does not perform as well for ROKS as it did for Δ SCF and TDDFT, we find that the simpler range-corrected GGA, LC- ω PBE, performs quite well for ROKS excitation energies on this test set. However, note that the mean error (ME) and root-mean-square

deviations (RMSD) for LC- ω PBE0 are of similar magnitude. Given the tendency, observed in the smaller organic dyes, for additional diffuse basis functions to lower the predicted excitation energy by 0.1 eV or more, we suspect that using a more complete basis set would significantly reduce both the ME and RMSD of the LC- ω PBE0 excitation energies to more favorable values, while adversely affecting the performance of PBE0 to some extent.

Next we move away from ground-state equilibrium geometries and consider how ROKS excitation energies compare with Δ SCF and TDDFT away from the Franck-Condon region.

5.4.3 Comparison of potential energy surfaces from ROKS, Δ SCF and TDDFT

As one of the simplest meaningful model chromophores for isomerization of retinal, formalimine and its excited states have been the subject of several theoretical investigations.^{282,307,308} A *cis-trans* isomerization about the C=N double bond can take place entirely in-plane via rotation of the C-N-H bond angle ϕ ; entirely out-of-plane via rotation of the H-C-N-H dihedral angle ϑ ; or through any linear combination of these two motions.³⁰⁷ Here we study the variation of ROKS, Δ SCF and TDDFT excitation energies along two one-dimensional cuts of the (ϑ, ϕ) PES. It should be stressed that these calculations are not intended to faithfully reproduce minimum-energy paths along either the ground- or excited-state adiabatic PES, but rather to compare how parallel the different descriptions of the S_1 state remain as the geometry is distorted from equilibrium.

The S_0 and S_1 torsional profiles of formalimine presented in Figure 5-4a show the same qualitative behavior observed in previous multireference configuration interaction and diffusion Monte Carlo studies,^{307,308} although differences in the employed geometries make a direct comparison difficult to quantify. All of the excited state DFT methods predict the same general shape for the S_1 PES along this coordinate and along the bond angle in Figure 5-4b, with two notable exceptions. First, Δ SCF

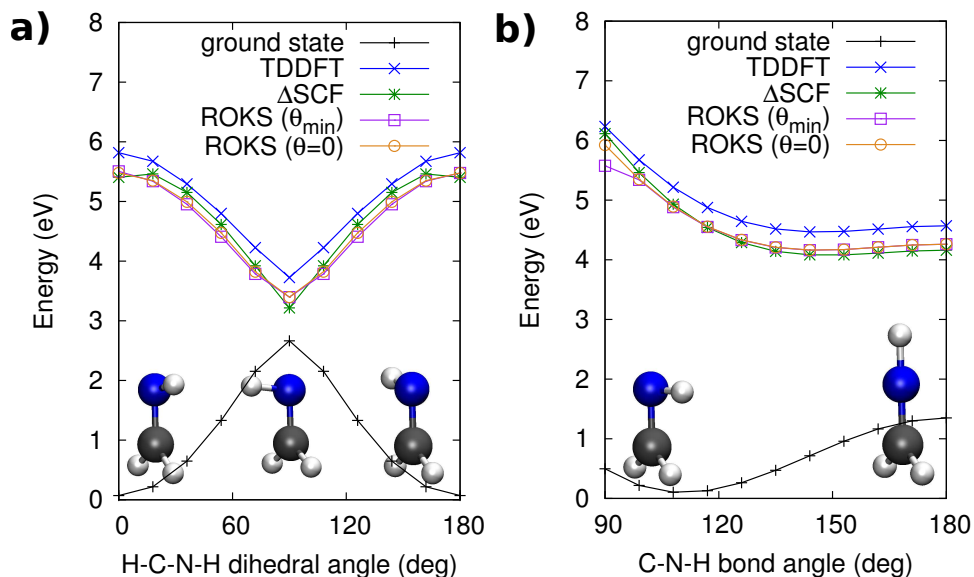


Figure 5-4: Potential energy curves for the S_0 and S_1 states of formaldehyde along (a) the purely out-of-plane isomerization pathway and (b) the purely in-plane isomerization pathway. The PBE0 functional and 6-31G* basis set were used for all constituent calculations.

predicts a small barrier to excited-state isomerization through the out-of-plane pathway (approximately 1 kcal/mol) while the other methods suggest a barrierless process, which was also inferred from ROKS-MD simulations on formaldehyde.²⁸² The second noteworthy difference between the curves concerns the ROKS open-shell mixing angle.

In general, the “canonical” ($\theta = 0$) and variational (θ_{\min}) ROKS excited state profiles are in very good agreement with one another. However, as the C–N–H angle approaches 90° , the variational approach predicts a lower excitation energy than the canonical approach by more than 0.3 eV, deviating also from the profile predicted by the other methods. This difference suggests that the distortion of the $S_0 \rightarrow S_1$ transition symmetry, induced by the close approach of the NH proton to the double bond, permits the same kind of artificial open-shell orbital mixing that arises in $\pi \rightarrow \pi^*$ states during full energy minimization. Fortunately, the canonical ROKS profile is in agreement with the other methods. Thus, for strained or highly asymmetric systems for which the symmetry of the transition is not clear, it seems that the canonical ROKS approach can still provide a reliable energy profile for the S_1 state.

Although the TDDFT predictions are uniformly higher than those of Δ SCF or ROKS, the curves obtained from the three methods are sufficiently parallel to justify the use of hybrid protocols where one of the methods is used for configurational sampling and another method is used to compute excitation energies. In fact, for the formalimine PES, we see no clear reason to prefer any one of these methods over the others.

In generating these potential energy curves, we found further evidence that the variational collapse problem of Δ SCF is a true hindrance in practical applications, not just a theoretical curiosity. Using a standard non-Aufbau occupation procedure,¹³⁹ more than half of the Δ SCF states in our PES scan collapsed to the ground state prior to convergence. Many of these collapsed states could be stabilized with MOM, but for several geometries, neither of these strategies were sufficient. Ultimately, we converged these final states by using Δ SCF states obtained with a simpler XC functional as an initial guess, and *then* applying MOM after a non-zero number of SCF iterations with the target XC functional. These convergence difficulties would clearly not be acceptable for MD simulations on Δ SCF states. Fortunately for equilibrium dynamics, convergence problems tend to occur less frequently for near-equilibrium geometries; however, they would present serious challenges for reactive dynamics. Conversely, ROKS converged rapidly to the state of interest for every point examined on the PES.

5.5 Conclusion

This study was motivated by the need for accurate, efficient excited state electronic structure methods for our ongoing studies of the electronic properties of organic semiconductors. We turned to the ROKS approach as a means of obtaining Δ SCF-like states without the specter of variational collapse; however, ROKS presents a different complication, the dependence of the energy on mixing between the two open shells.

We have presented and implemented an algorithm for solving the ROKS equations which forces the ROKS energy to be variational with respect to the open-shell mixing

angle. Encouragingly, we find that a single convergence strategy — a density-matrix approach using “canonical” ROKS orbitals — can deliver the proper ROKS excitation energy, regardless of whether the canonical orbitals represent a minimum or a maximum along the open-shell orbital mixing angle. As illustrated by the formalimine excited state profiles, extremizing the energy with respect to the open-shell mixing angle, while appealing from a theoretical standpoint, can lead to collapse to roughly the energy of the T_1 state if the symmetry of the transition changes along the reaction coordinate of interest. If a variational treatment is necessary, one could envision a strategy in which a composite ROKS energy expression of the form

$$E_{\text{ROKS}}[\{\phi_i\}] = cE_{\text{ROKS}}[\{\phi_i\}, \theta = \theta_{\text{min}}] + (1 - c)E_{\text{ROKS}}[\{\phi_i\}, \theta = \theta_{\text{max}}]$$

where the choice of the coefficient c would be tied to some measure of the symmetry of the transition.

Of pressing interest for future work is the implementation of gradients for the canonical and variational ROKS strategies. While the Hellmann-Feynman theorem should hold for the variationally optimized ROKS energy, additional terms may be necessary to obtain gradients for the canonical prescription. Currently, ROHF Hellmann-Feynman gradients have been implemented and agree with forces computed by finite difference, but ROKS gradients remain work in progress. Once gradients are implemented and validated, we expect ROKS to be a handy tool in our electronic structure toolkit for fast excited state MD simulations of large systems.

Chapter 6

Conclusion

Theoretical and computational models are a valuable asset for understanding the behavior of electronically excited states in the condensed phase. We have employed several methods based on DFT to characterize electronic excitations and charge transfer in a simple donor-acceptor dyad (FAAQ) and in a designer metal-ion sensor (ZP1). Furthermore, we investigated the applicability of additional DFT-based strategies for excited states — the Δ SCF and ROKS approaches — and addressed a potential pathology of the latter method by extremizing the energy with respect to a parameter describing mixing between the open shells.

The hybrid CDFT + explicit solvent model presented in Chapter 2 allowed us to predict the driving force, reorganization energy, and electronic coupling associated with charge recombination in the FAAQ dyad. The reorganization energy in particular is highly sensitive to solvent effects, yet our model’s prediction agrees with the experimentally inferred value to within the error bars of our DFT method. We also presented the first CDFT calculations of electronic couplings for an asymmetric ET system in solution; although our predicted couplings are too large, their strong solute conformation dependence suggests that the assumption of a constant coupling along the ET reaction coordinate is not justified for this dyad. Meanwhile, our computational analysis of ET in the Zinpyr-1 zinc sensor demonstrated an electronic state-reordering governing the Zn^{2+} -mediated fluorescence activation and predicted the direct involvement of both amino and pyridyl nitrogen lone pair density in the

ET process. Our computational work on ZP1³⁰⁹ led to a follow-up kinetic modeling study to predict the zinc-binding affinities necessary to achieve a desired degree of fluorescence turn-on in future ratiometric sensors. These preliminary efforts were later extended by the Lippard group and have been directly used in their sensor design efforts.³¹⁰

Our assessment of the Δ SCF approach in Chapter 4 demonstrated that excitation energies of large organic chromophores can be predicted with anticipated errors of roughly 0.3 eV with the best hybrid functionals. This level of accuracy is commensurate with that of linear response TDDFT, so we consider Δ SCF to be a viable excited state DFT method for future characterization and simulations of organic semiconductor materials. Likewise, our density-matrix based implementation of the ROKS equations seems to provide a robust avenue to S_1 excited states that are quantitatively similar to Δ SCF states but avoid the risk of variational collapse to the ground state.

While providing answers to some important questions, this research raises additional questions and thus provides some direction for future work. On the applications side, it would be very interesting to extend the CDFT/MMpol approach to more complex ET systems like donor-bridge-acceptor systems, and to include additional electronic states in the analysis. In order to achieve longer timescales for MD configurational sampling, one could employ a force-matched MM model for the dynamics but retain a QM description for the energy gap. This approach would require a re-weighting of the QM energy gaps to reflect the fact that the snapshots are obtained from a different ensemble (the MM ensemble). In our experience, these re-weighting schemes tend to reject most of the QM data because $E_{\text{QM}} - E_{\text{MM}}$ frequently exceeds the thermal energy. We are optimistic that a cumulant re-weighting scheme currently under investigation might improve the outlook for using MM configurational sampling in multi-state ET simulations.

Another area where our computational tools for ET should prove useful is in condensed phase electrochemistry. We are actively modeling the catalytic cycle of a cobalt-oxide water oxidation catalyst,⁹ where four proton-coupled ET reactions

facilitate the transformation of water into hydrogen and oxygen gas. Furthermore, we are beginning to develop strategies for calculating Tafel slopes for metal-oxide redox chemistry from first principles.

An important next step for putting excited state DFT to good use is to parameterize approximate Hamiltonians for exact quantum dynamics in the condensed phase. In this scheme, the goal is to extract system-specific spectral densities from time-correlation functions, which in turn are calculated from ground- and excited-state DFT molecular dynamics simulations. These models can then be used to propagate quantum dynamics using, for example, path integral methods, or the generalized Langevin approach developed in our group.¹⁴⁷

On the fundamental theoretical side, the relationship between Δ SCF and TDDFT raises the question of precisely how making the adiabatic approximation affects excitation energies from the two methods. XC kernels with memory, which could be used to study this question, exist for TDDFT; but it is not clear how the effect of the adiabatic approximation could be studied within Δ SCF. There are also lingering fundamental questions concerning how to optimally define constraints in CDFT for modestly-separated donor-acceptor systems.¹⁹⁹ While we have been considering novel atomic population schemes as a way to approach this problem, it could turn out that a more general strategy such as partition density functional theory³¹¹ will provide a better way forward.

Regarding future directions in methodology for excited states, one would ideally like to develop methods that are simultaneously faster and more accurate than those discussed here. In the absence of a clear path towards this goal, two more modest but complementary strategies should be considered: (1) improve accuracy without sacrificing too much computational efficiency, and (2) make the calculations faster without sacrificing too much accuracy. We are pursuing a method in the first category as an extension of the Δ SCF study. The goal is to describe ground and excited states on the same footing by constructing a small configuration interaction problem in a basis of Δ -Hartree-Fock states with a first-order wavefunction correction from Møller-Plesset perturbation theory. This Δ SCF(2) method is slower than Δ SCF-DFT

(scaling as N^5) but (we hope) should prove to be more accurate. In the direction of faster calculations with comparable accuracy to the methods described in this thesis, a promising next step is to extend some of these excited state DFT strategies to semiempirical frameworks such as density functional tight-binding (DFTB).³¹² If excited state DFTB methods can be parameterized to achieve something close to the accuracy of the analogous excited state DFT methods, then excited state DFTB-MD will have a lot to teach us about the electronic properties and dynamics of organic semiconductors and other advanced materials in the condensed phase.

Appendix A

Energies of key structures

A.1 ZP1 vertical excitation energies

Below we tabulate relevant CIS, TDDFT and CDFT vertical excitation energies for the various structures of ZP1 identified in Figure 3-2. All excitation energies are reported in eV. LE denotes a locally excited state on the xanthone chromophore, while CT denotes a charge-transfer excited state from DPA arm to DCF body.

Structure	CIS ^a	TDDFT ^b	TDDFT ^c	CDFT ^d
2			2.75 (CT1)	
			2.90 (LE)	
			3.06	
4	3.78 (LE)	1.75	2.86 (LE)	5.34
	5.15	1.84	2.89	
		2.06	3.17	
			3.20	
5	4.07 (LE)	1.79 (CT1)	2.44 (CT1)	3.00
	5.14	2.02	2.92 (LE)	
		2.16	3.03	
			3.13 (CT2)	
6	4.25 (LE)	1.60	3.02 (LE)	5.74
	4.80	1.94 (LE)	3.05	
		2.32	3.11	
			3.24 (CT1)	
			3.27 (CT2)	
7	3.86	2.30 (CT1)	2.21 (CT1)	2.39
	4.95	2.81 (LE)	2.85 (LE)	
		2.97 (CT2)	2.90 (CT2)	
8	4.03		2.84 (CT)	4.51
	5.05		2.92 (LE)	
9	4.02		2.33 (CT)	3.59
	4.54		2.89 (LE)	
10	3.92 (LE)		2.92 (LE)	4.46
	4.76		3.06	
			3.14 (CT)	
11	3.84 (LE)	2.62 (0.0097)	2.87 (0.5631)	7.74
	4.94	2.80 (0.0211)	3.20 (0.0036)	
		2.86 (0.5146)	3.41 (0.0049)	

Table A.1: Lowest vertical excitation energies for ZP1 structures **2** and **4–11**, in eV. Methods: ^aCIS/SV(P)/gas-phase; ^bTD-B3LYP/SV(P)/gas-phase; ^cTD-B3LYP/SV(P)/COSMO; ^dCB3LYP/SV(P)/SCRf.

A.2 ROKS excitation energies: small dye test set

Molecule	PBE0		LC- ω PBE		Best estimate
	$\theta = 0$	$\theta = \frac{\pi}{4}$	$\theta = 0$	$\theta = \frac{\pi}{4}$	
ethene	7.14	4.50	6.76	4.64	7.80
butadiene	5.15	3.29	4.89	3.32	6.18
hexatriene	4.12	2.66	4.00	2.64	5.10
octatetraene	3.47	2.26	3.48	2.24	4.47
cyclopropene	6.24	4.25	5.83	4.31	7.06
cyclopentadiene	4.83	3.23	4.51	3.27	5.55
norbornadiene	4.76	3.85	4.49	3.77	5.34
benzene	6.28	4.63	5.89	4.60	5.08
furan	5.78	4.18	5.49	4.26	6.32
pyrrole	5.27	6.28	5.71	4.59	6.37
imidazole	5.76	6.81	5.88	4.79	6.19
pyridine	4.72	5.25	4.58	4.93	4.59
pyrazine	3.92	3.87	3.58	3.53	3.95
pyrimidine	4.29	4.79	3.98	4.35	4.55
pyridazine	3.58	3.75	3.30	3.46	3.78
triazine	4.62	5.31	4.26	4.73	4.60
tetrazine	2.21	2.16	2.24		2.24
formaldehyde	3.59	4.57	3.64	4.34	3.88
acetone	4.08	5.03	4.40		4.40
benzoquinone	2.49	2.60	2.14	2.20	2.80
formamide	6.99	8.85	5.49	6.43	5.63
acetamide	6.55	8.37	5.48	6.37	5.80
propanamide	6.52	8.15	5.50	6.32	5.72
cytosine	4.58	4.13	4.30	4.01	4.66
thymine	4.81	3.79	4.48	3.72	4.82
uracil	4.96	4.05	4.63	3.96	4.80
adenine	4.82	3.98	4.53	3.84	5.25

Table A.2: Dependence of the ROKS PBE0/6-311+G* and LC- ω PBE/6-311+G* excitation energies (in eV) on the open-shell mixing angle for the same test set of Table 5.1. Naphthalene is omitted due to convergence difficulties.

Appendix B

Optimized geometries of key structures

The geometries are provided in .xyz format. All coordinates are specified in Å.

B.1 Protonation and zinc-binding states of ZP1

All geometries are optimized at the B3LYP/SV(P) level in COSMO water ($\epsilon = 80$) solution. Refer to Figure 3-2 for definitions of the bold-faced structure labels below.

Structure **2** (deprotonated relative to Figure 3-2):

```
100
ZP1 structure 2
Cl    -1.3427989    -4.9336680     1.3505239
Cl     7.1623441     0.6940560    -0.7194417
O     4.1751111    -5.3558594    -2.4711543
O     5.0829655     2.7162624    -1.2557708
O     1.3140164    -0.0266640    -0.4966919
O    -2.6263488    -2.4099915     0.6846059
C     3.7732486    -4.4011464    -1.7659569
C     4.1894292    -4.3972612    -0.2884465
C     4.9868151    -5.4369169     0.2130584
C     5.3901382    -5.4645161     1.5502826
C     4.9939528    -4.4337276     2.4112271
C     4.2002155    -3.3890985     1.9263418
C     3.7914458    -3.3598880     0.5800642
C     2.9356480    -2.2155374     0.1324105
C     3.5106798    -0.9843138    -0.2128917
```

C	4.9251855	-0.7707030	-0.2878318
C	5.4276671	0.4466008	-0.6389458
C	4.5875284	1.6142845	-0.9585904
C	3.1488295	1.3772514	-0.8987814
C	2.6672405	0.1318813	-0.5363673
C	0.7167657	-1.1767236	-0.0861348
C	-0.6833702	-1.1647687	0.0072116
C	-1.3583264	-2.3318554	0.5027862
C	-0.5303990	-3.4833893	0.7928113
C	0.8368687	-3.4724575	0.6749243
C	1.5137550	-2.3034751	0.2426948
H	5.2815785	-6.2244963	-0.4855554
H	6.0128496	-6.2848181	1.9223616
H	5.3021607	-4.4394180	3.4617571
H	3.8923300	-2.5845221	2.6020805
H	5.5989621	-1.5980101	-0.0589605
H	1.4116549	-4.3658332	0.9230537
O	3.0595963	-3.4355211	-2.1361452
C	2.2296790	2.5201505	-1.2619437
C	0.3986559	3.9932048	-0.5609665
C	0.8600846	5.2852378	-1.2249825
C	0.9457693	5.3973906	-2.6232233
C	1.4071866	6.5891474	-3.1884020
C	1.7728143	7.6372223	-2.3389799
C	1.6525290	7.4371661	-0.9595173
C	2.2089244	3.5019517	1.0291684
C	1.4533688	3.2936693	2.3355750
C	0.4430948	2.3261824	2.4508094
C	-0.1949599	2.1443082	3.6790810
C	0.2034122	2.9318078	4.7644090
C	1.2226770	3.8675190	4.5556279
C	-1.4138315	0.1230527	-0.3319881
C	-3.3204421	1.2875121	-1.3160455
C	-4.1826878	1.8727418	-0.2118234
C	-4.3973041	3.2521339	-0.1119517
C	-5.2846835	3.7330456	0.8528003
C	-5.9289786	2.8236762	1.6984926
C	-5.6476920	1.4676736	1.5475183
C	-2.7330726	-0.9143536	-2.1695484
C	-4.1105135	-1.4999057	-2.4242714
C	-4.5240662	-1.8589926	-3.7114900
C	-5.7731789	-2.4604207	-3.8813273
C	-6.5772697	-2.6822414	-2.7593320
C	-6.0961510	-2.2851086	-1.5126709
H	0.1760857	1.7414650	1.5691105
H	-0.9925007	1.3999799	3.7806094
H	-0.2636116	2.8307259	5.7485044
H	1.5602989	4.5047959	5.3840330
H	-3.8710509	-1.6671826	-4.5671715
H	-6.1160270	-2.7488022	-4.8795009
H	-7.5618403	-3.1491245	-2.8427388
H	-6.6911558	-2.4390543	-0.6077916
N	1.4594922	3.0759985	-0.1415785
N	-2.7323195	-0.0262650	-0.9972362

N	1.2073565	6.3002079	-0.4129051
N	-4.7996073	1.0097387	0.6120845
H	2.8550850	3.2861521	-1.7616524
H	1.4865516	2.1688718	-2.0018131
H	-0.1962382	4.2597435	0.3297235
H	-0.2638118	3.4485453	-1.2589548
H	0.6459511	4.5601155	-3.2607304
H	1.4767334	6.6981621	-4.2756309
H	2.1373557	8.5911436	-2.7313090
H	1.9244133	8.2406305	-0.2619211
H	2.5334965	4.5612089	0.9917313
H	3.1313353	2.8965232	1.0796185
H	-1.6026758	0.6944333	0.5953233
H	-0.7524205	0.7459351	-0.9588714
H	-3.9717873	1.1676380	-2.1993365
H	-2.5387868	2.0134972	-1.6092820
H	-3.8778440	3.9371978	-0.7875212
H	-5.4679388	4.8075213	0.9464863
H	-6.6295748	3.1555492	2.4686812
H	-6.1097497	0.7172172	2.1967940
H	-2.0346618	-1.7444919	-1.9746549
H	-2.3644074	-0.4005376	-3.0770040
H	-3.5878849	0.0446245	3.1609397
O	-3.0600915	-0.3680074	2.4522952
H	-2.6304452	-1.1428935	2.8608807
Zn	-4.0380039	-0.9823939	0.5127237
H	-6.4709327	-1.8341802	1.6383627
O	-5.5026514	-1.8606517	1.7460696
H	-5.3003338	-2.6673932	2.2568203
N	1.8302141	4.0522769	3.3770758
N	-4.8963104	-1.7078513	-1.3511102

Structure 4:

93

ZP1 structure 4

H	4.5069419	-1.3103825	-2.7858630
H	5.5675292	-3.1008130	-4.1896911
H	6.1420497	-5.3080936	-3.0924574
H	5.6435721	-5.5889099	-0.6568607
C	4.5162475	-2.5258795	-0.9895256
C	4.7716165	-2.2771585	-2.3472486
C	5.3616325	-3.2745738	-3.1287247
C	5.6792413	-4.4941131	-2.5270715
C	5.3954144	-4.6470748	-1.1647189
N	4.8356817	-3.6956524	-0.4131622
H	3.0403943	1.1443311	2.9584106
H	4.2279790	0.8974632	5.1536294
H	4.6419829	-1.4301441	6.0525544
H	3.8353969	-3.3815715	4.7095607
C	2.8328438	-1.0049656	2.6820498
C	3.2451415	0.1500556	3.3701531
C	3.8991613	0.0131847	4.5979439
C	4.1301082	-1.2702846	5.0992329
C	3.6790427	-2.3578494	4.3430152

N	3.0454978	-2.2357960	3.1729602
C	3.8884158	-1.4691703	-0.0997379
H	4.5089125	-1.3974048	0.8086619
H	3.9449457	-0.4810445	-0.6170859
C	2.0713909	-0.8844282	1.3727120
H	1.0152015	-1.1303210	1.5814999
H	2.0921438	0.1821468	1.0552242
N	2.5235641	-1.7766907	0.3153968
C	1.6054317	-1.8138237	-0.8359363
H	2.0225717	-2.5483949	-1.5431009
H	1.5761610	-0.8274669	-1.3490950
C	-0.8684389	-1.3880294	-0.4209952
C	0.2068460	-2.2613724	-0.4941838
C	0.0158185	-3.6879194	-0.2581546
C	-1.3426129	-4.0668598	0.1518561
C	-2.3759606	-3.1797245	0.2606203
C	-2.1861755	-1.7959886	-0.0336403
O	0.9243211	-4.5249121	-0.4110806
Cl	-1.6098889	-5.7732193	0.4879642
H	-3.3665860	-3.5269285	0.5587767
C	-3.2265617	-0.8443711	0.0202199
C	-5.6393849	-1.6682148	-0.2443450
C	-6.8604700	-1.9939150	0.3669355
C	-7.0400577	-1.8885929	1.7476132
C	-5.9789606	-1.4478478	2.5469929
C	-4.7559615	-1.1193083	1.9547559
C	-4.5706639	-1.2238161	0.5633594
C	-5.5095952	-1.8058972	-1.7707344
O	-6.5270098	-2.2010951	-2.3903010
O	-4.3955805	-1.5104170	-2.2645775
H	-7.6684124	-2.3342692	-0.2855169
H	-8.0022830	-2.1481326	2.2009852
H	-6.1004534	-1.3581337	3.6312216
H	-3.9277784	-0.7736825	2.5816982
O	-0.6422212	-0.0760059	-0.7295481
C	-2.9480771	0.5003325	-0.3085546
C	-3.9368576	1.5287920	-0.2953966
C	-3.6351585	2.7962464	-0.7085011
C	-2.3146359	3.1936873	-1.2064119
C	-1.3059870	2.1415079	-1.1795928
C	-1.6321878	0.8672878	-0.7401481
H	-4.9483780	1.2879798	0.0360807
Cl	-4.8754879	4.0439375	-0.6953738
O	-2.0812940	4.3409062	-1.6371430
C	0.0593607	2.5146322	-1.7083034
H	0.6400740	1.6001030	-1.9462453
H	-0.0988604	3.0560959	-2.6565792
N	0.7922194	3.4307957	-0.8336114
C	1.7318286	4.3193275	-1.5097066
H	2.1274257	5.0313741	-0.7645232
H	1.1674324	4.8990077	-2.2610182
C	2.9132352	3.6314659	-2.1826613
C	2.8898584	3.3146456	-3.5516888
C	3.9758425	2.6444603	-4.1196874

C	5.0562436	2.3032998	-3.3012277
C	4.9943935	2.6598786	-1.9498838
N	3.9610277	3.3087271	-1.4025252
H	2.0305482	3.6005380	-4.1654722
H	3.9799176	2.3957309	-5.1856964
H	5.9319993	1.7816108	-3.6976816
H	5.8287735	2.4166365	-1.2789454
C	1.2336897	2.8944549	0.4369773
H	2.2698551	2.5016853	0.4145393
H	0.5834243	2.0370837	0.6863304
C	1.1350488	3.8833108	1.5890523
C	1.8465841	4.4681000	3.7019008
C	0.9659336	5.5518116	3.7710261
C	0.1329934	5.7915446	2.6729424
C	0.2159786	4.9451802	1.5654310
N	1.9356283	3.6563083	2.6423364
H	2.5164740	4.2485645	4.5435924
H	0.9386267	6.1877956	4.6604618
H	-0.5740844	6.6276219	2.6821284
H	-0.4123216	5.0802313	0.6808667

Structure 5:

94

ZP1 structure 5

H	6.7346855	-0.7683862	-1.8741958
H	7.8634844	-2.7863765	-2.8398109
H	6.7215430	-5.0342754	-2.6332475
H	4.4970205	-5.1299670	-1.4685418
C	5.0374503	-1.9030211	-1.1450255
C	6.2723865	-1.7565105	-1.7971031
C	6.8976496	-2.8803173	-2.3344135
C	6.2702817	-4.1276922	-2.2224515
C	5.0395024	-4.1837964	-1.5736182
N	4.4471681	-3.1006570	-1.0480539
H	2.3467038	1.6398160	3.1581852
H	3.4943293	1.4763988	5.3835221
H	5.1376294	-0.4085086	5.7656335
H	5.5518072	-2.0185285	3.8949606
C	3.3528023	-0.1260659	2.3717630
C	3.0663277	0.8371008	3.3589549
C	3.7021240	0.7448483	4.5962049
C	4.6130140	-0.2961847	4.8127709
C	4.8387443	-1.1933782	3.7676965
N	4.2278536	-1.1158058	2.5776432
C	4.3554145	-0.7008243	-0.5173218
H	4.9973593	-0.3642390	0.3120583
H	4.3467973	0.1309927	-1.2611670
C	2.6213987	-0.0370398	1.0395948
H	1.5521429	-0.2196976	1.2467466
H	2.6751275	1.0142174	0.6749114
N	3.0369442	-0.9792545	0.0163064
C	2.0168595	-1.1376091	-1.0266569
H	2.4769572	-1.6756837	-1.8714444
H	1.6844551	-0.1591885	-1.4254329

C	-0.4716229	-1.3834823	-0.5121234
C	0.8204125	-1.9326517	-0.5435299
C	0.9959557	-3.2714546	-0.1145160
C	-0.1516562	-4.0044786	0.3154661
C	-1.4122303	-3.4490786	0.3184799
C	-1.6092652	-2.1133363	-0.0960819
H	3.0062629	-3.3743528	-0.3841733
O	2.1576099	-3.8964042	-0.0859850
Cl	0.0707901	-5.6603364	0.8408112
H	-2.2646162	-4.0457228	0.6443889
C	-2.8995904	-1.4810789	-0.1198599
C	-4.9083774	-3.0283549	-0.3682955
C	-6.0035278	-3.6770219	0.2206111
C	-6.2918344	-3.5251626	1.5787046
C	-5.4775362	-2.7061606	2.3694661
C	-4.3849573	-2.0483105	1.7958156
C	-4.0894553	-2.2032554	0.4295749
C	-4.6201345	-3.2158726	-1.8627279
O	-5.4051248	-3.9436279	-2.5122615
O	-3.6074943	-2.6143518	-2.3008094
H	-6.6217718	-4.3063344	-0.4244492
H	-7.1506292	-4.0401440	2.0207298
H	-5.6916894	-2.5744186	3.4345411
H	-3.7520263	-1.4066896	2.4163475
O	-0.5981399	-0.0877235	-0.8968342
C	-2.9781003	-0.1342040	-0.4768814
C	-4.2107598	0.5990564	-0.4880320
C	-4.2398729	1.9061682	-0.8657291
C	-3.0415613	2.6577394	-1.2809183
C	-1.7923174	1.9036074	-1.2588070
C	-1.7919010	0.5754409	-0.8842971
H	-5.1297762	0.0911420	-0.1929739
Cl	-5.7533480	2.7881886	-0.8835266
O	-3.1014160	3.8469109	-1.6322038
C	-0.5413894	2.6583369	-1.6466399
H	0.2654774	1.9514007	-1.9201450
H	-0.7797547	3.2481220	-2.5474232
N	-0.1219118	3.6142960	-0.6248709
C	0.5294505	4.8105763	-1.1136042
H	0.7433834	5.4616340	-0.2445331
H	-0.1808578	5.3751184	-1.7454799
C	1.8271775	4.6252243	-1.9015588
C	2.1175005	5.4596737	-2.9943589
C	3.3232034	5.2950600	-3.6797637
C	4.2013858	4.2912759	-3.2612471
C	3.8224183	3.5036103	-2.1698139
N	2.6741923	3.6627188	-1.5050681
H	1.4014917	6.2275324	-3.3024988
H	3.5695110	5.9354729	-4.5325113
H	5.1553656	4.1178328	-3.7667729
H	4.4840645	2.7020194	-1.8152260
C	0.3486916	3.0849893	0.6375892
H	1.4497878	3.1203727	0.7278418
H	0.0834201	2.0146668	0.6894436

C	-0.2512835	3.7536954	1.8672315
C	-0.1045432	4.0731563	4.1460017
C	-1.2706943	4.8441862	4.1799134
C	-1.9454030	5.0650613	2.9753156
C	-1.4305995	4.5113800	1.8007029
N	0.3969730	3.5447743	3.0250344
H	0.4527040	3.8771313	5.0711393
H	-1.6341372	5.2580408	5.1246443
H	-2.8635130	5.6610373	2.9522884
H	-1.9195952	4.6449756	0.8330330

Structure 6:

98

ZP1 structure 6

H	-0.6763386	3.6241835	3.6431836
O	-0.8128640	4.2380404	4.3933984
H	-0.7816940	5.0777511	3.8761195
Cl	5.1111321	3.1545154	0.0168728
Cl	-5.1861814	2.6494443	-1.4546053
O	4.7169277	0.3004751	0.3839992
O	0.0227184	0.2340163	-0.2219522
O	-4.6449400	-0.1524819	-0.9109621
C	-0.4386602	5.0649954	1.4130316
H	-0.4033056	7.5668517	0.3297200
H	-0.0914240	8.2026595	-2.0826834
H	0.2321206	6.4072159	-3.7936229
H	0.2448650	4.0206034	-3.1081559
H	2.4604511	4.0951019	-0.4762460
H	-2.6045417	3.8445448	-1.2115272
O	-0.4075955	3.8200721	1.6328103
O	-0.6015007	5.9741579	2.2599586
C	-0.2537657	5.4610831	-0.0420890
C	-0.2597189	6.8037931	-0.4394636
C	-0.0859581	7.1507301	-1.7815919
C	0.0952400	6.1463249	-2.7398970
C	0.1027142	4.8012979	-2.3550393
C	-0.0716538	4.4519262	-1.0056175
C	-0.0560829	3.0065151	-0.6233569
C	1.1783644	2.3374251	-0.3946938
C	2.4245754	3.0160480	-0.3249182
C	3.5809674	2.3229582	-0.0669944
C	3.5738741	0.9049336	0.1435354
C	2.3461614	0.2032273	0.0803263
C	1.1820755	0.9321123	-0.1838136
C	-1.1670364	0.8208561	-0.4928572
C	-2.2851561	-0.0177731	-0.5416170
C	-3.5420334	0.5606113	-0.8435551
C	-3.6231753	1.9714637	-1.0842189
C	-2.5109217	2.7740166	-1.0291400
C	-1.2374458	2.2209256	-0.7272229
H	-4.4481102	-1.1033537	-0.5647538
H	4.5656515	-0.7186606	0.3588922
C	2.2882236	-1.2799317	0.3973500
C	3.5675071	-2.2118027	-1.4514048

C	4.9360785	-2.6398513	-1.9489882
C	5.0689237	-3.6710722	-2.8906014
C	6.3440927	-3.9963051	-3.3624390
C	7.4430975	-3.2885676	-2.8700716
C	7.2091753	-2.2831757	-1.9244034
C	3.7073915	-3.2305484	0.7606373
C	4.0517733	-2.9929068	2.2196300
H	6.0290597	-1.0063301	3.9208699
H	5.1437993	-2.3439403	5.8452949
H	-4.0401193	-3.1672857	4.0109572
H	-6.3296066	-3.5560395	4.9658039
H	-8.3389642	-2.7926962	3.6322433
H	-7.9478694	-1.6831668	1.4209283
N	3.5139559	-1.9917694	0.0001811
N	-3.3523045	-2.1373923	0.1998694
N	5.9926946	-1.9622894	-1.4777215
N	-4.6717137	-3.0228250	-2.1763236
C	5.3043545	-1.8123565	3.7483509
C	4.8107084	-2.5569945	4.8257715
C	3.8834990	-3.5667639	4.5567270
C	-2.1484172	-1.5212229	-0.3814386
C	-3.4640876	-3.5623044	-0.1290613
C	-3.7654148	-3.8205741	-1.5941802
C	-3.1503231	-4.8777757	-2.2810605
C	-3.5030618	-5.1154284	-3.6125925
C	-4.4476873	-4.2821314	-4.2168991
C	-4.9968973	-3.2466727	-3.4522209
C	-3.4473287	-1.8869282	1.6441169
C	-4.8130690	-2.2021296	2.2264814
C	-4.9329401	-2.8431625	3.4685716
C	-6.2084940	-3.0604871	3.9975870
C	-7.3206270	-2.6416967	3.2633214
C	-7.0983217	-2.0210395	2.0285559
H	2.1709640	-1.3966805	1.4894064
H	1.3935031	-1.7380731	-0.0643421
H	3.3036903	-1.2567933	-1.9408666
H	2.8046067	-2.9518510	-1.7676771
H	4.1865375	-4.2108926	-3.2458249
H	6.4757627	-4.7953785	-4.0984617
H	8.4607637	-3.5082007	-3.2048513
H	8.0489385	-1.7091075	-1.5117096
H	4.5483337	-3.7744612	0.2971356
H	2.8187408	-3.8893708	0.6846297
H	-1.9937415	-1.9651016	-1.3808446
H	-1.2483304	-1.7647476	0.2136298
H	-4.2971595	-3.9733135	0.4664385
H	-2.5512570	-4.1159360	0.1717074
H	-2.4069569	-5.5035220	-1.7789305
H	-4.7525722	-4.4243046	-5.2574748
H	-5.7366399	-2.5669226	-3.8944994
H	-3.2401429	-0.8140666	1.8091463
H	-2.6655013	-2.4476542	2.1955432
N	-5.8818996	-1.8017954	1.5236388
C	3.4917870	-3.7854339	3.2326999

H	2.7595661	-4.5597270	2.9867581
N	4.9418554	-2.0250490	2.4807038
H	3.4636377	-4.1721391	5.3659597
H	-3.0402467	-5.9354715	-4.1702778

Structure 7:

95
ZP1 structure 7

H	6.6912463	-0.9038951	-1.9453118
H	7.7513412	-2.9446290	-2.9410254
H	6.5595239	-5.1653393	-2.7198655
H	4.3564194	-5.2117276	-1.5106645
C	4.9822029	-1.9993979	-1.1858667
C	6.2070274	-1.8810932	-1.8620713
C	6.7938839	-3.0173918	-2.4164586
C	6.1389450	-4.2496853	-2.2965529
C	4.9202778	-4.2789649	-1.6235698
N	4.3653438	-3.1834635	-1.0821194
H	2.5066514	1.6347160	3.1431057
H	3.6953142	1.4456137	5.3464754
H	5.2564254	-0.5105203	5.7178602
H	5.5474087	-2.1651186	3.8624271
C	3.4083122	-0.1876620	2.3621435
C	3.1912322	0.8010936	3.3407572
C	3.8496863	0.6943233	4.5652899
C	4.7148589	-0.3861799	4.7757683
C	4.8722027	-1.3079330	3.7392464
N	4.2375066	-1.2172360	2.5627805
C	4.3430803	-0.7838283	-0.5393917
H	5.0065778	-0.4715199	0.2830153
H	4.3481028	0.0541086	-1.2767285
C	2.6475588	-0.0839915	1.0471783
H	1.5803334	-0.2523323	1.2776021
H	2.7097282	0.9680895	0.6860961
N	3.0256603	-1.0287544	0.0117804
C	1.9862944	-1.1615156	-1.0142490
H	2.4210003	-1.7024182	-1.8705451
H	1.6642580	-0.1750589	-1.4021791
C	-0.4938849	-1.3659270	-0.4568278
C	0.7847612	-1.9379927	-0.5142113
C	0.9436864	-3.2823606	-0.0908661
C	-0.2101821	-3.9961143	0.3620033
C	-1.4600831	-3.4195307	0.3900078
C	-1.6404262	-2.0776494	-0.0213766
H	2.9522337	-3.4241216	-0.4031086
O	2.0894361	-3.9281215	-0.0890269
Cl	-0.0058063	-5.6535196	0.8814258
H	-2.3136652	-4.0028108	0.7368390
C	-2.9103663	-1.4137368	-0.0181393
C	-4.9632251	-2.9424669	-0.3482380
C	-6.0714710	-3.5885716	0.2277758
C	-6.3592372	-3.4629309	1.5856102
C	-5.5317051	-2.6769479	2.3931031
C	-4.4271965	-2.0269421	1.8352525

C	-4.1236278	-2.1447600	0.4683807
C	-4.7752799	-3.1628862	-1.8182308
O	-5.5113909	-3.8540613	-2.4928365
O	-3.7177647	-2.5293346	-2.3361490
H	-3.6691143	-2.7301148	-3.2947418
H	-6.7068064	-4.1954439	-0.4206155
H	-7.2263842	-3.9748803	2.0120701
H	-5.7423662	-2.5662745	3.4608525
H	-3.7832723	-1.4138275	2.4719188
O	-0.6079661	-0.0683135	-0.8371019
C	-2.9858885	-0.0789551	-0.3967005
C	-4.2136124	0.6695099	-0.4043235
C	-4.2287341	1.9731143	-0.7884042
C	-3.0187072	2.7052395	-1.2223110
C	-1.7752608	1.9371685	-1.2022848
C	-1.7885099	0.6156236	-0.8165121
H	-5.1372213	0.1775970	-0.0964522
Cl	-5.7241110	2.8759475	-0.8012931
O	-3.0685663	3.8869121	-1.5867228
C	-0.5208775	2.6713333	-1.6188654
H	0.2700318	1.9493412	-1.9008265
H	-0.7683921	3.2532534	-2.5220908
N	-0.0698204	3.6306412	-0.6145843
C	0.5824386	4.8164923	-1.1348658
H	0.8507707	5.4613209	-0.2768816
H	-0.1447712	5.3940893	-1.7348274
C	1.8366530	4.5985101	-1.9816707
C	2.0461511	5.3434272	-3.1541167
C	3.2145217	5.1417414	-3.8935394
C	4.1361964	4.1908223	-3.4471032
C	3.8379518	3.4906825	-2.2732219
N	2.7267012	3.6865712	-1.5572310
H	1.2980885	6.0716534	-3.4813872
H	3.3979314	5.7136332	-4.8087684
H	5.0631349	3.9915098	-3.9922290
H	4.5357549	2.7319925	-1.8938838
C	0.4377252	3.1027805	0.6351853
H	1.5424629	3.0969129	0.6759427
H	0.1322503	2.0446677	0.7160307
C	-0.0812579	3.8125270	1.8784458
C	0.1823548	4.1644254	4.1419569
C	-0.9564346	4.9728415	4.2161686
C	-1.6798244	5.1959253	3.0404324
C	-1.2378954	4.6067130	1.8532795
N	0.6143696	3.6022762	3.0083998
H	0.7762368	3.9659522	5.0436694
H	-1.2621025	5.4136030	5.1692998
H	-2.5790328	5.8206864	3.0487465
H	-1.7676103	4.7414803	0.9072559

Structure 8:

103			
ZP1 structure 8			
Cl	-0.6285049	-5.0050612	2.7349797

C1	6.4960483	0.7348743	-2.2216250
O	3.3863932	-5.5063976	-2.5002936
O	4.2731023	2.6746430	-2.1270299
O	1.0646660	-0.1246877	-0.0769558
O	-2.2404372	-2.6215305	2.2553631
C	3.1973410	-4.5088961	-1.7663678
C	4.0772147	-4.3808696	-0.5156721
C	5.0448315	-5.3566033	-0.2361004
C	5.8643644	-5.2646699	0.8914460
C	5.7220746	-4.1764777	1.7609674
C	4.7634495	-3.1936240	1.4944741
C	3.9356631	-3.2856673	0.3607584
C	2.9218599	-2.2070641	0.1382323
C	3.2885324	-0.9896532	-0.4490315
C	4.5906520	-0.7478113	-0.9949777
C	4.8987546	0.4538794	-1.5572011
C	3.9523541	1.5793358	-1.6348117
C	2.6230818	1.3140227	-1.0901873
C	2.3325967	0.0783076	-0.5417466
C	0.6905494	-1.2656013	0.5619240
C	-0.6259065	-1.3212671	1.0496988
C	-1.0611081	-2.4876211	1.7614221
C	-0.1025156	-3.5613515	1.8916774
C	1.1711974	-3.4911914	1.3857195
C	1.6141230	-2.3300109	0.7033777
H	5.1336858	-6.1913112	-0.9360975
H	6.6141012	-6.0364025	1.0932500
H	6.3575472	-4.0888916	2.6477039
H	4.6545687	-2.3436095	2.1750117
H	5.3360208	-1.5433226	-0.9550237
H	1.8515959	-4.3351398	1.5049858
O	2.3581314	-3.5895346	-1.9376053
C	1.6131182	2.4323192	-1.1576663
C	0.2782251	4.0981963	0.0429645
C	0.5603850	5.3286392	-0.8094728
C	0.2090766	5.3767837	-2.1689664
C	0.5154982	6.5173639	-2.9152598
C	1.1657204	7.5791185	-2.2811019
C	1.4729426	7.4446253	-0.9230602
C	2.5242331	3.5539575	0.8667314
C	2.3127651	3.6197491	2.3713012
C	1.3883305	2.7929407	3.0294264
C	1.2822721	2.8625330	4.4198855
C	2.1068354	3.7524961	5.1153263
C	2.9998988	4.5322997	4.3739241
C	-1.5394146	-0.1313778	0.8745330
C	-2.8546271	1.2115001	-0.7015497
C	-3.9817276	1.8197825	0.1064178
C	-4.0011439	3.1705941	0.4649570
C	-5.1181645	3.6783967	1.1332895
C	-6.1782668	2.8187869	1.4339023
C	-6.0739839	1.4807850	1.0553175
C	-2.0208070	-0.9354751	-1.4622197
C	-3.1305896	-1.1982396	-2.4641545

C	-2.8526145	-1.3777664	-3.8230047
C	-3.8987774	-1.6848559	-4.6955765
C	-5.1968177	-1.7958832	-4.1884724
C	-5.3926834	-1.5912135	-2.8240780
H	0.7697966	2.1123717	2.4402411
H	0.5674921	2.2296598	4.9557244
H	2.0609984	3.8440745	6.2042520
H	3.6637025	5.2426523	4.8843058
H	-1.8275587	-1.2771529	-4.1891159
H	-3.7023098	-1.8308510	-5.7617124
H	-6.0456252	-2.0322096	-4.8344648
H	-6.3885076	-1.6681855	-2.3781581
N	1.3536660	3.1061137	0.1266410
N	-2.4975118	-0.1674570	-0.2975415
N	1.1791185	6.3569615	-0.2032077
N	-5.0073229	1.0028687	0.3995339
H	1.9768802	3.1404044	-1.9268553
H	0.6413139	2.0361972	-1.5046430
H	0.0444787	4.4409281	1.0648225
H	-0.6165052	3.5865729	-0.3548588
H	-0.3064301	4.5321838	-2.6350266
H	0.2468109	6.5768458	-3.9746269
H	1.4246194	8.4948510	-2.8201732
H	1.9766010	8.2617325	-0.3899951
H	2.9113793	4.5391716	0.5404237
H	3.3331595	2.8254241	0.6840265
H	-2.1493364	0.0122624	1.7782799
H	-0.9051059	0.7628685	0.7605107
H	-3.1874252	1.1909396	-1.7528629
H	-1.9683309	1.8693132	-0.6711311
H	-3.1546371	3.8180503	0.2230229
H	-5.1551497	4.7326100	1.4222080
H	-7.0680515	3.1711134	1.9609413
H	-6.8666316	0.7644828	1.2901376
H	-1.6566405	-1.9084732	-1.0960655
H	-1.1746784	-0.4375218	-1.9715842
H	-5.0255294	-1.4761473	2.7634442
O	-4.2906369	-1.0846652	2.2578432
H	-3.4585270	-1.6341634	2.4383458
Zn	-4.5198354	-1.0757608	0.1510716
H	-7.3175187	-1.2858411	-0.0942400
O	-6.5446887	-1.6910019	0.3401516
H	-6.8022766	-2.6029190	0.5719515
N	3.1013418	4.4748964	3.0413963
N	-4.3850650	-1.2983564	-1.9890296
O	-3.8294422	-3.0861126	0.2525223
H	-4.3755007	-3.8800498	0.1147939
H	-3.2703918	-3.2065555	1.0743216

ZP1 Structure 9:

105			
ZP1 structure 9			
H	4.5087374	-0.0443821	-5.8374339
H	6.7293919	-0.7109462	-4.8334688

C	4.6206890	-0.1685060	-4.7566515
H	2.5520890	0.3191916	-4.3079043
C	5.8514405	-0.5387594	-4.2067939
C	3.5290369	0.0354422	-3.9090431
H	-6.7199208	-4.7794197	-1.9348844
H	-1.9117912	7.4035244	-2.3136458
H	-6.8984226	-6.7280402	-0.3752488
C	5.9395811	-0.6938061	-2.8253419
C	-5.8565775	-5.0766012	-1.3238747
C	-5.9605377	-6.1709260	-0.4562745
H	-1.2183422	5.0271707	-2.1867311
C	3.6997182	-0.1293906	-2.5323240
H	6.8777309	-0.9842315	-2.3441507
Cl	-5.8112417	1.7731995	-2.7889399
N	-4.7445033	-4.3542974	-1.4749095
C	-2.1474459	6.8182523	-1.4200510
N	4.8881552	-0.4936077	-2.0142275
H	1.6014426	0.0161737	-2.0671196
H	-2.1108839	-1.9088186	-2.5816893
O	-4.3068298	-0.7581676	-2.8038700
H	-2.1918156	-3.9035766	-2.0597674
C	-1.7576868	5.4777188	-1.3490203
C	-4.8321451	-6.5266366	0.2849462
C	-4.2523907	1.4962247	-2.0623237
C	2.5717673	0.1514986	-1.5568773
C	-3.7132645	0.1179459	-2.1759598
C	-3.6639056	-4.6811005	-0.7493794
H	-4.8573417	-7.3784141	0.9720362
H	-4.0122770	3.5081159	-1.4159366
H	2.6378141	1.2099552	-1.2573858
C	-3.5805398	2.5072358	-1.4571712
H	2.7926644	-2.2944098	-1.6786258
H	-3.1444741	8.4500563	-0.3985018
C	-3.6663333	-5.7701938	0.1343208
C	-2.8349191	7.4022788	-0.3522459
H	5.5941815	1.9270457	-0.4940284
C	-2.4225368	-0.1162429	-1.5167251
C	-2.4116665	-3.8467720	-0.9811303
C	-1.8919497	-1.5285839	-1.5734039
C	-2.2867530	2.2799543	-0.8644389
C	-1.7643999	0.9273804	-0.9170778
C	-2.0434594	4.6943722	-0.2180540
N	-2.5434880	-2.4357854	-0.6239614
H	-2.7659315	-6.0193064	0.7025133
C	-1.5598934	3.2779129	-0.2412834
C	2.4356447	-2.1027008	-0.6526270
H	-0.7858059	-1.5223539	-1.4525979
N	2.6783261	-0.6742520	-0.3357542
H	-1.5522315	-4.3241434	-0.4584367
O	-0.5509566	0.6742314	-0.3346473
H	1.3553050	-2.3312596	-0.6579104
O	5.2518946	1.3868398	0.2413045
H	7.5388389	-1.6614068	0.0950660
C	-0.2788345	2.9590901	0.3421093

C	-3.1266325	6.6370911	0.7757392
Zn	4.9005548	-0.6950375	0.0978449
H	7.5379105	-0.1348327	0.4652380
C	0.1804585	1.6267791	0.2899552
O	6.9657183	-0.9185086	0.3605172
C	-2.7409160	5.2880769	0.8636850
H	4.8046136	1.9826614	0.8819073
H	0.2280646	4.9571031	1.0291541
C	0.5405682	3.9137596	0.9812239
H	-6.2805981	-2.6268887	2.6469947
C	3.1715202	-3.0579218	0.2610601
C	1.3995233	1.2130041	0.8689125
N	-4.4111716	-2.4192125	1.7782940
N	4.4146300	-2.6913681	0.6222508
H	-3.6668060	7.0734179	1.6185054
C	1.7897463	-0.2473876	0.8063918
C	-2.2096626	-2.1378135	0.7591562
H	0.8561685	-0.8283246	0.7534136
C	1.7371133	3.5383412	1.5574491
C	-5.2270264	-2.9320309	2.7017536
H	-2.2843990	-1.0457484	0.8914973
H	1.6216854	-4.5643949	0.3426090
C	2.1727609	2.1875697	1.5312013
C	2.6351737	-4.2887757	0.6450195
C	-3.1154880	-2.7677265	1.8036119
H	-1.1535625	-2.4219232	0.9938354
Cl	2.7377387	4.7274666	2.3468942
C	5.1670017	-3.5190617	1.3660716
O	3.3452551	1.9341093	2.1382513
C	-3.1256102	4.5822691	2.1277268
H	6.1630923	-3.1623009	1.6431272
H	3.5539722	0.9775044	2.3013364
H	2.2798159	-0.5539186	1.7419773
O	-2.7691874	3.2930247	2.1626503
C	-4.8055367	-3.8063321	3.7114816
C	3.4162661	-5.1576459	1.4111948
O	4.7191836	-0.3329397	2.3083491
C	-2.5976747	-3.6302214	2.7814634
C	4.7080438	-4.7685999	1.7776225
H	-5.5196708	-4.1923039	4.4444715
H	4.4712202	-1.0814423	2.8872522
O	-3.7099879	5.1194364	3.0459174
H	5.5332150	0.0413709	2.7035151
H	3.0175408	-6.1270079	1.7227541
C	-3.4549161	-4.1561219	3.7524927
H	-1.5349787	-3.8891734	2.7806179
H	-3.0502967	2.9112826	3.0210293
H	5.3507392	-5.4156207	2.3787784
H	-3.0726575	-4.8315951	4.5242852

Structure 10:

105			
ZP1 structure 10			
H	6.0563202	-2.8708585	-4.8392916

H	3.8765406	-1.9769745	-5.7528497
C	5.3101429	-2.4150744	-4.1843779
C	4.1031238	-1.9177693	-4.6844940
H	6.4734955	-2.6984077	-2.3716020
C	5.5461960	-2.3238086	-2.8142142
C	3.1831989	-1.3480470	-3.8010203
H	2.2280781	-0.9557838	-4.1591351
N	4.6610767	-1.7728256	-1.9694836
H	7.3771355	-2.9787364	-0.0039023
C	3.4992089	-1.2841705	-2.4409805
H	7.6028715	-1.4284753	0.0867552
O	6.9511476	-2.1377728	0.2440291
H	2.2900307	-3.0130261	-1.1023258
H	5.7953635	0.7827360	-1.1382476
C	2.5754362	-0.6097106	-1.4433072
H	1.5393032	-0.6315031	-1.8287322
Zn	4.9216568	-1.5598534	0.1518321
O	5.6874690	0.3974320	-0.2502661
H	5.9512764	-4.0531248	1.8227562
H	2.8688859	0.4498840	-1.3703210
N	4.1765020	-3.3841787	0.9774390
C	2.1507520	-2.5843077	-0.0953414
C	4.8714661	-4.2185320	1.7639100
C	2.8423961	-3.5125299	0.8807340
N	2.6877101	-1.2039775	-0.0990264
C	4.2610687	-5.2450867	2.4829893
H	1.0611131	-2.5846102	0.0892468
H	5.3196053	1.0895675	0.3564342
H	4.8633963	-5.9089750	3.1073916
C	2.1525849	-4.5045647	1.5825301
C	2.8737978	-5.3869841	2.3910655
H	1.0661834	-4.5861643	1.4953404
H	2.3553114	-6.1723300	2.9483253
H	-1.8618960	-1.5770356	-1.5981292
O	5.0324206	-0.8684786	2.1521919
H	5.9180210	-0.8889074	2.5583501
H	-1.1966338	-1.3710654	0.0350896
H	-2.5461857	-3.5105987	-1.3476603
H	-0.0830131	4.8445138	-2.4835299
C	2.0566162	-0.3993250	1.0123118
H	4.7064857	0.0771829	2.1675095
O	4.1597033	1.5361344	1.6090246
C	-2.1006070	-1.2122940	-0.5842357
H	1.0373897	-0.7846437	1.1751767
C	1.9553268	1.0947345	0.8142114
H	-0.3565219	7.2458222	-3.0333432
H	2.6241697	-0.6104730	1.9297302
C	3.0501332	1.9606299	1.1737076
O	-0.2368488	0.8189865	0.0211633
H	-2.7794188	-4.0358203	0.3267793
C	0.7714387	1.6620680	0.3482856
H	-4.4155641	-1.0782711	-1.0233572
C	-3.2142224	-3.4084685	-0.4751460
C	-2.4126118	0.2694315	-0.6751389

C	-0.4970906	5.5262562	-1.7357974
C	-1.4506434	1.2465893	-0.4055403
C	2.8426376	3.3983301	1.0010820
O	-4.6480635	-0.1612115	-1.4116390
Cl	4.1772183	4.4366580	1.4186114
C	-3.6827355	0.6912301	-1.1377437
C	0.5776166	3.0745240	0.1978572
C	-0.6519547	6.8806384	-2.0456176
C	1.6725400	3.9274255	0.5443376
N	-3.2456685	-1.9906297	-0.0880203
C	-1.6931227	2.6367384	-0.5738788
C	-0.6578679	3.5574010	-0.2551624
C	-4.5722060	-3.9556906	-0.8858301
H	1.5646962	5.0073169	0.4389307
C	-3.9330728	2.0884633	-1.3232805
N	-5.3064488	-3.1769846	-1.6910014
C	-2.9708646	3.0306963	-1.0519796
C	-0.8650592	5.0232053	-0.4768846
H	-4.3719488	-5.8427798	0.1677712
Cl	-5.5022623	2.5711210	-1.9055645
H	-2.6641160	-2.3045183	1.9344757
H	-3.1927338	4.0878453	-1.1992040
C	-4.9940640	-5.2338892	-0.4945758
C	-6.4833160	-3.6332778	-2.1272447
H	-7.0573742	-2.9622800	-2.7790600
C	-3.4521527	-1.7812423	1.3549381
C	-1.1809841	7.7583281	-1.0948108
H	-3.3385886	-0.7015036	1.5503931
H	-1.3050094	8.8192992	-1.3284092
C	-6.2213223	-5.7125789	-0.9620406
C	-6.9880864	-4.8959551	-1.7969351
H	-6.5749968	-6.7067254	-0.6717231
C	-1.4019828	5.9126550	0.4863555
H	-7.9566125	-5.2241334	-2.1843669
C	-1.5506075	7.2713414	0.1580244
C	-4.8201112	-2.1973220	1.8587049
H	-4.0852605	-3.6906310	3.2513046
O	-1.6620735	4.2214753	2.1368473
N	-5.8704110	-1.5441774	1.3388024
C	-4.9642766	-3.1810712	2.8467615
C	-1.8341518	5.5200852	1.8660968
H	-1.9648761	7.9410226	0.9145476
H	-1.9681191	4.0409004	3.0509661
C	-7.0922582	-1.8553134	1.7740521
C	-6.2471735	-3.4962858	3.3061067
O	-2.2982212	6.2987633	2.6726520
H	-7.9277873	-1.3030328	1.3244479
H	-6.3883680	-4.2585980	4.0785483
C	-7.3393991	-2.8224467	2.7571125
H	-8.3624605	-3.0332097	3.0811908

Structure 11:

114
ZP1 structure 11

H	-5.2104275	5.7913296	-0.1549799
H	-7.3247549	4.7667322	0.7762319
C	-5.2696292	4.7194112	0.0537711
H	-3.2364550	4.3030851	-0.5855193
C	-6.4415352	4.1579453	0.5693156
C	-4.1688903	3.8941671	-0.1882352
C	-6.4620078	2.7883910	0.8246923
C	-4.2723309	2.5272176	0.0853332
H	-7.3533989	2.2998101	1.2285546
H	2.6840308	2.6037767	4.5813356
N	-5.4031681	1.9988088	0.5879717
H	4.3718084	3.2026678	2.9440458
H	-2.1789764	2.1197287	-0.2223655
C	-3.1374044	1.5684481	-0.2245355
H	-2.9694093	-1.1884122	6.3070558
H	-3.1262950	1.8943583	2.1981323
C	-3.4600297	-0.9506682	5.3588615
H	2.1472176	2.1029317	1.5865591
C	-2.7675901	-0.2614634	4.3596955
H	-6.3856152	-1.3129921	3.6611620
C	-4.7830208	-1.3358375	5.1261076
H	-0.0196752	1.9379002	-5.4151447
O	4.1358186	2.5229232	-0.0192271
H	-7.9561838	-0.5724379	0.5926308
H	-3.2844877	1.1845609	-1.2471198
H	-7.9329291	-0.0373742	2.0679456
H	4.3840311	2.4988073	1.4882365
O	-7.3769034	-0.4154019	1.3622685
O	2.8731478	1.6475928	4.5947932
H	0.4224133	2.0315501	-7.8524449
Cl	5.0434814	2.8270930	-2.7667111
C	-5.3595953	-1.0158431	3.8978992
C	-3.4221967	0.0315589	3.1603421
O	4.5901655	2.3763386	2.4792039
H	2.8056522	1.3683055	5.5266829
H	-5.3599940	-1.8809094	5.8767160
H	0.6845121	1.1956278	1.1718627
C	-2.7760260	0.8565033	2.0674576
H	-6.1189026	0.4019820	-1.7108200
N	-4.6954254	-0.3407540	2.9489972
C	3.3299189	1.9772611	-0.8116991
Zn	-5.3290371	-0.1240130	0.9187327
O	-5.9401755	-0.3494930	-1.1177016
H	-5.3603168	-1.0047530	-1.5948721
C	3.5906520	2.0104248	-2.2532182
C	1.7806078	1.2034493	1.0721383
H	-1.7324180	0.0554246	4.5116859
H	-1.6805731	0.8867906	2.2094456
N	-3.1242053	0.4168653	0.6961155
C	2.1215351	1.2944106	-0.3936648
H	0.9471553	0.4045265	3.3377265
C	0.5491834	1.1351961	-5.8920880
C	2.7686165	1.4264817	-3.1702351
C	0.7982920	1.1876892	-7.2666103

H	3.0245609	1.4575900	-4.2298539
C	1.2672082	0.7701133	-1.3588930
C	1.5640828	0.7749764	-2.7584437
O	0.1073688	0.2013883	-0.9304133
H	6.1407668	1.4249672	4.6692832
C	-2.2360442	-0.7316220	0.2724881
Zn	4.0707679	0.5063828	3.1903565
H	6.4857336	-0.0854138	4.4883826
N	2.3237599	-0.0002025	1.8213644
C	0.7022806	0.1105965	-3.6456051
C	-0.7913003	-0.3856453	-1.7685418
C	1.3325038	-0.4802606	2.8022937
H	-1.2640324	-0.6116706	0.7761317
O	5.7460756	0.5499503	4.4947885
C	1.0178492	0.0683090	-5.1081228
C	-1.9724296	-0.8785659	-1.2071567
C	-0.4933450	-0.4699342	-3.1588343
H	0.4776638	-0.9767051	2.3050161
C	1.5243560	0.1648621	-7.8836553
O	-5.0387493	-2.2151684	0.7547152
H	1.7247339	0.1972763	-8.9581490
H	-2.6870315	-1.6533841	0.6659140
C	-2.9170414	-1.5611215	-2.0511669
C	-1.4406084	-1.1288481	-3.9937726
O	-4.0068158	-2.0593450	-1.6190824
H	-1.2477233	-1.2130040	-5.0639067
C	-2.5901810	-1.6484485	-3.4647580
H	-5.8451550	-2.7607521	0.7917785
C	1.9339508	-1.4226613	3.8267241
H	-4.5972857	-2.3699995	-0.1350766
N	3.1942448	-1.1635674	4.2222749
N	5.0863101	-0.3936236	1.5293655
C	2.8261145	-1.1064388	0.9811003
H	2.2132966	-1.2620499	0.0797526
H	6.9990574	0.1970530	2.0755693
Cl	-3.7456901	-2.4542602	-4.4955651
C	1.7527255	-0.9693357	-5.7338913
C	1.9924253	-0.9017444	-7.1181161
H	0.1872130	-2.6847052	4.0239183
C	4.2858134	-0.9512034	0.6051364
C	6.4023405	-0.2824497	1.2943543
C	1.2025164	-2.4799773	4.3734512
C	3.7625842	-1.9211008	5.1722645
H	4.7830223	-1.6573905	5.4624199
H	2.7410091	-2.0378487	1.5662504
C	4.7960987	-1.4273100	-0.6059780
C	6.9904240	-0.7450861	0.1193315
H	2.5587204	-1.7117174	-7.5824871
O	2.1081043	-2.1897645	-3.7119798
C	1.7903053	-3.2713986	5.3641187
H	4.1243899	-1.8638667	-1.3499571
H	8.0672388	-0.6409656	-0.0326023
C	2.3055481	-2.1758739	-5.0391471
C	3.0949488	-2.9868491	5.7745087

C	6.1673059	-1.3265066	-0.8500624
H	1.2357336	-4.1044856	5.8051130
H	6.5888944	-1.6925472	-1.7906399
H	3.5949286	-3.5794886	6.5439621
H	2.4650689	-3.0301272	-3.3553036
O	2.8816635	-3.0756432	-5.6134306

B.2 Test set of large organic dyes

All geometries are optimized at the B3LYP/6-31G* level in the gas phase.

1: β -carotene

96			
beta-carotene			
C	12.745662	-0.445000	0.701009
C	14.041652	0.396507	0.629154
C	13.778523	1.897929	0.708324
C	12.915735	2.321017	-0.479297
C	11.742468	1.399574	-0.741787
C	11.630196	0.169005	-0.179960
C	10.439094	-0.680888	-0.364302
C	9.148869	-0.282707	-0.247826
C	7.972372	-1.119059	-0.420817
C	6.740902	-0.546373	-0.251680
C	5.449240	-1.158543	-0.372973
C	4.283616	-0.475280	-0.179269
C	2.947185	-1.007309	-0.286088
C	1.886951	-0.163011	-0.061397
C	0.490913	-0.461292	-0.120562
C	10.755529	1.987546	-1.723955
C	13.102178	-1.874152	0.226580
C	12.250384	-0.529161	2.164423
C	8.169985	-2.571767	-0.780451
C	2.780483	-2.465140	-0.645739
H	14.554973	0.182279	-0.319794
H	14.719882	0.073345	1.430309
H	13.265698	2.143773	1.647179
H	14.722762	2.456344	0.712260
H	12.534639	3.342823	-0.333063
H	13.533249	2.375759	-1.391502
H	10.626799	-1.734158	-0.559650
H	8.948649	0.755148	0.015647
H	6.726710	0.513693	0.006058
H	5.400044	-2.212738	-0.631502
H	4.355597	0.581984	0.079809
H	2.131007	0.869468	0.192862
H	0.182044	-1.474305	-0.372187
H	10.076483	1.243603	-2.144590
H	10.146153	2.776458	-1.259889
H	11.299300	2.468301	-2.549302
H	13.331463	-1.893456	-0.845586

H	13.988645	-2.228985	0.766098
H	12.299578	-2.593707	0.418643
H	11.308674	-1.084945	2.226756
H	12.990344	-1.039787	2.793978
H	12.073395	0.465653	2.587547
H	8.756821	-3.089381	-0.010416
H	7.227016	-3.109378	-0.893469
H	8.726185	-2.668928	-1.721466
H	3.297365	-3.107554	0.078324
H	3.217168	-2.677224	-1.630067
H	1.734714	-2.774933	-0.673402
C	-12.745662	0.445000	-0.701009
C	-14.041652	-0.396507	-0.629154
C	-13.778523	-1.897929	-0.708324
C	-12.915735	-2.321017	0.479297
C	-11.742468	-1.399574	0.741787
C	-11.630196	-0.169005	0.179960
C	-10.439094	0.680888	0.364302
C	-9.148869	0.282707	0.247826
C	-7.972372	1.119059	0.420817
C	-6.740902	0.546373	0.251680
C	-5.449240	1.158543	0.372973
C	-4.283616	0.475280	0.179269
C	-2.947185	1.007309	0.286088
C	-1.886951	0.163011	0.061397
C	-0.490913	0.461292	0.120562
C	-10.755529	-1.987546	1.723955
C	-13.102178	1.874152	-0.226580
C	-12.250384	0.529161	-2.164423
C	-8.169985	2.571767	0.780451
C	-2.780483	2.465140	0.645739
H	-14.554973	-0.182279	0.319794
H	-14.719882	-0.073345	-1.430309
H	-13.265698	-2.143773	-1.647179
H	-14.722762	-2.456344	-0.712260
H	-12.534639	-3.342823	0.333063
H	-13.533249	-2.375759	1.391502
H	-10.626799	1.734158	0.559650
H	-8.948649	-0.755148	-0.015647
H	-6.726710	-0.513693	-0.006058
H	-5.400044	2.212738	0.631502
H	-4.355597	-0.581984	-0.079809
H	-2.131007	-0.869468	-0.192862
H	-0.182044	1.474305	0.372187
H	-10.076483	-1.243603	2.144590
H	-10.146153	-2.776458	1.259889
H	-11.299300	-2.468301	2.549302
H	-13.331463	1.893456	0.845586
H	-13.988645	2.228985	-0.766098
H	-12.299578	2.593707	-0.418643
H	-11.308674	1.084945	-2.226756
H	-12.990344	1.039787	-2.793978
H	-12.073395	-0.465653	-2.587547
H	-8.756821	3.089381	0.010416

H	-7.227016	3.109378	0.893469
H	-8.726185	2.668928	1.721466
H	-3.297365	3.107554	-0.078324
H	-3.217168	2.677224	1.630067
H	-1.734714	2.774933	0.673402

2: free-base phthalocyanine

58

H2Pc

N	2.024207	0.000523	0.000726
N	-0.000438	1.949624	-0.000863
N	2.381999	2.399727	0.000049
N	2.383101	-2.398535	0.000026
C	2.789998	-1.145223	-0.000053
C	4.174414	-0.705704	-0.000395
C	5.372561	-1.424876	-0.000757
C	6.562483	-0.703569	-0.001130
C	6.562170	0.706635	-0.001121
C	5.371931	1.427419	-0.000739
C	4.174100	0.707719	-0.000387
C	2.789486	1.146607	-0.000042
C	1.096134	2.762416	0.000083
C	0.701097	4.175005	0.000305
C	1.423448	5.365679	0.000596
C	0.701095	6.561599	0.000892
C	-0.704271	6.561247	0.000896
C	-1.426031	5.364969	0.000602
C	-0.703089	4.174653	0.000300
C	1.097416	-2.761861	0.000052
H	5.363154	-2.510165	-0.000785
H	7.510925	-1.233476	-0.001453
H	7.510378	1.236963	-0.001435
H	5.362047	2.512703	-0.000751
H	2.509090	5.357985	0.000629
H	1.232569	7.509455	0.001151
H	-1.236218	7.508838	0.001155
H	-2.511668	5.356735	0.000635
H	1.010120	0.000333	0.001808
N	0.000438	-1.949624	-0.000863
C	-1.096134	-2.762416	0.000083
N	-2.381999	-2.399727	0.000049
C	-2.789486	-1.146607	-0.000042
N	-2.024207	-0.000523	0.000726
C	-2.789998	1.145223	-0.000053
N	-2.383101	2.398535	0.000026
C	-1.097416	2.761861	0.000052
C	-4.174414	0.705704	-0.000395
C	-5.372561	1.424876	-0.000757
C	-6.562483	0.703569	-0.001130
C	-6.562170	-0.706635	-0.001121
C	-5.371931	-1.427419	-0.000739
C	-4.174100	-0.707719	-0.000387
H	-5.362047	-2.512703	-0.000751
H	-7.510378	-1.236963	-0.001435

H	-7.510925	1.233476	-0.001453
H	-5.363154	2.510165	-0.000785
H	-1.010120	-0.000333	0.001808
C	-0.701097	-4.175005	0.000305
C	-1.423448	-5.365679	0.000596
C	-0.701095	-6.561599	0.000892
C	0.704271	-6.561247	0.000896
C	1.426031	-5.364969	0.000602
C	0.703089	-4.174653	0.000300
H	2.511668	-5.356735	0.000635
H	1.236218	-7.508838	0.001155
H	-1.232569	-7.509455	0.001151
H	-2.509090	-5.357985	0.000629

3: zinc phthalocyanine

57			
ZnPc			
Zn	0.000000	0.000000	0.000000
N	2.906374	1.727951	0.000086
N	0.490205	1.928681	0.000066
N	-1.727957	2.906371	-0.000023
N	-1.928695	0.490211	-0.000107
C	1.771642	2.421274	0.000077
C	1.714336	3.880351	0.000041
C	2.708259	4.859110	-0.000003
C	2.305381	6.193802	-0.000062
C	0.940874	6.541820	-0.000059
C	-0.053634	5.564562	-0.000007
C	0.347809	4.228406	0.000029
C	-0.400001	2.973987	0.000030
C	-2.421297	1.771647	-0.000070
C	-3.880385	1.714334	-0.000045
C	-4.859201	2.708209	0.000001
C	-6.193878	2.305268	0.000071
C	-6.541847	0.940750	0.000098
C	-5.564544	-0.053709	0.000032
C	-4.228412	0.347798	-0.000044
C	-2.973993	-0.399996	-0.000092
N	-0.490205	-1.928681	-0.000066
N	1.928695	-0.490211	0.000107
C	2.973993	0.399996	0.000092
N	-2.906374	-1.727951	-0.000086
C	-1.771642	-2.421274	-0.000077
C	0.400001	-2.973987	-0.000030
C	2.421297	-1.771647	0.000070
C	4.228412	-0.347798	0.000044
C	-1.714336	-3.880351	-0.000041
N	1.727957	-2.906371	0.000023
C	-0.347809	-4.228406	-0.000029
C	3.880385	-1.714334	0.000045
C	5.564544	0.053709	-0.000032
C	-2.708259	-4.859110	0.000003
C	0.053634	-5.564562	0.000007
C	4.859201	-2.708209	-0.000001

C	6.541847	-0.940750	-0.000098
C	-2.305381	-6.193802	0.000062
C	-0.940874	-6.541820	0.000059
C	6.193878	-2.305268	-0.000071
H	5.827925	1.106935	-0.000054
H	7.591846	-0.659481	-0.000191
H	6.981000	-3.054942	-0.000122
H	4.581682	-3.757757	0.000014
H	3.757783	4.581505	0.000000
H	3.055091	6.980889	-0.000125
H	0.659647	7.591830	-0.000109
H	-1.106842	5.828019	0.000000
H	-4.581682	3.757757	-0.000014
H	-6.981000	3.054942	0.000122
H	-7.591846	0.659481	0.000191
H	-5.827925	-1.106935	0.000054
H	-3.757783	-4.581505	0.000000
H	-3.055091	-6.980889	0.000125
H	-0.659647	-7.591830	0.000109
H	1.106842	-5.828019	0.000000

4: *N,N'*-diphenyl-*N,N'*-bis(3-methylphenyl)-1,1'-biphenyl-4-4'-diamine (TPD)

72

TPD

N	5.099263	0.251313	0.116701
N	-4.905755	0.085956	-0.211313
C	3.681498	0.224920	0.071445
C	3.004510	-0.106021	-1.113701
H	3.575168	-0.346900	-2.004877
C	1.615093	-0.142109	-1.149769
H	1.124091	-0.431559	-2.074625
C	0.837206	0.172834	-0.021457
C	1.527396	0.513680	1.155114
H	0.967674	0.784673	2.045745
C	2.916755	0.528131	1.209703
H	3.418007	0.787682	2.136750
C	-0.643469	0.148095	-0.070924
C	-1.344691	0.487516	-1.241412
H	-0.794152	0.793998	-2.126228
C	-2.733609	0.455762	-1.296926
H	-3.243079	0.715593	-2.219381
C	-3.487941	0.105634	-0.165087
C	-2.800286	-0.224749	1.014062
H	-3.362189	-0.501506	1.900322
C	-1.410372	-0.214514	1.050494
H	-0.910181	-0.505248	1.969989
C	-5.611710	1.089977	-0.928631
C	-5.214619	2.435116	-0.855490
H	-4.362487	2.706134	-0.240192
C	-5.906172	3.412729	-1.568201
H	-5.583931	4.448604	-1.499377
C	-7.013121	3.073857	-2.349110
H	-7.553787	3.839628	-2.898093
C	-7.416428	1.738587	-2.416121

C	-6.719699	0.751207	-1.722427
H	-7.028887	-0.287086	-1.790250
C	-5.627059	-0.935748	0.467288
C	-6.775009	-0.618332	1.209205
H	-7.097313	0.417755	1.263661
C	-7.506838	-1.605974	1.875310
C	-7.058668	-2.932244	1.815740
H	-7.607901	-3.710955	2.339471
C	-5.912005	-3.255145	1.089539
H	-5.573138	-4.287059	1.043577
C	-5.199983	-2.271031	0.407840
H	-4.314440	-2.526674	-0.165096
C	-8.762521	-1.245275	2.636120
H	-8.919226	-1.912017	3.490847
H	-9.650608	-1.324620	1.994717
H	-8.724419	-0.216788	3.010409
C	5.773571	1.264909	0.850125
C	6.897925	0.949735	1.630534
H	7.243828	-0.078153	1.676172
C	7.564471	1.947109	2.339522
H	8.433465	1.684103	2.937322
C	7.114551	3.268481	2.301487
H	7.631978	4.041844	2.862091
C	5.991472	3.583622	1.533678
H	5.633063	4.608828	1.486906
C	5.329719	2.596760	0.805751
H	4.465470	2.850406	0.200024
C	5.853702	-0.736774	-0.576407
C	5.474372	-2.085045	-0.526401
H	4.600060	-2.365029	0.055061
C	6.196232	-3.069824	-1.210958
C	7.327868	-2.689232	-1.941096
H	7.902914	-3.442196	-2.474281
C	7.719897	-1.349456	-1.986744
H	8.597148	-1.061942	-2.560698
C	6.988445	-0.371939	-1.319285
H	7.285920	0.670670	-1.366861
C	5.759049	-4.515753	-1.142256
H	4.765564	-4.655292	-1.586819
H	5.697611	-4.866584	-0.104840
H	6.457368	-5.168809	-1.674927
H	-8.271934	1.457555	-3.025073

5: 2,9-dimethyl-1,3,8,10-tetraazaperopyrene

60			
RiehmGade			
C	5.533782	0.018361	-0.018383
C	3.576010	1.217551	-0.012843
C	2.827083	0.016273	-0.009645
C	3.577442	-1.187494	-0.011537
C	2.861482	2.459484	-0.011193
C	1.403649	0.016404	-0.004683
C	0.712098	1.265638	-0.002766
C	1.496962	2.471175	-0.006297

C	0.710913	-1.233305	-0.001832
C	1.496566	-2.440318	-0.003620
C	2.859832	-2.430041	-0.008319
H	3.436755	-3.349277	-0.009484
H	0.990052	-3.398640	-0.000895
H	3.439224	3.378191	-0.013975
H	0.991210	3.429927	-0.005230
N	4.919262	-1.179441	-0.015960
N	4.923461	1.210860	-0.017289
C	7.065265	-0.016892	-0.023671
C	7.542462	-0.777935	1.234777
C	7.533708	-0.778768	-1.284910
C	7.662104	1.399010	-0.026173
H	7.250961	-0.249068	2.150118
H	7.114278	-1.783770	1.269202
H	8.635700	-0.863509	1.228925
H	7.235606	-0.250646	-2.198555
H	8.626968	-0.864140	-1.286757
H	7.105579	-1.784767	-1.315514
H	8.756673	1.333740	-0.030462
H	7.346280	1.966796	-0.906583
H	7.353206	1.967059	0.856529
C	-0.710922	-1.233306	0.002733
C	-1.403662	0.016402	0.005056
C	-1.496572	-2.440320	0.004988
C	-2.827096	0.016270	0.009989
C	-0.712114	1.265637	0.002583
C	-2.859838	-2.430045	0.009642
H	-0.990057	-3.398641	0.002656
C	-3.576025	1.217548	0.012617
C	-3.577452	-1.187499	0.012334
C	-1.496981	2.471174	0.005536
H	-3.436760	-3.349282	0.011172
C	-2.861501	2.459482	0.010404
N	-4.923476	1.210856	0.017056
N	-4.919272	-1.179448	0.016745
H	-0.991231	3.429926	0.004006
H	-3.439245	3.378188	0.012722
C	-5.533793	0.018355	0.018988
C	-7.065280	-0.016901	0.022840
C	-7.541255	-0.778820	-1.235542
C	-7.534934	-0.777900	1.284156
C	-7.662123	1.399002	0.023765
H	-7.248965	-0.250523	-2.150958
H	-7.112925	-1.784633	-1.268904
H	-8.634487	-0.864520	-1.230646
H	-7.237512	-0.249266	2.197729
H	-8.628212	-0.863049	1.285119
H	-7.107028	-1.783962	1.315760
H	-8.756694	1.333733	0.027086
H	-7.347116	1.967428	0.904055
H	-7.352407	1.966414	-0.859063

6: 10-(4-dimethylamino-phenyl ethynyl)-anthracene-9-carbonitrile (DMAPEAC)

45

DMAPEAC

C	3.626515	-3.668541	-0.000382
C	2.205880	-3.671714	-0.000115
C	4.317776	-2.484552	-0.000418
C	3.630350	-1.233409	-0.000187
C	2.192778	-1.234562	0.000070
C	1.513209	-2.488280	0.000098
C	4.322835	0.002930	-0.000202
C	3.628770	1.238386	0.000067
C	2.191187	1.237757	0.000346
C	1.482295	0.001142	0.000307
C	4.314623	2.490392	0.000071
C	3.621885	3.673520	0.000337
C	2.201251	3.674916	0.000623
C	1.510053	2.490616	0.000624
C	5.750850	0.003833	-0.000496
N	6.916462	0.004535	-0.000736
C	0.067080	0.000158	0.000487
C	-1.153535	0.000060	0.000508
C	-2.570762	-0.000855	0.000327
C	-3.303220	-1.206633	-0.000832
C	-3.304867	1.203904	0.001233
C	-4.689552	1.208533	0.001020
C	-5.425554	-0.002821	-0.000109
C	-4.687893	-1.213167	-0.001097
N	-6.804290	-0.003735	-0.000192
C	-7.533381	-1.260560	-0.002039
C	-7.534981	1.252153	-0.000578
H	4.167378	-4.610804	-0.000560
H	1.669120	-4.616241	-0.000080
H	5.403414	-2.481497	-0.000616
H	0.428474	-2.483656	0.000302
H	5.400265	2.488718	-0.000141
H	4.161566	4.616460	0.000335
H	1.663301	4.618766	0.000844
H	0.425328	2.484615	0.000841
H	-2.766941	-2.151022	-0.001593
H	-2.769909	2.149043	0.002114
H	-5.205813	2.160718	0.001751
H	-5.202829	-2.166064	-0.002110
H	-7.306972	-1.864596	-0.892185
H	-8.604544	-1.053708	-0.001066
H	-7.306013	-1.867464	0.885863
H	-7.309373	1.857799	0.888646
H	-8.605877	1.043938	-0.001176
H	-7.308342	1.858018	-0.889409

7: ambipolar tri(p-phenylene vinylene)

78

OPV1a

C	8.063131	-0.528291	0.043519
C	7.601632	0.786181	0.068644
C	6.225566	1.023372	0.074751

C	5.287765	-0.021551	0.056063
C	5.793354	-1.340000	0.031885
C	7.155799	-1.593850	0.025508
H	5.110091	-2.183064	0.018546
H	7.536065	-2.610378	0.006952
O	9.404091	-0.887016	0.034831
H	8.281084	1.631637	0.083568
H	5.872681	2.051348	0.094005
C	3.861161	0.305731	0.062594
C	2.827260	-0.562535	0.035592
C	1.402326	-0.236284	0.041409
C	0.897123	1.078119	0.074065
C	0.463310	-1.288261	0.012821
C	-0.902425	-1.048182	0.016413
C	-1.407615	0.266215	0.048695
C	-0.468589	1.318196	0.077633
C	-2.832508	0.592553	0.053814
H	-1.583431	-1.893661	-0.005413
H	0.822658	-2.314561	-0.012156
H	-0.827953	2.344484	0.102830
H	1.578097	1.923603	0.096490
H	3.038971	-1.630550	0.005056
H	3.649286	1.373205	0.092052
C	-3.866550	-0.275381	0.022146
H	-3.044149	1.660484	0.087493
C	-5.293071	0.052421	0.027610
H	-3.654991	-1.342798	-0.011345
C	-5.798196	1.370917	0.058584
C	-6.231220	-0.991997	0.000631
C	-7.607219	-0.754310	0.004945
C	-8.068252	0.560171	0.036957
C	-7.160546	1.625250	0.063373
H	-5.878649	-2.019965	-0.024020
H	-8.286999	-1.599348	-0.017031
H	-5.114688	2.213644	0.078742
H	-7.540515	2.641779	0.087244
O	-9.409074	0.919436	0.044396
C	-10.369322	-0.106920	0.031472
C	-11.693267	0.664564	0.053400
H	-10.261252	-0.759218	0.909794
H	-10.272288	-0.727010	-0.871124
N	-12.962576	-0.180071	0.051802
H	-11.746580	1.315027	-0.822686
H	-11.731264	1.289193	0.948839
C	-13.030934	-1.058712	1.277230
H	-12.949462	-0.430964	2.166112
H	-12.217906	-1.783363	1.253923
H	-13.988857	-1.580958	1.277533
C	-13.043592	-1.034094	-1.190164
H	-12.969855	-0.388901	-2.067137
H	-14.001932	-1.555596	-1.191951
H	-12.231110	-1.759770	-1.188779
C	-14.145254	0.761091	0.068008
H	-14.094872	1.375374	0.967825

H	-15.063448	0.171734	0.068460
H	-14.106862	1.392538	-0.820484
C	10.363831	0.139809	0.046543
C	11.688214	-0.631020	0.028648
H	10.264962	0.762308	0.947292
H	10.256820	0.789690	-0.833698
N	12.957154	0.214372	0.031864
H	11.728769	-1.256921	-0.865780
H	11.739884	-1.280096	0.905852
C	13.035583	1.069213	1.273385
H	12.960913	0.424505	2.150641
H	12.222529	1.794230	1.270317
H	13.993529	1.591421	1.276373
C	14.140317	-0.726170	0.018478
H	14.092189	-1.340983	-0.881112
H	14.100411	-1.357152	0.907229
H	15.058235	-0.136374	0.019559
C	13.027110	1.092229	-1.194037
H	12.213658	1.816451	-1.172555
H	12.947532	0.463863	-2.082656
H	13.984750	1.615000	-1.193076

8: 1,1-didemethylretinal chromophore

57			
retinal B			
C	7.090168	-0.361093	0.172283
C	8.363423	0.445587	0.053805
C	8.163928	1.895802	-0.392077
C	7.004169	2.516471	0.385416
C	5.706066	1.752595	0.102384
C	5.854535	0.237317	0.164181
C	7.341717	-1.843118	0.277931
C	4.651393	-0.556410	0.174417
C	3.370221	-0.076572	0.071409
C	2.190082	-0.886509	0.056362
C	2.316418	-2.386047	0.171766
C	0.963008	-0.241997	-0.069861
C	-0.308436	-0.841376	-0.115597
C	-1.488584	-0.124324	-0.252384
C	-2.782969	-0.685257	-0.315714
C	-2.954817	-2.184624	-0.230880
C	-3.873629	0.187747	-0.464267
C	-5.208818	-0.185118	-0.564688
N	-6.223211	0.662463	-0.718823
C	-7.639879	0.293775	-0.807153
C	-8.465766	0.825512	0.370137
C	-9.948770	0.446371	0.246762
C	-10.790477	0.976731	1.411416
H	9.048198	-0.083394	-0.624119
H	8.864761	0.420594	1.035846
H	7.944549	1.926494	-1.467988
H	9.089838	2.461778	-0.241797
H	6.873329	3.572560	0.124963
H	7.226273	2.480404	1.460693

H	5.322558	2.033413	-0.890137
H	4.937106	2.065163	0.819991
H	8.186474	-2.023823	0.953884
H	7.639588	-2.248304	-0.699338
H	6.497037	-2.428973	0.643024
H	4.774749	-1.631354	0.242653
H	3.213407	0.994684	-0.017883
H	2.898822	-2.789018	-0.664885
H	1.354434	-2.898915	0.179943
H	2.841969	-2.658968	1.093712
H	0.987529	0.844406	-0.146083
H	-0.373356	-1.923059	-0.043992
H	-1.414568	0.959754	-0.322874
H	-2.435056	-2.678413	-1.059419
H	-3.996200	-2.505831	-0.262472
H	-2.525052	-2.568579	0.700596
H	-3.651519	1.252802	-0.514633
H	-5.505480	-1.229005	-0.527814
H	-7.689272	-0.798766	-0.855553
H	-8.035401	0.678134	-1.755633
H	-8.369382	1.919504	0.418207
H	-8.052447	0.431292	1.307680
H	-10.039143	-0.647338	0.194123
H	-10.344963	0.834171	-0.701695
H	-10.440830	0.575843	2.370027
H	-11.841426	0.693701	1.295046
H	-10.744019	2.070556	1.469297
H	-6.011691	1.655268	-0.748403

9: 5,6-dihydroretinal chromophore

65			
retinal D			
C	6.174197	-1.218460	0.100274
C	7.629792	-0.878688	0.487796
C	8.081940	0.525885	0.040141
C	6.972317	1.587578	0.238180
C	5.940769	1.130298	1.277320
C	5.192682	-0.168628	0.803194
C	4.985807	2.256218	1.695400
C	6.045567	-1.229658	-1.439596
C	5.819521	-2.624891	0.616970
C	4.017520	0.161087	-0.060970
C	2.734210	-0.184599	0.206476
C	1.585594	0.155258	-0.601951
C	1.790853	0.929354	-1.878511
C	0.339858	-0.244557	-0.149340
C	-0.906485	0.011591	-0.763477
C	-2.114833	-0.400999	-0.233565
C	-3.388709	-0.146947	-0.800395
C	-3.491197	0.627826	-2.093470
C	-4.514010	-0.632694	-0.122351
C	-5.840641	-0.463844	-0.514403
N	-6.885025	-0.945440	0.148446
C	-8.296069	-0.744818	-0.202362

C	-9.039843	0.114552	0.827407
C	-10.527032	0.272426	0.480368
C	-11.278905	1.134151	1.499526
H	8.299495	-1.637899	0.064269
H	7.729214	-0.967287	1.577103
H	8.398547	0.505852	-1.008557
H	8.971449	0.803046	0.617503
H	6.462573	1.799720	-0.712953
H	7.410915	2.541274	0.554763
H	6.495555	0.837134	2.178687
H	4.803269	-0.650448	1.709149
H	5.550057	3.079835	2.146880
H	4.249766	1.912332	2.432071
H	4.433570	2.667213	0.841194
H	6.254474	-0.255823	-1.894844
H	5.045424	-1.544297	-1.759415
H	6.761947	-1.944715	-1.860159
H	4.770726	-2.873215	0.409836
H	5.977295	-2.704232	1.699374
H	6.442552	-3.386222	0.132960
H	4.226982	0.734162	-0.961684
H	2.529768	-0.752759	1.113141
H	2.260425	1.897896	-1.670419
H	0.863976	1.121464	-2.419336
H	2.462247	0.384748	-2.552208
H	0.310931	-0.802556	0.785627
H	-0.916384	0.569286	-1.695410
H	-2.093866	-0.960295	0.700404
H	-3.043845	1.621291	-1.981564
H	-4.516150	0.767221	-2.437527
H	-2.947119	0.110982	-2.891578
H	-4.337467	-1.189538	0.796676
H	-6.096350	0.088960	-1.413420
H	-8.766306	-1.731638	-0.290437
H	-8.323579	-0.280833	-1.193207
H	-8.559017	1.099767	0.887532
H	-8.941375	-0.344591	1.821442
H	-10.993413	-0.720460	0.420609
H	-10.622186	0.717938	-0.519529
H	-11.228554	0.697480	2.503805
H	-12.335464	1.226158	1.228914
H	-10.858519	2.145218	1.552183
H	-6.703818	-1.460827	1.005266

10: rhodamine-6G

64			
C	2.858536	-1.842571	0.253880
C	3.945990	-0.956615	0.118093
C	3.716252	0.391105	-0.354986
C	2.435502	0.772403	-0.660118
C	1.313892	-0.099546	-0.533819
C	1.583944	-1.415316	-0.064969
C	-0.016304	0.270498	-0.819106
C	-1.036091	-0.696635	-0.682377

O	0.583511	-2.322371	0.084110
C	-0.701567	-1.995036	-0.216167
C	-1.657485	-2.970039	-0.031470
C	-3.020751	-2.717642	-0.305245
C	-3.396781	-1.418300	-0.818338
C	-2.408801	-0.470791	-0.972966
N	-3.884188	-3.761290	-0.116919
C	-5.314327	-3.749869	0.226460
C	-5.603794	-3.215459	1.632560
H	-3.417921	-4.596122	0.217096
N	5.203722	-1.348566	0.423003
C	5.583726	-2.672691	0.912407
C	7.088244	-2.744020	1.152514
H	5.949712	-0.680037	0.295742
C	-0.329643	1.626627	-1.367826
C	-0.320198	1.785079	-2.759554
C	-0.608644	3.021212	-3.339691
C	-0.909988	4.117870	-2.532173
C	-0.920001	3.974718	-1.146915
C	-0.632703	2.738560	-0.551572
C	-0.647631	2.578903	0.935468
O	-0.454731	1.517598	1.502514
O	-0.892580	3.731403	1.575036
C	-0.928792	3.667340	3.027141
C	-1.161967	5.073893	3.540177
H	2.994869	-2.858408	0.601796
C	4.872065	1.348478	-0.499263
H	2.257883	1.782956	-1.013199
H	-1.344925	-3.937264	0.350149
C	-4.800456	-1.066138	-1.256615
H	-2.688674	0.503302	-1.359981
H	-5.642675	-4.790170	0.142522
H	-5.873250	-3.193591	-0.524514
H	-5.088185	-3.808858	2.395370
H	-6.678913	-3.260139	1.837772
H	-5.278627	-2.174697	1.737485
H	5.280163	-3.431555	0.178430
H	5.039574	-2.882661	1.843014
H	7.646283	-2.560041	0.227530
H	7.361020	-3.738987	1.514811
H	7.405745	-2.014327	1.905714
H	-0.085368	0.932509	-3.390414
H	-0.597039	3.122862	-4.420916
H	-1.136263	5.081352	-2.978632
H	-1.152062	4.819624	-0.509291
H	0.019408	3.248151	3.376558
H	-1.727695	2.979203	3.320227
H	-0.354772	5.744863	3.230109
H	-1.196969	5.063098	4.634606
H	-2.110638	5.476411	3.171471
H	-5.513407	-1.042642	-0.425204
H	-5.179195	-1.772345	-2.004223
H	-4.805317	-0.073687	-1.715003
H	5.386550	1.513894	0.457132

H	4.525475	2.322304	-0.853937
H	5.618935	0.986835	-1.219570

11: (*Z*)-2-(3-((*E*)-4-(diphenylamino)styryl)-5,5-dimethylcyclohex-2-enylidene)-2-cyanoacetic acid

63

TAAS1

N	4.741370	-0.117929	-0.000764
C	5.691248	0.942882	-0.093737
C	5.228225	-1.457812	0.085270
C	3.361692	0.146468	0.044229
C	6.814353	0.952944	0.745779
C	7.757554	1.973701	0.642815
C	7.587500	3.003688	-0.284611
C	6.466881	2.997834	-1.118304
C	5.527508	1.971464	-1.034198
C	6.197845	-1.910634	-0.820924
C	6.692266	-3.210289	-0.725774
C	6.218825	-4.077336	0.261208
C	5.249941	-3.629103	1.161613
C	4.761683	-2.325653	1.083555
C	2.432130	-0.787852	-0.463199
C	1.071533	-0.540007	-0.407193
C	0.559855	0.655368	0.142714
C	1.500007	1.588841	0.625045
C	2.864471	1.345635	0.590606
C	-0.855500	0.966550	0.234316
C	-1.902435	0.139887	-0.029083
C	-3.297989	0.485170	0.098917
C	-4.244130	-0.489691	-0.089520
C	-3.720902	1.886616	0.477079
C	-5.161674	2.231055	0.041607
C	-6.109998	1.099774	0.495913
C	-5.653750	-0.281972	0.084063
C	-5.595038	3.544005	0.714385
C	-5.235509	2.405741	-1.489454
C	-6.536506	-1.339364	-0.084530
C	-6.041628	-2.620440	-0.475828
C	-8.015489	-1.259202	0.124914
N	-5.713555	-3.692974	-0.800447
O	-8.601367	-0.284016	0.546141
O	-8.724125	-2.375937	-0.178068
H	6.941316	0.158116	1.473861
H	8.623080	1.968488	1.299890
H	8.321129	3.801282	-0.358910
H	6.328421	3.788139	-1.851301
H	4.665908	1.958403	-1.694553
H	6.559638	-1.239606	-1.593918
H	7.443056	-3.548861	-1.434797
H	6.602061	-5.091428	0.329307
H	4.880328	-4.291231	1.940047
H	4.020955	-1.973276	1.794865
H	2.792305	-1.706775	-0.912693
H	0.392985	-1.278819	-0.823563

H	1.143390	2.519644	1.060380
H	3.553249	2.079261	0.994923
H	-1.070676	1.977067	0.577083
H	-1.704549	-0.887671	-0.329643
H	-3.909264	-1.488264	-0.358674
H	-3.026502	2.619079	0.049083
H	-3.639746	1.992050	1.570326
H	-7.125634	1.281336	0.143991
H	-6.184302	1.105645	1.594738
H	-5.559529	3.466045	1.807894
H	-6.620520	3.808999	0.431546
H	-4.941336	4.372083	0.413867
H	-4.920628	1.502798	-2.022208
H	-4.590654	3.230462	-1.816651
H	-6.260231	2.638843	-1.801547
H	-8.143325	-3.087027	-0.503878

12: 5,5',6,6'-tetrachloro-1,1'-diethyl-3,3'-di(4-sulfobutyl)-benzimidazolocarbo-cyanine (TDBC)

78
TDBC

C	3.659824	-2.199905	-3.717044
C	5.031426	-2.258027	-3.982076
C	5.915292	-1.307329	-3.441027
C	5.448205	-0.270128	-2.627782
C	4.083364	-0.214077	-2.374044
C	3.201551	-1.172766	-2.901154
Cl	5.611969	-3.555601	-5.005786
Cl	7.636109	-1.382707	-3.762468
N	1.923009	-0.857738	-2.452170
C	2.003860	0.255770	-1.653885
N	3.319449	0.671796	-1.626470
C	0.695943	-1.390492	-3.096418
C	0.523387	-0.870658	-4.522478
C	3.861593	1.534591	-0.562739
C	4.130743	0.738530	0.721194
C	4.318018	1.636189	1.951068
C	4.394384	0.857983	3.268633
S	2.824701	0.026038	3.748319
O	2.646687	-1.079600	2.746263
O	3.074967	-0.450295	5.130227
O	1.782189	1.087549	3.621922
C	0.965780	0.901275	-0.955737
C	-0.061608	0.250218	-0.284409
C	-1.157396	0.889925	0.293988
C	-2.067068	0.308660	1.185770
N	-1.835076	-0.673523	2.119967
N	-3.393065	0.688759	1.290274
C	-3.020468	-0.938634	2.791611
C	-4.007117	-0.086119	2.262451
C	-0.511380	-1.145583	2.579758
C	-0.165616	-2.561867	2.128602
C	-4.099082	1.428872	0.232902
C	-4.372657	0.541202	-0.988176

C	-4.704344	1.341653	-2.257255
C	-4.560117	0.515673	-3.539931
S	-2.821008	0.065375	-3.934129
O	-2.067514	1.348280	-3.819054
O	-2.427567	-0.943682	-2.891374
O	-2.891482	-0.504514	-5.304652
C	-3.310512	-1.822827	3.822967
C	-4.623861	-1.853894	4.304395
C	-5.613751	-1.017401	3.761392
C	-5.313891	-0.118252	2.732197
Cl	-4.994714	-2.976466	5.597475
H	-6.089816	0.521322	2.329932
H	2.993031	-2.940673	-4.140366
H	6.143711	0.450538	-2.215229
H	-0.178027	-1.102870	-2.513593
H	0.774511	-2.482413	-3.060286
H	0.361832	0.210963	-4.508889
H	-0.383528	-1.308084	-4.948791
H	1.378832	-1.108716	-5.164831
H	3.131466	2.324383	-0.377908
H	4.760427	2.018604	-0.960023
H	5.011356	0.097367	0.577755
H	3.287759	0.069157	0.913833
H	3.470219	2.328842	2.026651
H	5.227234	2.247692	1.840505
H	4.624245	1.537165	4.095410
H	5.165201	0.079614	3.242925
H	1.053633	1.977853	-0.848935
H	0.004120	-0.831015	-0.191473
H	-1.381839	1.901006	-0.028925
H	-0.515907	-1.079265	3.671971
H	0.239746	-0.430419	2.245403
H	-0.850072	-3.310859	2.544415
H	0.853193	-2.766053	2.468715
H	-0.193863	-2.656542	1.037370
H	-3.479408	2.284314	-0.047288
H	-5.012291	1.837229	0.678479
H	-5.181000	-0.165330	-0.754221
H	-3.478170	-0.054439	-1.194452
H	-4.017080	2.192966	-2.340897
H	-5.723525	1.753146	-2.200577
H	-4.912021	1.087626	-4.403916
H	-5.127468	-0.420313	-3.494977
H	-2.559836	-2.477299	4.248132
Cl	-7.266381	-1.066524	4.346446

13: chlorin

40			
chlorin			
C	0.930549	-4.219503	0.000273
C	-0.442208	-4.263680	0.000068
C	-0.932371	-2.915277	-0.000015
N	0.165868	-2.101802	0.000192
C	1.330040	-2.845137	0.000280

C	2.615911	-2.321331	0.000272
C	2.982035	-0.965842	0.000083
N	2.110050	0.083572	-0.000116
C	4.360086	-0.503473	-0.000086
C	4.303028	0.856014	-0.000240
C	2.891152	1.201909	-0.000194
C	2.415157	2.522675	-0.000246
C	1.091258	2.941394	-0.000134
C	-2.274506	-2.508319	-0.000343
C	-2.783081	-1.215743	-0.000404
C	-4.285684	-0.944747	-0.001558
N	-2.049587	-0.080830	0.000071
C	-4.350670	0.592492	0.001543
C	-2.875661	0.989099	0.000520
N	-0.010442	2.108125	0.000036
C	-1.169580	2.831960	0.000227
C	-0.788243	4.214740	0.000189
C	0.583724	4.279910	-0.000037
C	-2.474844	2.318918	0.000510
H	1.618533	-5.054854	0.000373
H	-1.076371	-5.140402	-0.000031
H	0.153363	-1.088153	0.000147
H	3.423860	-3.048139	0.000351
H	5.236411	-1.140500	-0.000050
H	5.123244	1.563889	-0.000357
H	3.161989	3.312153	-0.000345
H	-3.000569	-3.316761	-0.000667
H	-4.766687	-1.390626	0.876800
H	-4.763934	-1.386471	-0.883571
H	-4.864148	0.992608	0.883486
H	-4.867110	0.996497	-0.876835
H	0.053159	1.096498	0.000093
H	-1.489711	5.038599	0.000327
H	1.203774	5.166884	-0.000123
H	-3.263320	3.066731	0.000806

14: free-base porphyrin (porphin)

38			
porphin			
C	4.260039	-0.682826	0.000028
C	4.259003	0.689328	0.000043
C	2.894326	1.132289	0.000038
N	2.116259	0.001641	0.000000
C	2.896026	-1.127843	0.000036
C	2.423407	-2.439201	0.000036
C	1.086754	-2.854952	0.000016
N	0.001518	-2.029789	-0.000012
C	0.681409	-4.257724	-0.000024
C	-0.674911	-4.258786	0.000020
C	-1.082444	-2.856653	-0.000009
C	-2.419723	-2.442935	-0.000004
C	-2.894314	-1.132287	0.000001
C	2.419730	2.442931	0.000042
C	1.082441	2.856639	0.000011

C	0.674924	4.258781	-0.000130
N	-0.001516	2.029789	-0.000085
C	-0.681397	4.257729	0.000075
C	-1.086757	2.854965	-0.000017
N	-2.116248	-0.001641	-0.000003
C	-2.896014	1.127841	0.000009
C	-4.260027	0.682827	0.000044
C	-4.258991	-0.689328	0.000018
C	-2.423400	2.439205	0.000015
H	5.116594	-1.344007	0.000029
H	5.114567	1.351790	0.000055
H	1.100839	0.000898	-0.000036
H	3.182106	-3.216806	0.000039
H	1.356413	-5.105042	-0.000039
H	-1.348591	-5.107156	0.000039
H	-3.177266	-3.221668	0.000007
H	3.177262	3.221674	0.000042
H	1.348612	5.107144	-0.000207
H	-1.356392	5.105054	0.000160
H	-1.100827	-0.000898	-0.000016
H	-5.116574	1.344017	0.000073
H	-5.114548	-1.351800	0.000028
H	-3.182110	3.216801	0.000061

15: anthracene

24			
anthracene			
C	2.479534	-1.406965	-0.000055
C	3.660643	-0.713171	-0.000029
C	3.660643	0.713171	0.000029
C	2.479534	1.406965	0.000055
C	1.223879	0.722394	0.000021
C	1.223879	-0.722394	-0.000021
C	0.000000	-1.403267	0.000000
C	-1.223879	-0.722394	0.000021
C	-1.223879	0.722394	-0.000021
C	0.000000	1.403267	0.000000
C	-2.479534	1.406965	-0.000055
C	-3.660643	0.713171	-0.000029
C	-3.660643	-0.713171	0.000029
C	-2.479534	-1.406965	0.000055
H	2.476721	-2.494640	-0.000118
H	4.607477	-1.246598	-0.000079
H	4.607477	1.246598	0.000079
H	2.476721	2.494640	0.000118
H	0.000000	-2.491731	0.000000
H	0.000000	2.491731	0.000000
H	-2.476721	2.494640	-0.000118
H	-4.607477	1.246598	-0.000079
H	-4.607477	-1.246598	0.000079
H	-2.476721	-2.494640	0.000118

16: pentacene

36

pentacene

C	4.941789	-1.410408	0.000240
C	6.117814	-0.716617	0.000127
C	6.117814	0.716617	-0.000127
C	4.941789	1.410408	-0.000240
C	3.678571	0.727467	-0.000115
C	3.678571	-0.727467	0.000115
C	2.467682	-1.407697	0.000171
C	1.226431	-0.728336	0.000048
C	1.226431	0.728336	-0.000048
C	2.467682	1.407697	-0.000171
C	0.000000	1.408315	0.000000
C	-1.226431	0.728336	0.000048
C	-1.226431	-0.728336	-0.000048
C	0.000000	-1.408315	0.000000
H	4.939421	-2.498043	0.000427
H	7.066072	-1.247456	0.000230
H	7.066072	1.247456	-0.000230
H	4.939421	2.498043	-0.000427
H	2.467469	-2.496005	0.000300
H	2.467469	2.496005	-0.000300
H	0.000000	2.496525	0.000000
C	-2.467682	1.407697	0.000171
C	-2.467682	-1.407697	-0.000171
H	0.000000	-2.496525	0.000000
C	-3.678571	0.727467	0.000115
C	-3.678571	-0.727467	-0.000115
C	-4.941789	-1.410408	-0.000240
C	-6.117814	-0.716617	-0.000127
C	-6.117814	0.716617	0.000127
C	-4.941789	1.410408	0.000240
H	-2.467469	2.496005	0.000300
H	-2.467469	-2.496005	-0.000300
H	-4.939421	-2.498043	-0.000427
H	-7.066072	-1.247456	-0.000230
H	-7.066072	1.247456	0.000230
H	-4.939421	2.498043	0.000427

Bibliography

- [1] A. Facchetti. π -conjugated polymers for organic electronics and photovoltaic cell applications. *Chem. Mater.*, 23:733–758, 2011.
- [2] J. D. Myers and J. Xue. Organic semiconductors and their applications in photovoltaic devices. *Polym. Rev.*, 52:1–37, 2012.
- [3] S. Difley, L.-P. Wang, S. Yeganeh, S. Yost, and T. Van Voorhis. Electronic properties of disordered organic semiconductors via QM/MM simulations. *Acc. Chem. Res.*, 43:995–1004, 2010.
- [4] J. W. Verhoeven. On the role of spin correlation in the formation, decay, and detection of long-lived, intramolecular charge-transfer states. *J. Photochem. Photobiol. C*, 7:40–60, 2006.
- [5] N. Satoh, T. Nakashima, and K. Yamamoto. Metal-assembling dendrimers with a triarylamine core and their application to a dye-sensitized solar cell. *J. Am. Chem. Soc.*, 127:13030–13038, 2005.
- [6] P. A. Sullivan, A. J. P. Akelaitis, S. K. Lee, G. McGrew, S. K. Lee, D. H. Choi, and L. R. Dalton. Novel dendritic chromophores for electro-optics: Influence of binding mode and attachment flexibility on electro-optic behavior. *Chem. Mater.*, 18:344–351, 2006.
- [7] J. W. Verhoeven, H. J. van Ramesdonk, M. M. Groeneveld, A. C. Benniston, and A. Harriman. Long-lived charge-transfer states in compact donor-acceptor dyads. *ChemPhysChem*, 6:2251–2260, 2005.
- [8] A. Valdés, J. Brilliet, M. Grätzel, H. Gudmundsdóttir, H. A. Hansen, H. Jónsson, P. Klüpfel, G.-J. Kroes, F. Le Formal, I. C. Man, R. S. Martins, J. K. Nørskov, J. Rossmeisl, K. Sivula, A. Vojvodic, and M. Zäch. Solar hydrogen production with semiconductor metal oxides: new directions in experiment and theory. *Phys. Chem. Chem. Phys.*, 14:49–70, 2012.
- [9] L.-P. Wang and T. Van Voorhis. Direct-coupling O₂ bond forming a pathway in cobalt oxide water oxidation catalysts. *J. Phys. Chem. Lett.*, 2:2200–2204, 2011.
- [10] G. Ceder. Opportunities and challenges for first-principles materials design and applications to Li battery materials. *MRS Bull.*, 35:693–701, 2010.

- [11] J. Hachmann, R. Olivares-Amaya, S. Atahan-Evrenk, C. Amador-Bedolla, R. S. Sanchez-Carrera, A. Gold-Parker, L. Vogt, A. M. Brockway, and A. Aspuru-Guzik. The harvard clean energy project: Large-scale computational screening and design of organic photovoltaics on the World Community Grid. *J. Phys. Chem. Lett.*, 2:2241–2251, 2011.
- [12] G. Hautier, C. C. Fischer, A. Jain, T. Mueller, and G. Ceder. Finding Nature’s missing ternary oxide compounds using machine learning and density functional theory. *Chem. Mater.*, 22:3762–3767, 2010.
- [13] H. Kobayashi and P. L. Choyke. Target-cancer-cell-specific activatable fluorescence imaging probes: Rational design and *in vivo* applications. *Acc. Chem. Res.*, 44:83–90, 2011.
- [14] J. Michl and E. C. H. Sykes. Molecular rotors and motors: Recent advances and future challenges. *ACS Nano*, 3:1042–1048, 2009.
- [15] S. Shim, P. Rebentrost, S. Valleau, and A. Aspuru-Guzik. Atomistic study of the long-lived quantum coherences in the Fenna-Matthews-Olson complex. *Biophys. J.*, 102:649–660, 2012.
- [16] R. A. Marcus. On the theory of oxidation-reduction reactions involving electron transfer. 1. *J. Chem. Phys.*, 24:966–978, 1956.
- [17] R. A. Marcus. Chemical + electrochemical electron-transfer theory. *Ann. Rev. Phys. Chem.*, 15:155–196, 1964.
- [18] P. F. Barbara, T. J. Meyer, and M. A. Ratner. Contemporary issues in electron transfer research. *J. Phys. Chem.*, 100(31):13148–13168, 1996.
- [19] M. Bixon and J. Jortner. Electron-transfer — from isolated molecules to biomolecules. *Adv. Chem. Phys.*, 106:35–202, 2007.
- [20] R. A. Marcus. Electron transfers in chemistry and biology. *Biochim. Biophys. Acta*, 811:265–322, 1985.
- [21] I. R. Gould, D. Noukakis, L. Gomez-Jahn, R. H. Young, J. L. Goodman, and S. Farid. Radiative and nonradiative electron transfer in contact radical-ion pairs. *Chem. Phys.*, 176:439–456, 1993.
- [22] G. K. Schenter, B. C. Garrett, and D. G. Truhlar. The role of collective solvent coordinates and nonequilibrium solvation in charge-transfer reactions. *J. Phys. Chem. B*, 105:9672–9685, 2001.
- [23] D. V. Matyushov and G. A. Voth. New developments in the theoretical description of charge-transfer reactions in condensed phases. *Rev. Comp. Chem.*, 18:147–210, 2002.

- [24] I. R. Gould, D. Ege, J. E. Moser, and S. Farid. Efficiencies of photoinduced electron-transfer reactions: Role of the Marcus inverted region in return electron transfer within geminate radical-ion pairs. *J. Am. Chem. Soc.*, 112:4290–4301, 1990.
- [25] D. V. Matyushov and R. Schmid. Optical and radiationless intramolecular electron transitions in nonpolar fluids: Relative effects of induction and dispersion interactions. *J. Chem. Phys.*, 103:2034–2049, 1995.
- [26] R. Doolen, J. D. Simon, and K. K. Baldrige. Solvent, isotope, and substituent effects on the bimolecular electron transfer reaction between chlorine oxide and benzenes. *J. Phys. Chem.*, 99:13938–13947, 1995.
- [27] J. C. Goeltz, E. E. Benson, and C. P. Kubiak. Electronic structural effects in self-exchange reactions. *J. Phys. Chem. B*, 114:14729–14734, 2010.
- [28] S. F. Nelsen, S. C. Blackstock, and Y. Kim. Estimation of inner shell marcus terms for amino nitrogen compounds by molecular orbital calculations. *J. Am. Chem. Soc.*, 109:677–682, 1987.
- [29] T. Van Voorhis, T. Kowalczyk, B. Kaduk, L.-P. Wang, C.-L. Cheng, and Q. Wu. The diabatic picture of electron transfer, reaction barriers, and molecular dynamics. *Ann. Rev. Phys. Chem.*, 61:149–170, 2010.
- [30] R. J. Cave and M. D. Newton. Generalization of the Mulliken-Hush treatment for the calculation of electron transfer matrix elements. *Chem. Phys. Lett.*, 249:15–19, 1996.
- [31] A. Warshel and R. M. Weiss. An empirical valence bond approach for comparing reactions in solutions and in enzymes. *J. Am. Chem. Soc.*, 102:6218–6226, 1980.
- [32] T. A. Wesolowski and A. Warshel. Frozen density-functional approach for *ab initio* calculations of solvated molecules. *J. Phys. Chem.*, 97:8050–8053, 1993.
- [33] Q. Wu and T. Van Voorhis. Constrained density functional theory and its application in long-range electron transfer. *J. Chem. Theory Comput.*, 2(3):765–774, 2006.
- [34] P. Hohenberg and W. Kohn. Inhomogeneous electron gas. *Phys. Rev.*, 136:B864–B871, 1964.
- [35] B. J. Zhou, V. L. Ligneres, and E. A. Carter. Improving the orbital-free density functional theory description of covalent materials. *J. Chem. Phys.*, 122:044103, 2005.
- [36] W. Kohn and L. J. Sham. Self-consistent equations including exchange and correlation effects. *Phys. Rev.*, 140:A1133–A1138, 1965.

- [37] A. Szabo and N.S. Ostlund. *Modern Quantum Chemistry: Introduction to Advanced Electronic Structure Theory*. Dover Publications, New York, 1996.
- [38] J. P. Perdew, A. Ruzsinszky, L. A. Constantin, J. Sun, and G. I. Csonka. Some fundamental issues in ground-state density functional theory: A guide for the perplexed. *J. Chem. Theory Comput.*, 5:902–908, 2009.
- [39] A. D. Becke. Density-functional thermochemistry .3. The role of exact exchange. *J. Chem. Phys.*, 98:5648–5652, 1993.
- [40] J. Toulouse, F. Colonna, and A. Savin. Long-range–short-range separation of the electron-electron interaction in density-functional theory. *Phys. Rev. A*, 70:062505, 2004.
- [41] Y. Tawada, T. Tsuneda, S. Yanagisawa, T. Yanai, and K. Hirao. A long-range-corrected time-dependent density functional theory. *J. Chem. Phys.*, 120:8425–8433, 2004.
- [42] E. Runge and E. K. U. Gross. Density-functional theory for time-dependent systems. *Phys. Rev. Lett.*, 52:997–1000, 1984.
- [43] K. Burke, J. Werschnik, and E. K. U. Gross. Time-dependent density functional theory: Past, present, and future. *J. Chem. Phys.*, 123:62206, 2005.
- [44] F. Furche. On the density matrix based approach to time-dependent density functional response theory. *J. Chem. Phys.*, 114:5982–5992, 2001.
- [45] M. A. L. Marques and E. K. U. Gross. Time-dependent density functional theory. *Ann. Rev. Phys. Chem.*, 55:427–455, 2004.
- [46] A. Dreuw, J. L. Weisman, and M. Head-Gordon. Long-range charge-transfer excited states in time-dependent density functional theory require non-local exchange. *J. Chem. Phys.*, 119(6):2943–2946, 2003.
- [47] R. S. Mulliken. Electronic populations analysis on LCAO-MO molecular wave functions. *J. Chem. Phys.*, 23:1833–1840, 1955.
- [48] P. Löwdin. On the non-orthogonality problem connected with the use of atomic wave functions in the theory of molecules and crystals. *J. Chem. Phys.*, 18:365–375, 1950.
- [49] A. D. Becke. A multicenter numerical integration scheme for polyatomic molecules. *J. Chem. Phys.*, 88(4):2547–2553, 1988.
- [50] F. L. Hirshfeld. Bonded-atom fragments for describing molecular charge densities. *Theor. Chim. Acta*, 44:129–138, 1977.
- [51] O. V. Prezhdo, J. T. Kindt, and J. C. Tully. Perturbed ground state method for electron transfer. *J. Chem. Phys.*, 111:7818–7827, 1999.

- [52] R. Gaudoin and K. Burke. Lack of Hohenberg-Kohn theorem for excited states. *Phys. Rev. Lett.*, 93:173001, 2004.
- [53] M. Levy and A. Nagy. Variational density-functional theory for an individual excited state. *Phys. Rev. Lett.*, 83:4361–4364, 1999.
- [54] M. Hemanadhan and M. K. Harbola. Is it possible to construct excited-state energy functionals by splitting k -space? *J. Mol. Struct. Theochem.*, 943:152–157, 2010.
- [55] M. V. Basilevsky, G. E. Chudinov, I. V. Rostov, Y. P. Liu, and M. D. Newton. Quantum-chemical evaluation of energy quantities governing electron transfer kinetics: Application to intramolecular processes. *J. Mol. Struct. Theochem.*, 371:191–203, 1996.
- [56] C. J. Cramer and D. G. Truhlar. Implicit solvation models: Equilibria, structure, spectra, and dynamics. *Chem. Rev.*, 99:2161–2200, 1999.
- [57] M. A. Aguilar. Separation of the electric polarization into fast and slow components: A comparison of two partition schemes. *J. Phys. Chem. A*, 105:10393–10396, 2001.
- [58] J. Tomasi, B. Mennucci, and R. Cammi. Quantum mechanical continuum solvation models. *Chem. Rev.*, 105:2999–3093, 2005.
- [59] D. Frenkel and B. Smit. *Understanding Molecular Simulation: From Algorithms to Applications*. Academic Press, San Diego, 2nd edition, 2001.
- [60] L.-P. Wang and T. Van Voorhis. Hybrid ensembles for improved force matching. *J. Chem. Phys.*, 133:231101, 2010.
- [61] H. Lin and D. G. Truhlar. QM/MM: What have we learned, where are we, and where do we go from here? *Theor. Chim. Acta*, 117:185–199, 2007.
- [62] J.-K. Hwang and A. Warshel. Microscopic examination of free-energy relationships for electron transfer in polar solvents. *J. Am. Chem. Soc.*, 109:715–720, 1987.
- [63] M. Tachiya. Reaction coordinate in electron transfer: what physical quantity should we use for it? *J. Chem. Phys.*, 129:066102, 2008.
- [64] B. Kaduk, T. Kowalczyk, and T. Van Voorhis. Constrained density functional theory. *Chem. Rev.*, 112:321–370, 2012.
- [65] M.-H. Ham, J. H. Choi, A. A. Boghossian, E. S. Jeng, R. A. Graff, D. A. Heller, A. C. Chang, A. Mattis, T. H. Bayburt, Y. V. Grinkova, A. S. Zeiger, K. J. Van Vliet, E. K. Hobbie, S. G. Sligar, C. A. Wraight, and M. S. Strano. Photoelectrochemical complexes for solar energy conversion that chemically and autonomously regenerate. *Nature Chem.*, 2:929–936, 2010.

- [66] I. McConnell, G. H. Li, and G. W. Brudvig. Energy conversion in natural and artificial photosynthesis. *Chem. Biol.*, 17:434–447, 2010.
- [67] M. Grätzel. Photoelectrochemical cells. *Nature*, 414:338–344, 2001.
- [68] Veldman D., O. Ipek, S. C. J. Meskers, J. Sweelssen, M. M. Koetse, S. C. Veenstra, J. M. Kroon, S. S. van Bavel, J. Loos, and R. A. J. Janssen. Compositional and electric field dependence of the dissociation of charge transfer excitons in alternating polyfluorene copolymer/fullerene blends. *J. Am. Chem. Soc.*, 130:7721–7735, 2008.
- [69] J. Lee, K. Vandewal, S. Yost, M. E. Bahlke, L. Goris, M. A. Baldo, J. V. Manca, and T. Van Voorhis. Charge transfer state versus hot exciton dissociation in polymer-fullerene blended solar cells. *J. Am. Chem. Soc.*, 132:11878–11880, 2010.
- [70] R. E. Blankenship. *Molecular Mechanisms of Photosynthesis*. Blackwell Science, Oxford, 2002.
- [71] A. Hagfeldt and M. Grätzel. Molecular photovoltaics. *Acc. Chem. Res.*, 33:269–277, 2000.
- [72] R. Mauer, I. A. Howard, and F. Laquai. Effect of nongeminate recombination on fill factor in polythiophene/methanofullerene organic solar cells. *J. Phys. Chem. Lett.*, 1:3500–3505, 2010.
- [73] M. R. Wasielewski, M. P. Niemczyk, W. A. Svec, and E. B. Pewitt. Dependence of rate constants for photoinduced charge separation and dark charge recombination on the free-energy of reaction in restricted-distance porphyrin quinone molecules. *J. Am. Chem. Soc.*, 107:1080–1082, 1985.
- [74] T. Liu and A. Troisi. Absolute rate of charge separation and recombination in a molecular model of the P3HT/PCBM interface. *J. Phys. Chem. C*, 115:2406–2415, 2011.
- [75] H. Imahori, K. Tamaki, D. M. Guldi, C. P. Luo, M. Fukitsuka, O. Ito, Y. Sakata, and S. Fukuzumi. Modulating charge separation and charge recombination dynamics in porphyrin fullerene linked dyads and triads: Marcus-normal versus inverted region. *J. Am. Chem. Soc.*, 123:2607–2617, 2001.
- [76] H. Hoppea and N. S. Sariciftci. Organic solar cells: an overview. *J. Mater. Res.*, 19:1924–1945, 2004.
- [77] M. T. Lloyd, J. E. Anthony, and G. G. Malliaras. Photovoltaics from soluble small molecules. *Mater. Today*, 10:34–41, 2007.
- [78] A. Gouloumis, A. de la Escosura, P. Vazquez, T. Torres, A. Kahnt, D. M. Guldi, H. Neugebauer, C. Winder, M. Drees, and N. S. Sariciftci. Photoinduced electron transfer in a new bis(C₆₀)-phthalocyanine triad. *Org. Lett.*, 8:5187–5190, 2006.

- [79] F. X. L. I. Xamena, L. Teruel, M. Alvaro, and H. Garcia. Donor/conductor/acceptor triads spatially organized on the micrometer-length scale: An alternative approach to photovoltaic cells. *Chem. Eur. J.*, 13:515–519, 2007.
- [80] K. Hasharoni, H. Levanon, J. Tang, M. K. Bowman, J. R. Norris, D. Gust, T. A. Moore, and A. L. Moore. Singlet photochemistry in model photosynthesis: Identification of charge separated intermediates by Fourier transform and CW-EPR spectroscopies. *J. Am. Chem. Soc.*, 112:6477–6481, 1990.
- [81] J. R. Miller, J. V. Beitz, and R. K. Huddleston. Effect of free energy on rates of electron transfer between molecules. *J. Am. Chem. Soc.*, 106:5057–5068, 1984.
- [82] A. D. Clegg, N. V. Rees, O. V. Klymenko, B. A. Coles, and R. G. Compton. Experimental validation of Marcus theory for outer-sphere heterogeneous electron-transfer reactions: The oxidation of substituted 1,4-phenylenediamines. *ChemPhysChem*, 5:1234–1240, 2004.
- [83] J. Jortner. Temperature-dependent activation-energy for electron-transfer between biological molecules. *J. Chem. Phys.*, 64:4860–4867, 1976.
- [84] D. W. Small, D. V. Matyushov, and G. A. Voth. The theory of electron transfer reactions: What may be missing? *J. Am. Chem. Soc.*, 125:7470–7478, 2003.
- [85] J. Blumberger. Free energies for biological electron transfer from QM/MM calculation: method, application and critical assessment. *Phys. Chem. Chem. Phys.*, 10:5651–5667, 2008.
- [86] V. Tipmanee, H. Oberhofer, M. Park, K. S. Kim, and J. Blumberger. Prediction of reorganization free energies for biological electron transfer: A comparative study of Ru-modified cytochromes and a 4-helix bundle protein. *J. Am. Chem. Soc.*, 132:17032–17040, 2010.
- [87] A. Warshel. Dynamics of reactions in polar solvents. Semiclassical trajectory studies of electron-transfer and proton-transfer reactions. *J. Phys. Chem.*, 86:2218–2224, 1982.
- [88] R. A. Kuharski, J. S. Bader, D. Chandler, M. Sprik, M. L. Klein, and R. W. Impey. Molecular model for aqueous ferrous-ferric electron transfer. *J. Chem. Phys.*, 89:3248–3257, 1988.
- [89] A. Warshel and M. Levitt. Theoretical studies of enzymatic reactions: Dielectric, electrostatic and steric stabilization of the carbonium ion in the reaction of lysozyme. *J. Mol. Biol.*, 103:227–249, 1976.
- [90] M. H. M. Olsson, G. Y. Hong, and A. Warshel. Frozen density functional free energy simulations of redox proteins: Computational studies of the reduction potential of plastocyanin and rusticyanin. *J. Am. Chem. Soc.*, 125:5025–5039, 2003.

- [91] G. King and A. Warshel. Investigation of the free-energy functions for electron-transfer reactions. *J. Chem. Phys.*, 93:8682–8692, 1990.
- [92] Q. Wu and T. Van Voorhis. Direct optimization method to study constrained systems within density-functional theory. *Phys. Rev. A*, 72(2):024502, 2005.
- [93] P. H.-L. Sit, M. Cococcioni, and N. Marzari. Realistic quantitative descriptions of electron transfer reactions: Diabatic free-energy surfaces from first-principles molecular dynamics. *Phys. Rev. Lett.*, 97:028303, 2006.
- [94] H. Oberhofer and J. Blumberger. Charge constrained density functional molecular dynamics for simulation of condensed phase electron transfer reactions. *J. Chem. Phys.*, 131:064101, 2009.
- [95] K. Okamoto, T. Hasobe, N. V. Tkachenko, H. Lemmetyinen, P. V. Kamat, and S. Fukuzumi. Drastic difference in lifetimes of the charge-separated state of the formanilide-anthraquinone dyad versus the ferrocene-formanilide-anthraquinone triad and their photoelectrochemical properties of the composite films with fullerene clusters. *J. Phys. Chem. A*, 109:4662–4670, 2005.
- [96] H. J. Van Ramesdonk, B. H. Bakker, M. M. Groeneveld, J. W. Verhoeven, B. D. Allen, J. P. Rostron, and A. Harriman. Ultrafast intersystem crossing in 9,10-anthraquinones and intramolecular charge separation in an anthraquinone-based dyad. *J. Phys. Chem. A*, 110:13145–13150, 2006.
- [97] K. Hamanoue, T. Nakayama, H. Nanshow, T. Hanada, Y. Naruta, T. Kodo, and K. Maruyama. Photoinduced intramolecular charge separation in an anthraquinone-linked all-cis 5,10,15,20-meso-tetrakis (2-aminophenyl)porphyrin derivative studied by picosecond and nanosecond laser spectroscopy. *J. Chem. Soc. Faraday Trans.*, 89:3243–3250, 2003.
- [98] N. S. Allen, G. Pullen, M. Shah, M. Edge, D. Holdsworth, I. Weddell, R. Swart, and F. Catalina. Photochemistry and photoinitiator properties of 2-substituted anthraquinones. 1. Absorption and luminescence characteristics. *J. Photochem. Photobiol. A*, 91:73–79, 1995.
- [99] Q. Wu and T. Van Voorhis. Direct calculation of electron transfer parameters through constrained density functional theory. *J. Phys. Chem. A*, 110(29):9212–9218, 2006.
- [100] J. E. Subotnik, R. J. Cave, R. P. Steele, and N. Shenvi. The initial and final states of electron and energy transfer processes: Diabatization as motivated by system-solvent interactions. *J. Chem. Phys.*, 130:234102, 2009.
- [101] A. Dreuw and M. Head-Gordon. Failure of time-dependent density functional theory for long-range charge-transfer excited states: The zincbacteriochlorin-bacteriochlorin and bacteriochlorophyllspheroidene complexes. *J. Am. Chem. Soc.*, 126(12):4007–4016, 2004.

- [102] A. Dreuw and M. Head-Gordon. Single-reference *ab initio* methods for the calculation of excited states of large molecules. *Chem. Rev.*, 105:4009–4037, 2005.
- [103] E. M. Kosower and D. Huppert. Solvent motion controls the rate of intramolecular electron transfer in solution. *Chem. Phys. Lett.*, 96:433–435, 1983.
- [104] H. J. Kim and J. T. Hynes. Equilibrium and nonequilibrium solvation and solute electronic structure. i. Formulation. *J. Chem. Phys.*, 93:5194–5200, 1990.
- [105] A. Warshel and W. W. Parson. Computer simulations of electron-transfer reactions in solution and in photosynthetic reaction centers. *Ann. Rev. Phys. Chem.*, 42:279–309, 1991.
- [106] T. Simonson. Gaussian fluctuations and linear response in an electron transfer protein. *Proc. Nat'l. Acad. Sci., USA*, 99:6544–6549, 2002.
- [107] D. V. Matyushov and G. A. Voth. Modeling the free energy surfaces of electron transfer in condensed phases. *J. Chem. Phys.*, 113:5413–5424, 2000.
- [108] T. Ishida. Polarizable solute in polarizable and flexible solvents: Simulation study of electron transfer reaction systems. *J. Phys. Chem. B*, 109:18558–18564, 2005.
- [109] G. Lamoureux and B. Roux. Modeling induced polarization with classical Drude oscillators: Theory and molecular dynamics simulation algorithm. *J. Chem. Phys.*, 119:3025–3039, 2003.
- [110] B. R. Brooks, C. L. Brooks, III, A. D. Mackerell, Jr., L. Nilsson, R. J. Petrella, B. Roux, Y. Won, G. Archontis, C. Bartels, S. Boresch, A. Caffisch, L. Caves, Q. Cui, A. R. Dinner, M. Feig, S. Fischer, J. Gao, M. Hodoscek, W. Im, K. Kuczera, T. Lazaridis, J. Ma, V. Ovchinnikov, E. Paci, R. W. Pastor, C. B. Post, J. Z. Pu, M. Schaefer, B. Tidor, R. M. Venable, H. L. Woodcock, X. Wu, W. Yang, D. M. York, and M. Karplus. CHARMM: The biomolecular simulation program. *J. Comput. Chem.*, 30:1545–1614, 2009.
- [111] Y. Shao, L. F. Molnar, Y. Jung, J. Kussmann, C. Ochsenfeld, S. T. Brown, A. T. B. Gilbert, L. V. Slipchenko, Sergey V. Levchenko, D. P. O'Neill, R. A. DiStasio, Jr., R. C. Lochan, T. Wang, G. J. O. Beran, N. A. Besley, J. M. Herbert, C. Y. Lin, T. Van Voorhis, S. H. Chien, A. Sodt, R. P. Steele, V. A. Rassolov, P. E. Maslen, P. P. Korambath, R. D. Adamson, B. Austin, J. Baker, E. F. C. Byrd, H. Dachsel, R. J. Doerksen, A. Dreuw, B. D. Dunietz, A. D. Dutoi, T. R. Furlani, S. R. Gwaltney, A. Heyden, S. Hirata, C.-P. Hsu, G. Kedziora, R. Z. Khalliulin, P. Klunzinger, A. M. Lee, M. S. Lee, W. Liang, I. Lotan, N. Nair, B. Peters, E. I. Proynov, P. A. Pieniazek, Y. M. Rhee, J. Ritchie, E. Rosta, C. .D. Sherrill, A. C. Simmonett, J. E. Subotnik, H. .L. Woodcock, III, W. Zhang, A. T. Bell, A. K. Chakraborty, D. M. Chipman, F. J. Keil, A. Warshel, W. J. Hehre, H. F. Schaefer, III, J. Kong, A. I. Krylov, P. M. W.

- Gill, and M. Head-Gordon. Advances in methods and algorithms in a modern quantum chemistry program package. *Phys. Chem. Chem. Phys.*, 8(27):3172–3191, 2006.
- [112] H. L. Woodcock, M. Hodosceck, A. T. B. Gilbert, P. M. W. Gill, H. F. Schaefer III, and B. R. Brooks. Interfacing Q-Chem and CHARMM to perform QM/MM reaction path calculations. *J. Comput. Chem.*, 28:1485–1502, 2007.
- [113] M. L. Strader and S. E. Feller. A flexible all-atom model of dimethyl sulfoxide for molecular dynamics simulations. *J. Phys. Chem. A*, 106:1074–1080, 2002.
- [114] J.-P. Ryckaert, G. Ciccotti, and H. J. C. Berendsen. Numerical integration of the cartesian equations of motion of a system with constraints: molecular dynamics of *n*-alkanes. *J. Comp. Phys.*, 23:327–341, 1977.
- [115] Z. Lu and Y. Zhang. Interfacing *ab initio* quantum mechanical method with classical Drude oscillator polarizable model for molecular dynamics simulation of chemical reactions. *J. Chem. Theory Comput.*, 4:1237–1248, 2008.
- [116] Q. Wu and T. Van Voorhis. Extracting electron transfer coupling elements from constrained density functional theory. *J. Chem. Phys.*, 125:164105, 2006.
- [117] H. Oberhofer and J. Blumberger. Electronic coupling matrix elements from charge constrained density functional theory calculations using a plane wave basis set. *J. Chem. Phys.*, 133:244105, 2010.
- [118] M. M. Toutounji and M. A. Ratner. Testing the Condon approximation for electron transfer via the Mulliken-Hush model. *J. Phys. Chem. A*, 104:8566–8569, 2000.
- [119] H. Hu and W. Yang. Elucidating solvent contributions to solution reactions with *ab initio* QM/MM methods. *J. Phys. Chem. B*, 114:2755–2759, 2010.
- [120] G. M. Torrie and J. P. Valleau. Non-physical sampling distributions in Monte-Carlo free-energy estimation - umbrella sampling. *J. Comput. Phys.*, 23:187–199, 1977.
- [121] H. Levene. *Contributions to Probability and Statistics: Essays in Honor of Harold Hotelling*, pages 278–292. Stanford University Press, 1960.
- [122] M. Tachiya. Relation between the electron-transfer rate and the free energy change of reaction. *J. Phys. Chem.*, 93:7050–7052, 1989.
- [123] D. F. Underwood and D. A. Blank. Measuring the change in the intermolecular raman spectrum during dipolar solvation. *J. Phys. Chem. A*, 109:3295–3306, 2005.
- [124] A. E. Bragg, M. C. Cavanagh, and B. J. Schwartz. Linear response breakdown in solvation dynamics induced by atomic electron-transfer reactions. *Science*, 321:1817–1822, 2008.

- [125] H. Eyring. The activated complex in chemical reactions. *J. Chem. Phys.*, 3:107–115, 1935.
- [126] F. Ding, H. Wang, Q. Wu, T. Van Voorhis, S. Chen, and J. Konopelski. Computational study of bridge-assisted intervalence electron transfer. *J. Phys. Chem. A*, 114:6039–6046, 2010.
- [127] S. Yeganeh and T. Van Voorhis. Triplet excitation energy transfer with constrained density functional theory. *J. Phys. Chem. C*, 114:20756–20763, 2010.
- [128] S. S. Skourtis, D. H. Waldeck, and D. N. Beratan. Fluctuations in biological and bioinspired electron-transfer reactions. *Ann. Rev. Phys. Chem.*, 61:461–485, 2010.
- [129] G. Hong, E. Rosta, and A. Warshel. Using the constrained DFT approach in generative diabatic surfaces and off diagonal empirical valence bond terms for modeling reactions in condensed phases. *J. Phys. Chem. B*, 110:19570–19574, 2006.
- [130] F. Wallrapp, A. Voityuk, and V. Guallar. Solvent effects on donor-acceptor couplings in peptides. a combined QM and MD study. *J. Chem. Theory Comput.*, 5:3312–3320, 2009.
- [131] A. Troisi, M. A. Ratner, and M. B. Zimmt. Dynamic nature of the intramolecular electronic coupling mediated by a solvent molecule: A computational study. *J. Am. Chem. Soc.*, 126:2215–2224, 2004.
- [132] A. Warshel and J. K. Hwang. Simulation of the dynamics of electron-transfer reactions in polar solvents – semiclassical trajectories and dispersed polaron approaches. *J. Chem. Phys.*, 84:4938–4957, 1986.
- [133] J. C. Rasaiah and J. Zhu. Reaction coordinates for electron transfer reactions. *J. Chem. Phys.*, 129:214503, 2008.
- [134] A. V. Marenich, R. M. Olson, C. P. Kelly, C. J. Cramer, and D. G. Truhlar. Self-consistent reaction field model for aqueous and nonaqueous solutions based on accurate polarized partial charges. *J. Chem. Theory Comput.*, 3:2011–2033, 2007.
- [135] K. Mahata and P. Mahata. Maximizing correlation for supervised classification. In S. Sanei, J. A. Chambers, J. McWhirter, Y. Hicks, and A. G. Constantinides, editors, *Proceedings of the 2007 15th International Conference on Digital Signal Processing*, pages 107–110, New York, 2007. IEEE.
- [136] R. E. Buló, B. Ensing, J. Sikkema, and L. Visscher. Toward a practical method for adaptive QM/MM simulations. *J. Chem. Theory Comput.*, 5:2212–2221, 2009.

- [137] J. Chen and T. J. Martínez. QTPIE: Charge transfer with polarization current equilization. A fluctuating charge model with correct asymptotics. *Chem. Phys. Lett.*, 438:315–320, 2007.
- [138] T. Ziegler, A. Rauk, and E. J. Baerends. Calculation of multiplet energies by the Hartree-Fock-Slater method. *Theor. Chim. Acta*, 43:261–271, 1977.
- [139] T. Kowalczyk, S. R. Yost, and T. Van Voorhis. Assessment of the Δ SCF density functional theory approach for electronic excitations in organic dyes. *J. Chem. Phys.*, 134:054128, 2011.
- [140] S. Difley and T. Van Voorhis. Exciton/charge-transfer electronic couplings in organic semiconductors. *J. Chem. Theory Comput.*, 7:594–601, 2011.
- [141] T. D. M. Bell, K. P. Ghiggino, K. A. Jolliffe, M. G. Ranasinghe, S. J. Langford, M. J. Shephard, and M. N. Paddon-Row. Photoinduced energy and electron transfer in a giant zinc porphyrin-bridge- C_{60} system. *J. Phys. Chem. A*, 106:10089–10088, 2002.
- [142] M. E. El-Khouly, D. K. Ju, K.-Y. Kay, F. D’Souza, and S. Fukuzumi. Supramolecular tetrad of subphthalocyanine–triphenylamine–zinc porphyrin coordinated to fullerene as an antenna-reaction-center mimic: Formation of a long-lived charge-separated state in nonpolar solvent. *Chem. Eur. J.*, 16:6193–6202, 2010.
- [143] M. H. B. Stowell, T. M. Phillips, D. C. Rees, S. M. Soltis, E. Abresch, and G. Feher. Light-induced structural changes in photosynthetic reaction center: Implications for mechanism of electron-proton transfer. *Science*, 276:812–816, 1997.
- [144] V. Sundström, T. Pullerits, and R. van Grondelle. Photosynthetic light-harvesting: Reconciling dynamics and structure of purple bacterial LH2 reveals function of photosynthetic unit. *J. Phys. Chem. B*, 103:2327–2346, 1999.
- [145] J. T. Stockburger and C. H. Mak. A dynamical theory of electron transfer: Crossover from weak to strong electronic coupling. *J. Chem. Phys.*, 105:8126–8135, 1996.
- [146] N. Makri. Time-dependent quantum methods for large systems. *Ann. Rev. Phys. Chem.*, 50:167–191, 1999.
- [147] X. Song, H. Wang, and T. Van Voorhis. A Langevin equation approach to electron transfer reactions in the diabatic basis. *J. Chem. Phys.*, 129:144502, 2008.
- [148] T. Kowalczyk, L.-P. Wang, and T. Van Voorhis. Simulation of solution phase electron transfer in a compact donor–acceptor dyad. *J. Phys. Chem. B*, 115:12135–12144, 2011.

- [149] M. A. Fox and M. Chanon, editors. *Photoinduced Electron Transfer*. Elsevier, 1988.
- [150] R. S. Davidson. The chemistry of excited complexes - A survey of reactions. *Advances in Physical Organic Chemistry*, 19:1–130, 1983.
- [151] J. R. Lakowicz. *Principles of Fluorescence Spectroscopy*. Springer, 2006.
- [152] J. F. Callan, A. P. de Silva, and D. C. Magri. Luminescent sensors and switches in the early 21st century. *Tetrahedron*, 61(36):8551–8588, 2005.
- [153] A. P. de Silva, H. Q. Gunaratne, T. Gunnlaugsson, A. J. Huxley, C. P. McCoy, J. T. Rademacher, and T. E. Rice. Signaling recognition events with fluorescent sensors and switches. *Chem. Rev.*, 97(5):1515–1566, 1997.
- [154] E. M. Nolan and S. J. Lippard. Small-molecule fluorescent sensors for investigating zinc metalloneurochemistry. *Acc. Chem. Res.*, 42(1):193–203, 2009.
- [155] G. K. Walkup, S. C. Burdette, S. J. Lippard, and R. Y. Tsien. A new cell-permeable fluorescent probe for Zn²⁺. *J. Am. Chem. Soc.*, 122(23):5644–5645, 2000.
- [156] B. A. Wong, S. Friedle, and S. J. Lippard. Solution and fluorescence properties of symmetric dipicolylamine-containing dichlorofluorescein-based Zn²⁺ sensors. *J. Am. Chem. Soc.*, 131(20):7142–7152, 2009.
- [157] K. Rurack. Flipping the light switch ‘ON’ - the design of sensor molecules that show cation-induced fluorescence enhancement with heavy and transition metal ions. *Spectrochim. Acta A*, 57(11):2161–2195, 2001.
- [158] L. Serranoandres, M. Merchan, B. Roos, and R. Lindh. Theoretical study of the internal charge-transfer in aminobenzonitriles. *J. Am. Chem. Soc.*, 117(11):3189–3204, 1995.
- [159] T. Jin, K. Ichikawa, and T. Koyama. A fluorescent calix[4]arene as an intramolecular excimer-forming Na⁺ sensor in nonaqueous solution. *J. Chem. Soc., Chem. Commun.*, (6):499–501, 1992.
- [160] A. R. Clapp, I. L. Medintz, and H. Mattoussi. Förster resonance energy transfer investigations using quantum-dot fluorophores. *ChemPhysChem*, 7(1):47–57, 2006.
- [161] R. I. Cukier and D. G. Nocera. Proton-coupled electron transfer. *Ann. Rev. Phys. Chem.*, 49:337–369, 1998.
- [162] S. Prashanthi and P. R. Bangal. Reductive quenching of pyridine linked porphyrins by phenol: A case of proton coupled electron transfer. *Chem. Comm.*, (13):1757–1759, 2009.

- [163] S. Bhattacharya, T. K. Pradhan, A. De, S. R. Chaudhury, A. K. De, and T. Ganguly. Photophysical processes involved within the anisole-thioindoxyl dyad system. *J. Phys. Chem. A*, 110(17):5665–5673, 2006.
- [164] F. Han, L. Chi, X. Liang, S. Ji, S. Liu, F. Zhou, Y. Wu, K. Han, J. Zhao, and T. D. James. 3,6-disubstituted carbazole-based bisboronic acids with unusual fluorescence transduction as enantioselective fluorescent chemosensors for tartaric acid. *J. Org. Chem.*, 74(3):1333–1336, 2009.
- [165] M. H. Lim, B. A. Wong, W. H. Pitcock, Jr., D. Mokshagundam, M.-H. Baik, and S. J. Lippard. Direct nitric oxide detection in aqueous solution by copper(II) fluorescein complexes. *J. Am. Chem. Soc.*, 128(44):14364–14373, 2006.
- [166] I. D. Petsalakis, N. N. Lathiotakis, and G. Theodorakopoulos. Theoretical study on tertiary amine-fluorophore photoinduced electron transfer (PET) systems. *J. Mol. Struct. Theochem.*, 867(1-3):64–70, 2008.
- [167] I. D. Petsalakis, I. S. K. Kerkines, N. N. Lathiotakis, and G. Theodorakopoulos. Emitting and electron-transfer electronic states of tertiary amine-fluorophore sensor systems. *Chem. Phys. Lett.*, 474(4-6):278–284, 2009.
- [168] M. E. McCarroll, Y. Shi, S. Harris, S. Puli, I. Kimaru, R. Xu, L. Wang, and D. Dyer. Computational prediction and experimental evaluation of a photoinduced electron-transfer sensor. *J. Phys. Chem. B*, 110(46):22991–22994, 2006.
- [169] B. A. Wong, S. Friedle, and S. J. Lippard. Subtle modification of 2,2-dipicolylamine lowers the affinity and improves the turn-on of Zn(II)-selective fluorescent sensors. *Inorg. Chem.*, 48:7009–7011, 2009.
- [170] B. A. Sparano, S. P. Shahi, and K. Koide. Effect of binding and conformation on fluorescence quenching in new 2',7'-dichlorofluorescein derivatives. *Org. Lett.*, 6(12):1947–1949, 2004.
- [171] S. C. Burdette, C. J. Frederickson, W. Bu, and S. J. Lippard. ZP4, an improved neuronal Zn²⁺ sensor of the Zinpyr family. *J. Am. Chem. Soc.*, 125(7):1778–1787, 2003.
- [172] E. M. Nolan and S. J. Lippard. The Zinspy family of fluorescent zinc sensors: Syntheses and spectroscopic investigations. *Inorg. Chem*, 43(26):8310–8317, 2004.
- [173] E. M. Nolan, J. Jaworski, K. I. Okamoto, Y. Hayashi, M. Sheng, and S. J. Lippard. QZ1 and QZ2: Rapid, reversible quinoline-derivatized fluoresceins for sensing biological Zn(II). *J. Am. Chem. Soc.*, 127(48):16812–16823, 2005.
- [174] X. Zhang, D. Hayes, S. J. Smith, S. Friedle, and S. J. Lippard. New strategy for quantifying biological zinc by a modified Zinpyr fluorescence sensor. *J. Am. Chem. Soc.*, 130(47):15788–15789, 2008.

- [175] C. C. Woodrooffe, R. Masalha, K. R. Barnes, C. J. Frederickson, and S. J. Lippard. Membrane-permeable and -impermeable sensors of the Zinpyr family and their application to imaging of hippocampal zinc *in vivo*. *Chem. Biol.*, 11(12):1659–1666, 2004.
- [176] M. Malavolta, L. Costarelli, R. Giacconi, E. Muti, G. Bernardini, S. Tesei, C. Cipriano, and E. Mocchegiani. Single and three-color flow cytometry assay for intracellular zinc ion availability in human lymphocytes with Zinpyr-1 and double immunofluorescence: Relationship with metallothioneins. *Cytom. Part A*, 69A(10):1043–1053, 2006.
- [177] G. Anderegg, E. Hubmann, E. Podder, and N. G. Wenk. Pyridine-derivatives as complexing agents .11. Thermodynamics of metal-complex formation with bis[(2-pyridyl)methyl]-amine, tris[(2-pyridyl)methyl]-amine and tetrakis[(2-pyridyl)methyl]-amine. *Helv. Chim. Acta*, 60(1):123–140, 1977.
- [178] C. T. Lee, W. T. Yang, and R. G. Parr. Development of the Colle-Salvetti correlation-energy formula into a functional of the electron-density. *Phys. Rev. B*, 37(2):785–789, 1988.
- [179] R. Ahlrichs, M. Bar, M. Haser, H. Horn, and C. Kolmel. Electronic-structure calculations on workstation computers - The program system Turbomole. *Chem. Phys. Lett.*, 162(3):165–169, 1989.
- [180] F. Weigend and R. Ahlrichs. Balanced basis sets of split valence, triple zeta valence and quadruple zeta valence quality for H to Rn: Design and assessment of accuracy. *Phys. Chem. Chem. Phys.*, 7:3297–3305, 2005.
- [181] D Figgen, G Rauhut, M Dolg, and H Stoll. Energy-consistent pseudopotentials for group 11 and 12 atoms: Adjustment to multi-configuration Dirac-Hartree-Fock data. *Chem. Phys.*, 311(1-2):227–244, 2005.
- [182] A. Klamt and G. Schüürmann. COSMO: A new approach to dielectric screening in solvents with explicit expressions for the screening energy and its gradient. *J. Chem. Soc., Perkin Trans. 2*, (5):799–805, 1993.
- [183] M. A. Rohrdanz, K. M. Martins, and J. M. Herbert. A long-range-corrected density functional that performs well for both ground-state properties and time-dependent density functional theory excitation energies, including charge-transfer excited states. *J. Chem. Phys.*, 130(5):054112, 2009.
- [184] M. Head-Gordon, A. M. Graña, D. Maurice, and C. A. White. Analysis of electronic-transitions as the difference of electron-attachment and detachment densities. *J. Phys. Chem.*, 99(39):14261–14270, 1995.
- [185] S. Hirata and M. Head-Gordon. Time-dependent density functional theory within the Tamm-Dancoff approximation. *Chem. Phys. Lett.*, 314(3-4):291–299, 1999.

- [186] W. Humphrey, A. Dalke, and K. Schulten. VMD – Visual Molecular Dynamics. *J. Mol. Graphics*, 14:33–38, 1996.
- [187] T. H. Dunning, Jr. Gaussian basis sets for use in correlated molecular calculations. I. The atoms boron through neon and hydrogen. *J. Chem. Phys.*, 90:1007, 1989.
- [188] L. Onsager. Electric moments of molecules in liquids. *J. Am. Chem. Soc.*, 58(8):1486–1493, 1936.
- [189] J. B. Foresman, T. A. Keith, K. B. Wiberg, J. Snoonian, and M. J. Frisch. Solvent effects 5. Influence of the cavity shape, truncation of electrostatics, and electron correlation on *ab initio* reaction field calculations. *J. Phys. Chem.*, 100(40):16098–16104, 1996.
- [190] X.-F. Zhang, Q. Liu, A. Son, Q. Zhang, F. Zhao, and F. Zhang. Fluorescence properties of dibenzofluorescein in aqueous solution. *J. Fluoresc.*, 18(6):1051–1057, 2008.
- [191] R. Sjoback, J. Nygren, and M. Kubista. Absorption and fluorescence properties of fluorescein. *Spectrochim. Acta*, 51(6):L7–L21, 1995.
- [192] J. Casanovas, D. Jacquemin, E. A. Perpète, and C. Alemán. Fluorescein isothiocyanate: Molecular characterization by theoretical calculations. *Chem. Phys.*, 354:155–161, 2008.
- [193] M. Wanko, M. Garavelli, F. Bernardi, T. A. Niehaus, T. Frauenheim, and M. Elstner. A global investigation of excited state surfaces within time-dependent density-functional response theory. *J. Chem. Phys.*, 120(4):1674–1692, 2004.
- [194] K. B. Wiberg, R. E. Stratmann, and M. J. Frisch. A time-dependent density functional theory study of the electronically excited states of formaldehyde, acetaldehyde and acetone. *Chem. Phys. Lett.*, 297(1):60–64, 1998.
- [195] J. E. Del Bene, R. Ditchfield, and J. A. Pople. Self-consistent molecular orbital methods .10. Molecular orbital studies of excited states with minimal and extended basis sets. *J. Chem. Phys.*, 55(5):2236–2241, 1971.
- [196] J. B. Foresman, M. Head-Gordon, J. A. Pople, and M. J. Frisch. Toward a systematic molecular-orbital theory for excited-states. *J. Phys. Chem.*, 96(1):135–149, 1992.
- [197] J. Subotnik. Configuration interaction singles has a large systematic bias against charge-transfer states. *J. Chem. Phys.*, 135:071104, 2011.
- [198] M. A. Rohrdanz and J. M. Herbert. Simultaneous benchmarking of ground- and excited-state properties with long-range corrected density functional theory. *J. Chem. Phys.*, 129(3):034107, 2008.

- [199] S. Yeganeh and T. Van Voorhis. Optimal diabatic bases via thermodynamic bounds. *J. Chem. Phys.*, 135:104114, 2011.
- [200] N. Robertson. Optimizing dyes for dye-sensitized solar cells. *Angew. Chem. Int. Ed.*, 45:2338–2345, 2006.
- [201] B. O’Regan and M. Grätzel. A low-cost, high-efficiency solar cell based on dye-sensitized colloidal TiO₂ films. *Nature*, 353:737–740, 1991.
- [202] J. R. Sheats, H. Antoniadis, M. Hueschen, W. Leonard, J. Miller, R. Moon, D. Roitman, and A. Stocking. Organic Electroluminescent Devices. *Science*, 273:884–888, 1996.
- [203] U. Mitschke and P. Bäuerle. The electroluminescence of organic materials. *J. Mater. Chem.*, 10:1471–1507, 2000.
- [204] S. R. Forrest. The path to ubiquitous and low-cost organic electronic appliances on plastic. *Nature*, 428:911–918, 2004.
- [205] M. A. Baldo, D. F. O’Brien, Y. You, A. Shoustikov, S. Sibley, M. E. Thompson, and S. R. Forrest. Highly efficient phosphorescent emission from organic electroluminescent devices. *Nature*, 395:151–154, 1998.
- [206] C. D. Dimitrakopoulos and D. J. Masearo. Organic thin-film transistors: A review of recent advances. *IBM J. Res. Dev.*, 45:11–27, 2001.
- [207] P. Peumans, A. Yakimov, and S. R. Forrest. Small molecular weight organic thin-film photodetectors and solar cells. *J. Appl. Phys.*, 93:3693, 2003.
- [208] J. Cornil, D. Beljonne, J.-P. Calbert, and J.-L. Brédas. Interchain interactions in organic π -conjugated materials: Impact on electronic structure, optical response, and charge transport. *Adv. Mater.*, 13:1053–1067, 2001.
- [209] I. Kaur, W. Jia, R. P. Kopreski, S. Selvarasah, M. R. Dokmeci, C. Pramanik, N. E. McGruer, and G. P. Miller. Substituent effects in pentacenes: Gaining control over HOMO-LUMO gaps and photooxidative resistances. *J. Am. Chem. Soc.*, 130:16274–16286, 2008.
- [210] J. A. Pople, D. P. Santry, and G. A. Segal. Approximate Self-Consistent Molecular Orbital Theory. I. Invariant Procedures. *J. Chem. Phys.*, 43:S129, 1965.
- [211] J. Linderberg and Y. Ohrn. Derivation and analysis of the Pariser–Parr–Pople model. *J. Chem. Phys.*, 49:716, 1968.
- [212] B. Roos. The complete active space self-consistent field method and its applications in electronic structure calculations. *Adv. Chem. Phys.*, 69:399, 1987.
- [213] K. Emrich. An extension of the coupled cluster formalism to excited states. *Nucl. Phys. A*, 351:397–438, 1981.

- [214] E. Gross and W. Kohn. Local density-functional theory of frequency-dependent linear response. *Phys. Rev. Lett.*, 55:2850–2852, 1985.
- [215] R. Bauernschmitt and R. Ahlrichs. Treatment of electronic excitations within the adiabatic approximation of time dependent density functional theory. *Chem. Phys. Lett.*, 256:454–464, 1996.
- [216] F. Furche and R. Ahlrichs. Adiabatic time-dependent density functional methods for excited state properties. *J. Chem. Phys.*, 117:7433, 2002.
- [217] D. Jacquemin, V. Wathelet, E. A. Perpète, and C. Adamo. Extensive TD-DFT benchmark: Singlet-excited states of organic molecules. *J. Chem. Theory Comput.*, 5:2420–2435, 2009.
- [218] M. E. Casida, C. Jamorski, K. C. Casida, and D. R. Salahub. Molecular excitation energies to high-lying bound states from time-dependent density-functional response theory: Characterization and correction of the time-dependent local density approximation ionization threshold. *J. Chem. Phys.*, 108:4439, 1998.
- [219] D. J. Tozer and N. C. Handy. On the determination of excitation energies using density functional theory. *Phys. Chem. Chem. Phys.*, 2:2117–2121, 2000.
- [220] M. J. G. Peach, P. Benfield, T. Helgaker, and D. J. Tozer. Excitation energies in density functional theory: an evaluation and a diagnostic test. *J. Chem. Phys.*, 128:044118, 2008.
- [221] S. Grimme and M. Parac. Substantial errors from time-dependent density functional theory for the calculation of excited states of large π systems. *ChemPhysChem*, 4:292–5, 2003.
- [222] Z.-L. Cai, K. Sendt, and Jeffrey R. Reimers. Failure of density-functional theory and time-dependent density-functional theory for large extended π systems. *J. Chem. Phys.*, 117:5543, 2002.
- [223] D. Jacquemin, E. A. Perpète, G. E. Scuseria, I. Ciofini, and C. Adamo. TD-DFT performance for the visible absorption spectra of organic dyes: Conventional versus long-range hybrids. *J. Chem. Theory Comput.*, 4:123–135, 2008.
- [224] J.-W. Song, M. A. Watson, and K. Hirao. An improved long-range corrected hybrid functional with vanishing Hartree-Fock exchange at zero interelectronic distance (LC2gau-BOP). *J. Chem. Phys.*, 131:144108, 2009.
- [225] A. Görling. Density-functional theory for excited states. *Phys. Rev. A*, 54:3912–3915, 1996.
- [226] A. K. Theophilou. The energy density functional formalism for excited states. *J. Phys. C*, 12:5419–5430, 1979.

- [227] P. Ayers and M. Levy. Time-independent (static) density-functional theories for pure excited states: Extensions and unification. *Phys. Rev. A*, 80:012508, 2009.
- [228] C.-L. Cheng, Q. Wu, and T. Van Voorhis. Rydberg energies using excited state density functional theory. *J. Chem. Phys.*, 129:124112, 2008.
- [229] E. Artacho, M. Rohlfing, M. Côté, P. Haynes, R. Needs, and C. Molteni. Structural relaxations in electronically excited poly(para-phenylene). *Phys. Rev. Lett.*, 93:116401, 2004.
- [230] N. A. Besley, A. T. B. Gilbert, and P. M. W. Gill. Self-consistent-field calculations of core excited states. *J. Chem. Phys.*, 130:124308, 2009.
- [231] J. Liu and W. Liang. Analytical Hessian of electronic excited states in time-dependent density functional theory with Tamm-Dancoff approximation. *J. Chem. Phys.*, 135:014113, 2011.
- [232] T. Ziegler, M. Seth, M. Krykunov, J. Autschbach, and F. Wang. On the relation between time-dependent and variational density functional theory approaches for the determination of excitation energies and transition moments. *J. Chem. Phys.*, 130:154102, 2009.
- [233] T. Liu, W.-G. Han, F. Himo, G. M. Ullmann, D. Bashford, A. Toutchkine, K. M. Hahn, and L. Noodleman. Density functional vertical self-consistent reaction field theory for solvatochromism studies of solvent-sensitive dyes. *J. Phys. Chem. A*, 108:3545–3555, 2004.
- [234] D. Ceresoli, E. Tosatti, S. Scandolo, G. Santoro, and S. Serra. Trapping of excitons at chemical defects in polyethylene. *J. Chem. Phys.*, 121:6478–6484, 2004.
- [235] J. Gavnholt, T. Olsen, M. Englund, and J. Schiøtz. Δ self-consistent field method to obtain potential energy surfaces of excited molecules on surfaces. *Phys. Rev. B*, 78:075441, 2008.
- [236] M. Schreiber, M. R. Silva-Junior, S. P. A Sauer, and W. Thiel. Benchmarks for electronically excited states: CASPT2, CC2, CCSD, and CC3. *J. Chem. Phys.*, 128:134110, 2008.
- [237] D. Jacquemin, E. A. Perpète, I. Ciofini, C. Adamo, R. Valero, Y. Zhao, and D. G. Truhlar. On the performances of the M06 family of density functionals for electronic excitation energies. *J. Chem. Theory Comput.*, 6:2071–2085, 2010.
- [238] L. Goerigk and S. Grimme. Assessment of TD-DFT methods and of various spin scaled CIS(D) and CC2 versions for the treatment of low-lying valence excitations of large organic dyes. *J. Chem. Phys.*, 132:184103, 2010.

- [239] B. Mennucci, R. Cammi, and J. Tomasi. Excited states and solvatochromic shifts within a nonequilibrium solvation approach: A new formulation of the integral equation formalism method at the self-consistent field, configuration interaction, and multiconfiguration self-consistent field level. *J. Chem. Phys.*, 109:2798, 1998.
- [240] F. Inagaki, M. Tasumi, and T. Miyazawa. Excitation profile of the resonance Raman effect of β -carotene. *J. Mol. Spectrosc.*, 50:286–303, 1974.
- [241] L. Edwards and M. Gouterman. Porphyrins XV. Vapor absorption spectra and stability: Phthalocyanines. *J. Mol. Spectrosc.*, 33:292–310, 1970.
- [242] H. Mattoussi, H. Murata, C. D. Merritt, Y. Iizumi, J. Kido, and Z. H. Kafafi. Photoluminescence quantum yield of pure and molecularly doped organic solid films. *J. Appl. Phys.*, 86:2642, 1999.
- [243] T. Riehm, G. De Paoli, A. E. Konradsson, L. De Cola, H. Wadepohl, and L. H. Gade. Tetraazaperopyrenes: a new class of multifunctional chromophores. *Chem. Eur. J.*, 13:7317–7329, 2007.
- [244] K.-Y. Lai, T.-M. Chu, F. C.-N. Hong, A. Elangovan, K.-M. Kao, S.-W. Yang, and T.-I. Ho. Excimer emission from a novel ethyne-based fluorescent dye in organic light-emitting devices. *Surf. Coat. Technol.*, 200:3283–3288, 2006.
- [245] K. Tajima, L.-S. Li, and S. I. Stupp. Nanostructured oligo(p-phenylene vinylene)/silicate hybrid films: one-step fabrication and energy transfer studies. *J. Am. Chem. Soc.*, 128:5488–54895, 2006.
- [246] J. Rajput, D. B. Rahbek, L. H. Andersen, A. Hirshfeld, M. Sheves, P. Altoè, G. Orlandi, and M. Garavelli. Probing and modeling the absorption of retinal protein chromophores in vacuo. *Angew. Chem. Int. Ed*, 49:1790–1793, 2010.
- [247] Y. Lu and A. Penzkofer. Absorption behaviour of methanolic Rhodamine 6G solutions at high concentration. *Chem. Phys.*, 107:175–184, 1986.
- [248] Z. Ning, Q. Zhang, W. Wu, H. Pei, B. Liu, and H. Tian. Starburst triarylamine based dyes for efficient dye-sensitized solar cells. *J. Org. Chem.*, 73:3791–3797, 2008.
- [249] C. Bonnand, J. Bellessa, and J. Plenet. Properties of surface plasmons strongly coupled to excitons in an organic semiconductor near a metallic surface. *Phys. Rev. B*, 73:245330, 2006.
- [250] U. Eisner and R. P. Linstead. Chlorophyll and related substances. Part I. The synthesis of chlorin. *J. Chem. Soc.*, page 3742, 1955.
- [251] L. Edwards, D. H. Dolphin, M. Gouterman, and A. D. Adler. Porphyrins XVII. Vapor absorption spectra and redox reactions: Tetraphenylporphins and porphin. *J. Mol. Spectrosc.*, 38:16–32, 1971.

- [252] D. Biermann and W. Schmidt. Diels-Alder reactivity of polycyclic aromatic hydrocarbons. 1. Acenes and benzologs. *J. Am. Chem. Soc.*, 102:3163–3173, 1980.
- [253] M. Dolg, U. Wedig, H. Stoll, and H. Preuss. Energy-adjusted *ab initio* pseudopotentials for the first row transition elements. *J. Chem. Phys.*, 86:866–872, 1987.
- [254] Y. Zhao and D. G. Truhlar. The M06 suite of density functionals for main group thermochemistry, thermochemical kinetics, noncovalent interactions, excited states, and transition elements: two new functionals and systematic testing of four M06-class functionals and 12 other functionals. *Theor. Chim. Acta*, 120:215–241, 2008.
- [255] J. Fabian, L. A. Diaz, G. Seifert, and T. Niehaus. Calculation of excitation energies of organic chromophores: A critical evaluation. *J. Mol. Struct. Theochem.*, 594:41–53, 2002.
- [256] A. T. B. Gilbert, N. A. Besley, and P. M. W. Gill. Self-consistent field calculations of excited states using the maximum overlap method (MOM). *J. Phys. Chem. A*, 112:13164–13171, 2008.
- [257] A. Touthkine, W.-G. Han, M. Ullmann, T. Liu, D. Bashford, L. Noodleman, and K. M. Hahn. Experimental and DFT studies: novel structural modifications greatly enhance the solvent sensitivity of live cell imaging dyes. *J. Phys. Chem. A*, 111:10849–10860, 2007.
- [258] W. Liang, C. M. Isborn, and X. Li. Obtaining Hartree-Fock and density functional theory doubly excited states with Car-Parrinello density matrix search. *J. Chem. Phys.*, 131:204101, 2009.
- [259] J. Tao and G. Vignale. Time-dependent density-functional theory beyond the local-density approximation. *Phys. Rev. Lett.*, 97:036403, 2006.
- [260] J. Tao, G. Vignale, and I. Tokatly. Time-dependent density functional theory: Derivation of gradient-corrected dynamical exchange-correlational potentials. *Phys. Rev. B*, 76:195126, 2007.
- [261] G. Onida, L. Reining, and A. Rubio. Electronic excitations: density-functional versus many-body Green’s-function approaches. *Rev. Mod. Phys.*, 74:601–659, 2002.
- [262] S. Hirata, S. Ivanov, I. Grabowski, and R. J. Bartlett. Time-dependent density functional theory employing optimized effective potentials. *J. Chem. Phys.*, 116:6468, 2002.
- [263] Y. Kurzweil and R. Baer. Adapting approximate-memory potentials for time-dependent density functional theory. *Phys. Rev. B*, 77:085121, 2008.

- [264] G. Vignale. Real-time resolution of the causality paradox of time-dependent density-functional theory. *Phys. Rev. A*, 77:062511, 2008.
- [265] Y. Kurzweil and R. Baer. Generic Galilean-invariant exchange-correlation functionals with quantum memory. *Phys. Rev. B*, 72:035106, 2005.
- [266] M. E. Casida. Time-dependent density functional response theory for molecules. In D. P. Chong, editor, *Recent Advances in Density Functional Methods*, pages 155–192. World Scientific, Singapore, 1995.
- [267] M. Seth and T. Ziegler. Calculation of excitation energies of open-shell molecules with spatially degenerate ground states. I. Transformed reference via an intermediate configuration Kohn-Sham density-functional theory and applications to d^1 and d^2 systems with octahedral and tetrahedral symmetries. *J. Chem. Phys.*, 123:144105, 2005.
- [268] M. Seth and T. Ziegler. Calculation of excitation energies of open-shell molecules with spatially degenerate ground states. II. Transformed reference via intermediate configuration Kohn-Sham time dependent density functional theory oscillator strengths and magnetic circular dichroism C terms. *J. Chem. Phys.*, 124:144105, 2006.
- [269] F. Wang and T. Ziegler. The performance of time-dependent density functional theory based on a noncollinear exchange-correlation potential in the calculations of excitation energies. *J. Chem. Phys.*, 122:074109, 2005.
- [270] Y. Shao, M. Head-Gordon, and A. I. Krylov. The spin-flip approach within time-dependent density functional theory: Theory and applications to diradicals. *J. Chem. Phys.*, 118:4807, 2003.
- [271] F. Wang and T. Ziegler. Time-dependent density functional theory based on a noncollinear formulation of the exchange-correlation potential. *J. Chem. Phys.*, 121:12191–12196, 2004.
- [272] N. Maitra, K. Burke, and C. Woodward. Memory in time-dependent density functional theory. *Phys. Rev. Lett.*, 89:023002, 2002.
- [273] A. Görling. Orbital- and state-dependent functionals in density-functional theory. *J. Chem. Phys.*, 123:62203, 2005.
- [274] C. Ullrich, U. Gossmann, and E. Gross. Time-dependent optimized effective potential. *Phys. Rev. Lett.*, 74:872–875, 1995.
- [275] M. Levy. Universal variational functionals of electron densities, first-order density matrices, and natural spin-orbitals and solution of the v -representability problem. *Proc. Nat'l. Acad. Sci., USA*, 76:6062–6065, 1979.
- [276] D. Cremer. Density functional theory: Coverage of dynamic and non-dynamic electron correlation effects. *Mol. Phys.*, 99:1899–1940, 2001.

- [277] E. Ruiz, J. Cano, S. Alvarez, and P. Alemany. Broken symmetry approach to calculation of exchange coupling constants for homobinuclear and heterobinuclear transition metal complexes. *J. Comput. Chem.*, 20:1391–1400, 1999.
- [278] J. Cabrero, N. Ben Amor, C. de Graaf, F. Illas, and R. Caballol. *Ab initio* study of the exchange coupling in oxalato-bridged Cu(II) dinuclear complexes. *J. Phys. Chem. A*, 104:9983–9989, 2000.
- [279] E. Ruiz, A. Rodríguez-Forteza, J. Cano, S. Alvarez, and P. Alemany. About the calculation of exchange coupling constants in polynuclear transition metal complexes. *J. Comput. Chem.*, 24:982–989, 2003.
- [280] I. Rudra, Q. Wu, and T. Van Voorhis. Predicting exchange coupling constants in frustrated molecular magnets using density functional theory. *Inorg. Chem*, 46:10539–10548, 2007.
- [281] M. Filatov and S. Shaik. A spin-restricted ensemble-referenced Kohn–Sham method and its application to diradicaloid situations. *Chem. Phys. Lett.*, 304:429–437, 1999.
- [282] I. Frank, J. Hutter, D. Marx, and M. Parrinello. Molecular dynamics in low-spin excited states. *J. Chem. Phys.*, 108:4060, 1998.
- [283] M. Filatov and S. Shaik. Application of spin-restricted open-shell Kohn–Sham method to atomic and molecular multiplet states. *J. Chem. Phys.*, 110:116, 1999.
- [284] Y. Mochizuki, Y. Komeiji, T. Ishikawa, T. Nakano, and H. Yamataka. A fully quantum mechanical simulation study on the lowest $n \rightarrow \pi^*$ state of hydrated formaldehyde. *Chem. Phys. Lett.*, 437:66–72, 2007.
- [285] U. F. Röhrig, I. Frank, J. Hutter, A. Laio, J. VandeVondele, and U. Rothlisberger. QM/MM Car-Parrinello molecular dynamics study of the solvent effects on the ground state and on the first excited singlet state of acetone in water. *ChemPhysChem*, 4:1177–82, 2003.
- [286] M. Sulpizi, U. F. Röhrig, J. Hutter, and U. Rothlisberger. Optical properties of molecules in solution via hybrid TDDFT/MM simulations. *Int. J. Quantum Chem.*, 101:671–682, 2005.
- [287] F. Santoro, A. Lami, R. Improta, and V. Barone. Effective method to compute vibrationally resolved optical spectra of large molecules at finite temperature in the gas phase and in solution. *J. Chem. Phys.*, 126:184102, 2007.
- [288] F. Santoro, A. Lami, R. Improta, J. Bloino, and V. Barone. Effective method for the computation of optical spectra of large molecules at finite temperature including the Duschinsky and Herzberg-Teller effect: The Q_x band of porphyrin as a case study. *J. Chem. Phys.*, 128:224311, 2008.

- [289] B. Baumeier, F. May, C. Lennartz, and D. Andrienko. Challenges for *in silico* design of organic semiconductors. *J. Mater. Chem.*, in press, 2012.
- [290] I. Okazaki, F. Sato, T. Yoshihiro, T. Ueno, and H. Kashiwagi. Development of a restricted open shell Kohn-Sham program and its application to a model heme complex. *J. Mol. Struct. Theochem.*, 451(1-2):109–119, 1998.
- [291] M. Schulte and I. Frank. Restricted open-shell kohn–sham theory: n unpaired electrons. *Chem. Phys.*, 373:283–288, 2010.
- [292] V. N. Glushkov, N. I. Gidopoulos, and S. Wilson. Alternative technique for the constrained variational problem based on an asymptotic projection method: II. Applications to open-shell self-consistent field theory. In *Frontiers in Quantum Systems in Chemistry and Physics*, pages 451–489. Springer, 2008.
- [293] J. Cullen, M. Krykunov, and T. Ziegler. The formulation of a self-consistent constricted variational density functional theory for the description of excited states. *Chem. Phys.*, 391:11–18, 2011.
- [294] T. Ziegler, M. Krykunov, and J. Cullen. The application of constricted variational density functional theory to excitations involving electron transitions from occupied lone-pair orbitals to virtual π^* orbitals. *J. Chem. Theory Comput.*, 7:2485–2491, 2011.
- [295] S. Grimm, C. Nonnenberg, and I. Frank. Restricted open-shell Kohn–Sham theory for π – π^* transitions. I. Polyenes, cyanines, and protonated imines. *J. Chem. Phys.*, 119:11574, 2003.
- [296] C. Nonnenberg, C. Bräuchle, and I. Frank. Restricted open-shell Kohn–Sham theory for π – π^* transitions. III. Dynamics of aggregates. *J. Chem. Phys.*, 122:14311, 2005.
- [297] S. R. Billeter and D. Egli. Calculation of nonadiabatic couplings with restricted open-shell Kohn–Sham density-functional theory. *J. Chem. Phys.*, 125(22):224103, 2006.
- [298] M. Odellius, D. Laikov, and J. Hutter. Excited state geometries within time-dependent and restricted open-shell density functional theories. *J. Mol. Struct. Theochem.*, 630:163–175, 2003.
- [299] J. Friedrichs, K. Damianos, and I. Frank. Solving restricted open-shell equations in excited state molecular dynamics simulations. *Chem. Phys.*, 347:17–24, 2008.
- [300] C. Roothaan. Self-consistent field theory for open shells of electronic systems. *Rev. Mod. Phys.*, 32:179–185, 1960.
- [301] U. von Barth. Local-density theory of multiplet structure. *Phys. Rev. A*, 20:1693–1703, 1979.

- [302] A. Görling. Symmetry in density-functional theory. *Phys. Rev. A*, 47:2783–2799, 1993.
- [303] K. Hirao and H. Nakatsuji. General SCF operator satisfying correct variational condition. *J. Chem. Phys.*, 59:1457, 1973.
- [304] S. Goedecker and C. J. Umrigar. Critical assessment of the self-interaction-corrected local-density-functional method and its algorithmic implementation. *Phys. Rev. A*, 55:1765–1771, 1997.
- [305] P. Pulay. Convergence acceleration of iterative sequences. The case of SCF iteration. *Chem. Phys. Lett.*, 73:393–398, 1980.
- [306] V. R. Saunders and I. H. Hillier. A level-shifting method for converging closed shell Hartree-Fock wave functions. *Int. J. Quantum Chem.*, 7:699–705, 1973.
- [307] V. Bonačić-Koutecký and J. Michl. Photochemical *syn-anti* isomerization of a Schiff base: A two-dimensional description of a conical intersection in formaldehyde. *Theor. Chim. Acta*, 68:45–55, 1985.
- [308] F. Schautz, F. Buda, and C. Filippi. Excitations in photoactive molecules from quantum Monte Carlo. *J. Chem. Phys.*, 121:5836–5844, 2004.
- [309] T. Kowalczyk, Z. Lin, and T. Van Voorhis. Fluorescence quenching by photoinduced electron transfer in the Zn^{2+} sensor Zinpyr-1: A computational investigation. *J. Phys. Chem. A*, 114:10427–10434, 2010.
- [310] D. Buccella, J. A. Horowitz, and S. J. Lippard. Understanding zinc quantification with existing and advanced ditopic fluorescent Zinpyr sensors. *J. Am. Chem. Soc.*, 133:4101–4114, 2011.
- [311] Y. Zhang and A. Wasserman. Transferability of atomic properties in molecular partitioning: A comparison. *J. Chem. Theory Comput.*, 6:3312–3318, 2010.
- [312] G. Seifert and O. Joswig. Density-functional tight binding – an approximate density-functional theory method. *WIREs Comput. Mol. Sci.*, 2:456–465, 2012.